Università degli Studi di Padova

Thesis of Laurea Magistrale in
Aerospace Engineering

Debris Mitigation in LEO Orbits: Performance Analysis and Comparison of different Deorbit Systems

Candidate:
Pastore Guido Student ID: 1033323
Supervisor:
Prof. Lorenzini Enrico

Abstract

This thesis deals with the major problem of finding the best way to deorbit inactive spacecrafts and upper stages from LEO region, that is the most densely populated. Consequently, it is the region where implementation of deorbit capability, for spacecrafts launched in the future, is most necessary and urgent. Deorbit has been proven to be the most effective measure for long-term space debris mitigation. Different solutions have been proposed in literature, but an exhaustive comparison between them has never been performed. Solutions for deorbit considered in this work are: *Natural Decay*, *Drag Augmentation devices*, *Chemical Propulsion*, *Electrical Propulsion*, *Electro-Dynamic Tether (EDT)* system. The principal drivers for comparison are: deorbit time (constrained to a maximum of 25 years by international guidelines), risk of collision, in terms of Area-Time Product (ATP), and additional mass, comprising any component and consumable that would not be present onboard, were deorbit not implemented. Data about orbital debris in LEO region will be presented, and a detailed description of each deorbit system will follow. A personally written set of*Matlab*® codes, plus simulations with software Stela®, are used for numerical analysis of performance of each system. Computational codes are successfully validated. The option that leads to the lowest additional mass is the *EDT system*, for all inclinations and all initial altitudes above 600 km. Considering deorbit time and ATP, the best option is always *chemical propulsion*, since it provides a *direct* deorbit, but at altitudes higher than about 800 km, the required mass of propellant would be too large. *EDT system* and *electrical propulsion* are competitors at higher altitudes: the EDT system performs better, on all drivers, in a much wider range of initial orbital altitudes and inclinations. The *electrical propulsion* has the major problem of requiring the largest additional mass among all deorbit systems, due to additional solar panels. The selection of the optimal deorbit system requires, often, a compromise, since in certain cases there is not one single solution that outperforms all the others on every aspect. However, the *EDT system* results as the option that is optimal for the highest number of satellites in LEO, and therefore deserves particular attention and further development in the future.

Contents

List of Figures

List of Tables

List of Symbols

List of Acronyms

ATP Area-Time Product

CCSA Collisional Cross-Sectional Area

CM Center of Mass

CP Chemical Propulsion

DATP Drag Area-Time Product

DGRF Definitive Geomagnetic Reference Field

DoD Department of Defense (United States)

ECP Electrodynamic Center of Pressure

EDT ElectroDynamic Tether

EP Electrical Propulsion

FEAC Field Emitter Array Cathode

IAGA International Association of Geomagnetism and Aeronomy

IGRF International Geomagnetic Reference Field

IRI International Reference Ionosphere

JD Julian Day

LEO Low Earth Orbit

OML Orbit Motion Limited

RAAN Right Ascension of Ascending Node

TRL Technology Readiness Level

WCCSA Weighted Collisional Cross-Sectional Area

Chapter 1

Introduction

Measures to reduce the debris population in Earth orbits are becoming every day more urgent for the future of space missions, given that the increasing population of debris constantly augments the risk of collision, and consequent generation of new debris that, in cascade, increment even more the collision risk. This can be considered a spiraling effect that can be interrupted only with the implementation of debris mitigation strategies, that would lead, in the long run, to a very consistent debris removal from space. The most effective and essential mitigation measure has been demonstrated to be the implementation of deorbit capability on every future satellite launched in space (as reported in Ref.[23]).

As it will be shown in Sec.[1.1] the vast majority of space debris is concentrated in the LEO region of Earth orbits. For this reason, but not only, the main focus of mitigation measures is cast upon deorbit of satellites and spent stages orbiting in LEO.

The principal purpose of this thesis is to perform a thorough investigation about different solutions for *deorbit* of LEO satellites after their operational life, and to elicit the optimal choice among the pool of different options. The selection is performed following a critical comparison, based on results from numerical analysis, once boundary conditions are set, i.e. initial orbital parameters and features of the object to deorbit.

The analysis will consider the following solutions, that have been proposed in literature for spacecraft deorbit:

1. **Natural Decay**
2. ***Active* systems**:
    - *Chemical Propulsion*
    - *Electrical Propulsion*
3. ***Passive* systems** (a very low amount of energy might be required only for deployment of the device):

- *Drag Augmentation devices*, subdivided into two categories: inflatable devices (*aerodynamic drag balloons*)and non-inflatable devices supported by rigid booms (*aerodynamic drag sails*)
- *Bare Electro-Dynamic Tether (EDT)* system

Combined, or *hybrid*, solutions for deorbit have been proposed too, but they will not be considered in this work, because of the very low Technology Readiness Level (TRL, see Ref. [22] pg. 44). Moreover, a deorbit time lower than 25 years is always achievable by using a single deorbit device, hence it is hardly conceivable as convenient to increase complexity (and decrease reliability) of the system using simultaneously two different deorbit devices. The only combination that will be discussed is the partnership between a hardware system used for deorbit, i.e. an *active* or *passive* system, and *natural decay*. For example, it can be employed a *chemical propulsion* system to only partially deorbit a spacecraft, instead of performing a direct re-entry, and then just exploit the aerodynamic drag (i.e. *natural decay*) for the remaining phase of deorbit.

A critical comparison, based on analysis results, will be performed between all deorbit solutions metioned above. The main drivers employed for the comparison are:

- **Deorbit Time**, i.e. the total time required to lower the orbit to a level at which atmosphere will rapidly burn out the object, or to an higher altitude such that compliance with the time constraint imposed by international guidelines is achieved.
- **Additional mass** due to the presence of deorbit system, i.e.the mass of everything (hardware components, or consumables) that would not be present onboard, were deorbit not implemented. For example, if using *chemical* or *electrical propulsion*, the propellant required for deorbit is additional mass. Moreover, if the spacecraft is designed to work during its life without *chemical* or *electrical propulsion*, the additional mass for deorbit needs to account for the propulsion system dry mass too.
- Risk of collision and consequent generation of new debris associated to the deorbit phase. This parameter can be efficiently evaluated by computing a **"Weighted" Collisional Area-Time Product (ATP)**, as will be described in Sec.[3.2] at pg.65.
- **Technology Readiness Level (TRL)**

In the current work, a cost estimation will not be implemented since it is not feasible without knowing precise information on components prices, that is not publicly available in literature. Anyhow, as a "rule of thumb" the more complex is the system, the higher is the mass, and the lower is the TRL level, the higher the total cost will be. Therefore, an estimate of cost can be easily performed subsequently, after knowing the performance of each deorbit system on all drivers considered in this analysis, listed above.

1.1 Data about Orbital Debris

The following graph schematically shows a classification of all the objects orbiting around the Earth.

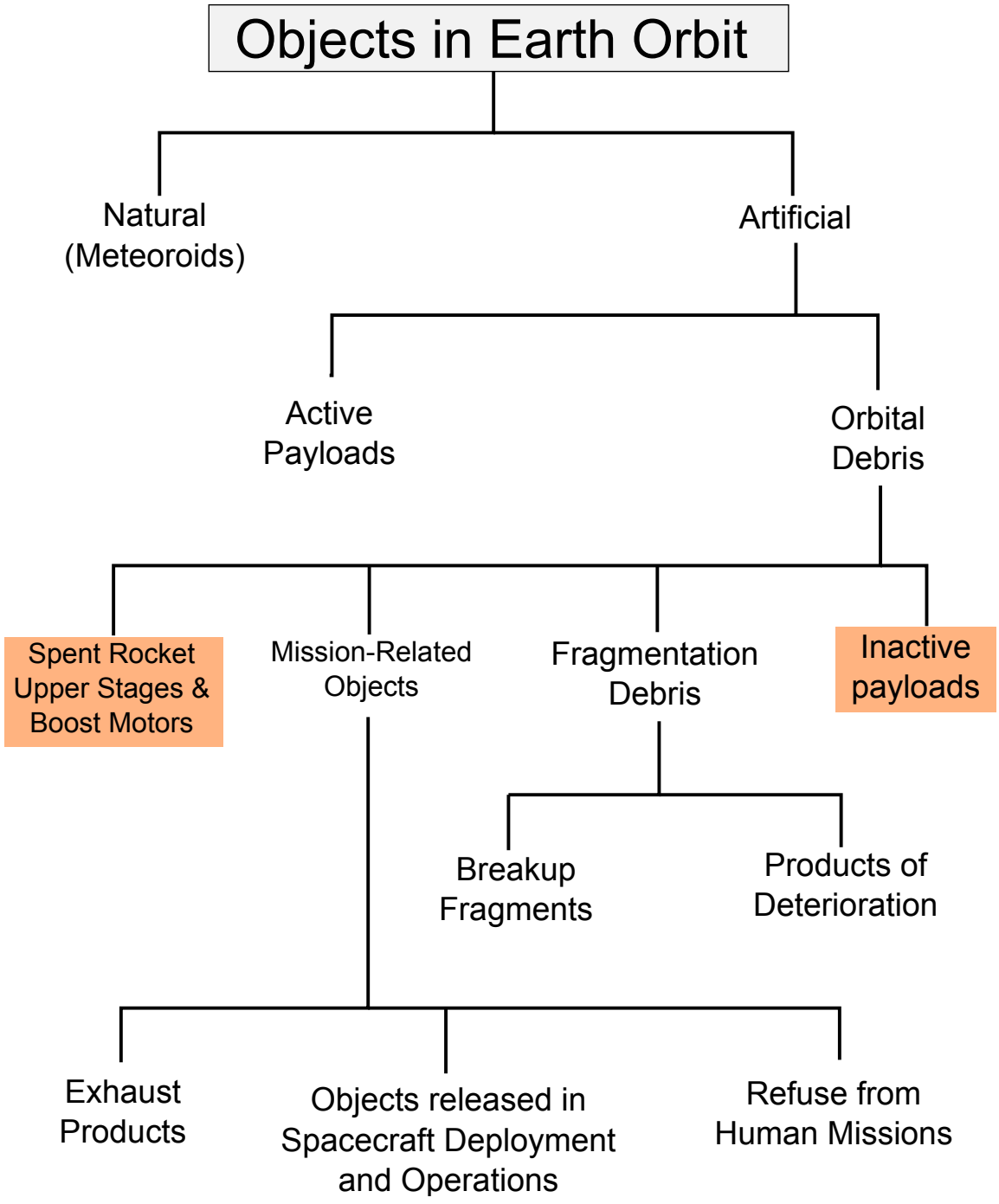

Figure 1.1: *Classification of objects in Earth orbits. Highlighted in orange boxes are the elements that need deorbit capability implementation.*

The graph posted next in this page shows the amount of debris for each main category

of debris type. It is interesting to note that only 6% is made of active payloads, and that most of debris come from fragmentation events, i.e. 40% of the total. Inactive payloads and spent rocket stages, that already amount to 44% of LEO cataloged objects population, are the two categories of objects whose abandonment in space can be avoided in future missions, once deorbit systems are finally implemented onboard new LEO satellites before launching them. Solutions have been proposed in literature also for deorbit of massive objects that are already in space, without deorbit system onboard; however, this is not a topic of this thesis, so it is suggested to refer to open scientific literature for additional information about this.

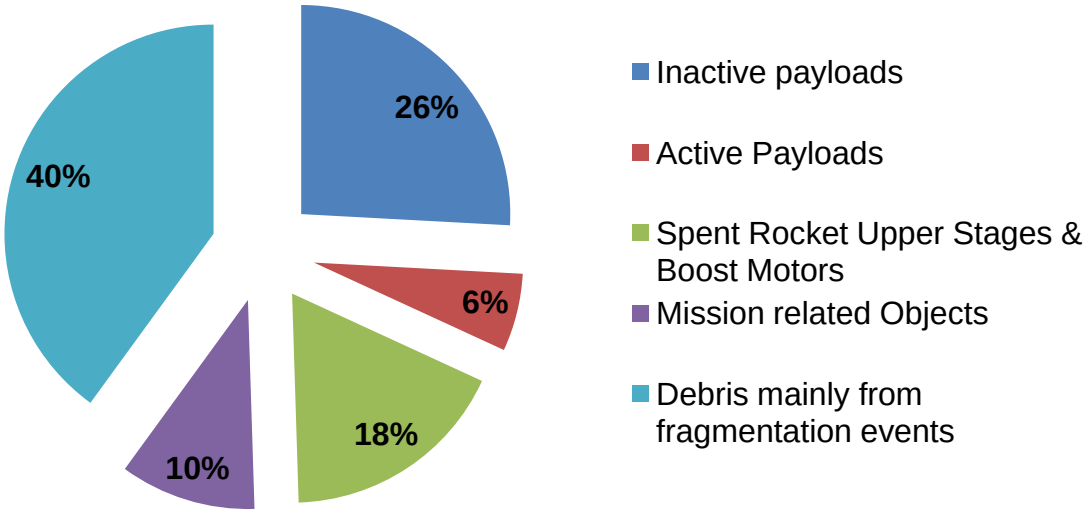

Figure 1.2: *All cataloged space objects, classified by object type, as of January 2002. Values from Ref.[23].*

Since the start of space activity in the late '50s, the debris population showed a constantly increasing trend, as shown in the following diagram.

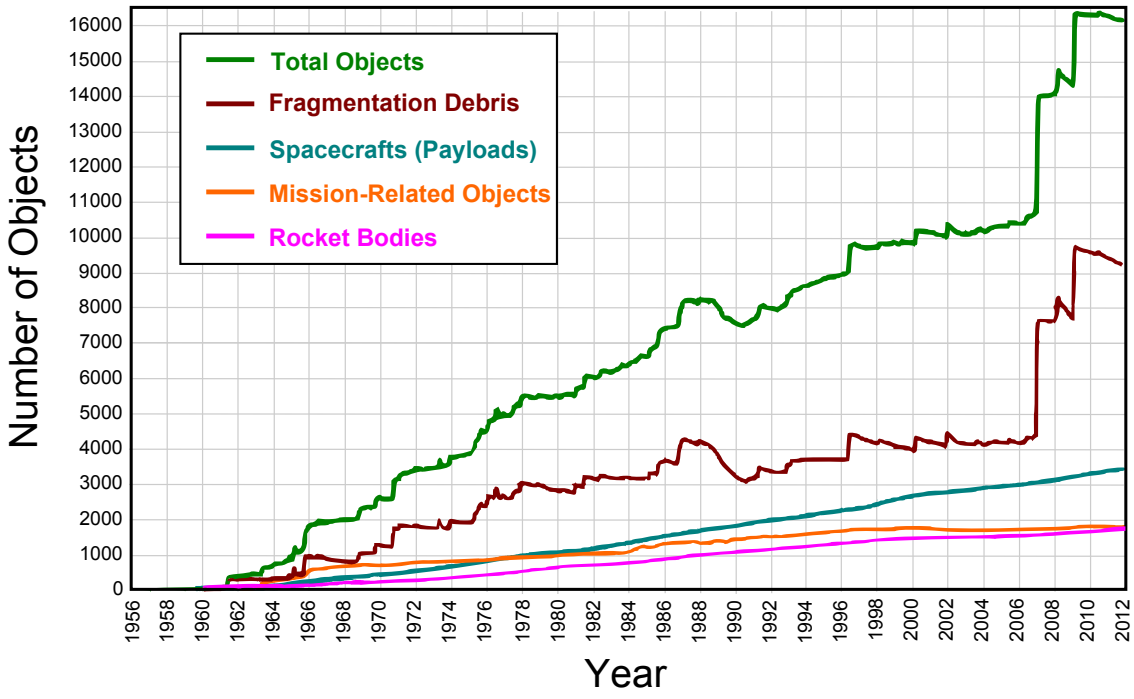

Figure 1.3: *Evolution in number of artificial cataloged objects in space, from 1956 to 2012.*

This trend increased mainly due to the fact that any man-made object, launched to any terrestrial orbit, was left in space at the end of its life. Large objects like inactive satellites and upper stages are the main potential source of debris propagation, due to their large cross section that makes them statistically the most likely objects to be involved in a collision event. In case of collision, their mass is so high that thousands of new debris can be generated, covering a broad spectrum of sizes. Unfortunate recent occurrences practically prove this fact. An example is the collision between a defunct Russian communication satellite, *Cosmos 2251*, with an operational Iridium spacecraft in February 2009, resulting in nearly 2000 new trackable objects and, most likely, tens of thousands of smaller, but still very dangerous, fragments.

In cascade, any collision determines an increase in debris population density and augments the probability of subsequent additional collisions. In fact, as displayed in Fig.[1.2], the vast majority of cataloged orbital debris is made of fragments from collisional events. This is the reason why, in order to limit, in the short term, the increase in debris population, and to decrease it, in the long term, the most effective measure to take is the removal of any future satellite and spent stage after its end of life.

The focus of this work is cast upon the LEO region, given that, as shown in the image below, it is the region of terrestrial orbits that shows, to a large extent, the highest density of debris. LEO orbits are conventionally considered as any orbit constrained in the approximate altitude range between 200 km to 2000 km.

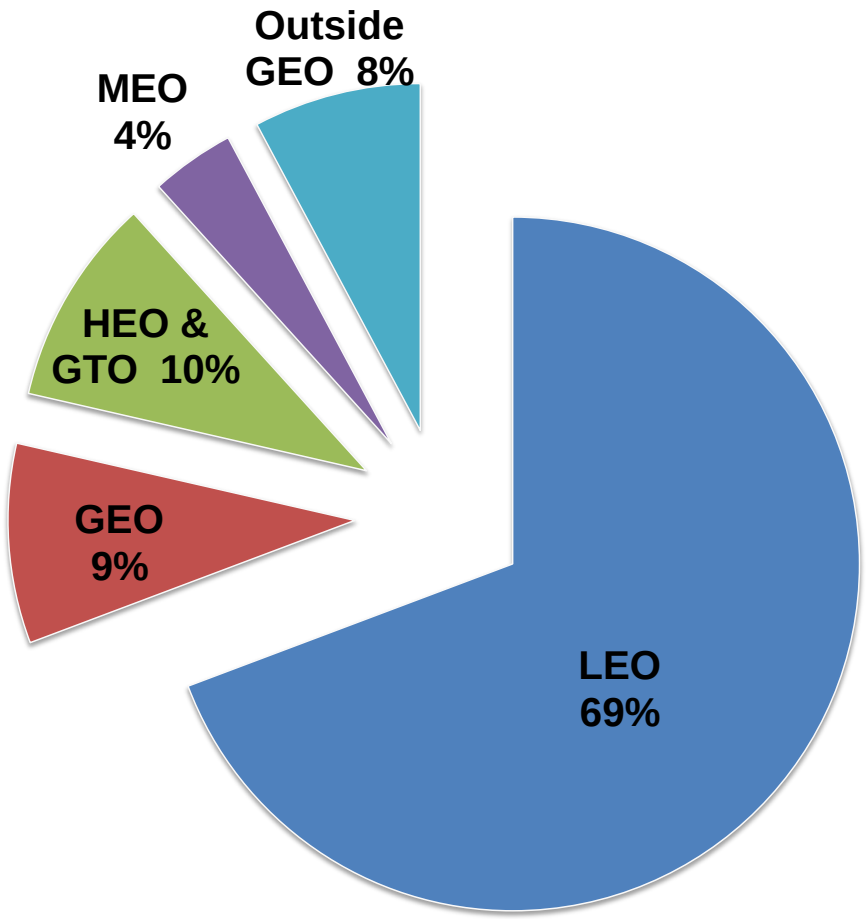

Figure 1.4: *All cataloged space objects, classified by orbital region, as of January 2002. Values from Ref.[23].*

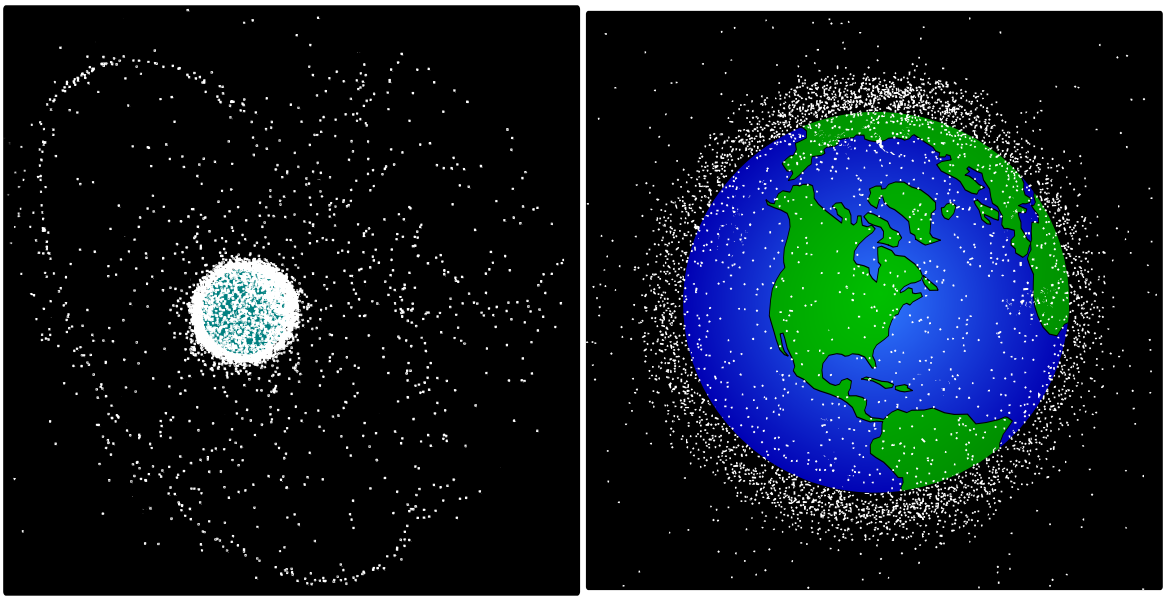

Figure 1.5: *On the left: View of debris in all terrestrial orbits. On the right: View of orbital debris in LEO region (based on image from pg. 4 of Ref.[22], with data from NASA Orbital Debris Program Office, 2007).*

The peak in space cataloged debris with characteristic diameter larger than 10 cm is around an altitude of about 900 km and with inclinations around 83°. There are other significant peaks in debris density near 800 km and 1400 km of altitude. As shown in the histogram below, the number of objects with perigee altitudes lower than 600 km is indeed limited with respect to the total number (about 10–15% of the total of LEO catalog objects). Consequently, a special attention must be directed towards orbits between 600 km and 1500 km.

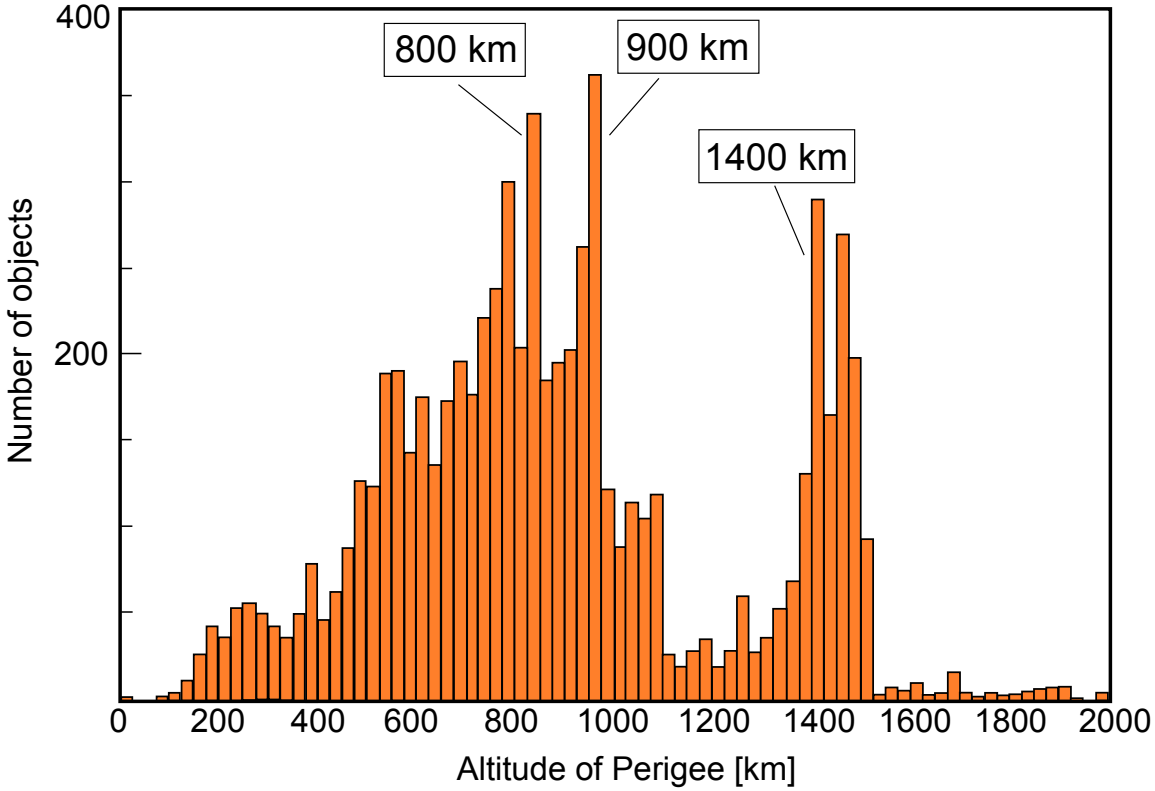

Figure 1.6: *Histogram reporting the number of catalog objects in LEO orbits, at every perigee altitude. Peaks in number of objects are located at approximate altitudes of* 800 km, 900 km *and* 1400 km, *with the highest concentration at* 900 km. *Data updated to June 2003. Every column in the histogram spans a perigee altitude range of* $\Delta h_{pe} = 25$ km. *Values from Ref.[23].*

It is also important to point out that the largest number of catalog objects, orbiting around the Earth, has a very low, close to zero, orbital eccentricity. Refer to the image posted below.

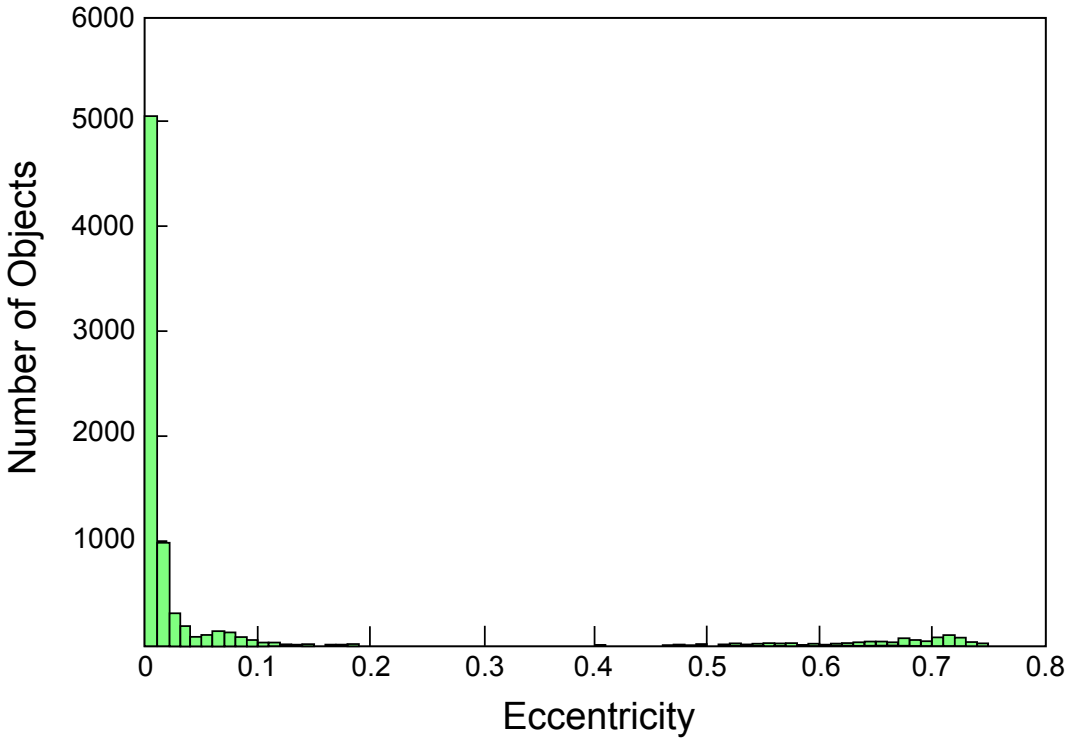

Figure 1.7: *Histogram reporting the number of catalog objects, as of June 2003, for each value of eccentricity. The single class of the histogram spans an eccentricity range of* $\Delta e = 0.01$. *Values from Ref.[23].*

From the orbital inclination standpoint, the number of orbital debris is maximum at approximately 65°, 74°, 83° and 98° (this last inclination is associated to the cluster of satellites in Sun-Synchronous orbits). The peak density is around 83°.

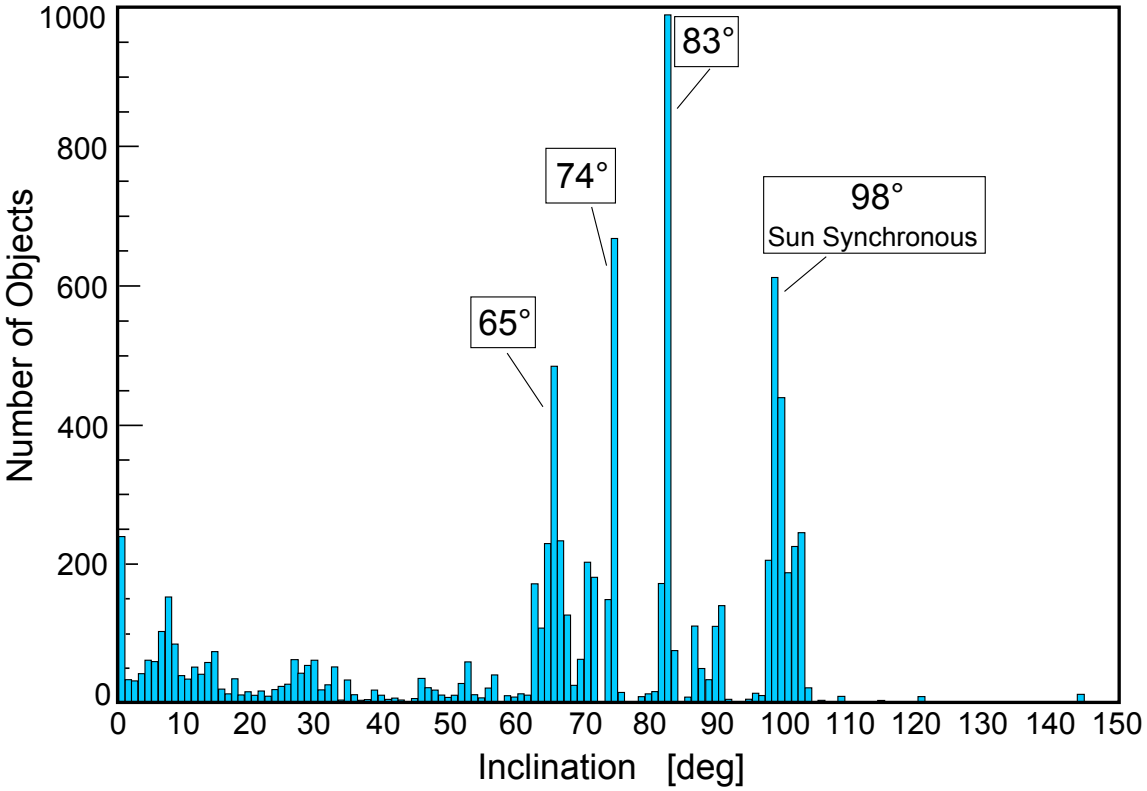

Figure 1.8: *Inclination distribution of cataloged debris population, as of June 2003. Peaks in number of objects are found at approximate inclinations of* 65°, 74°, 83° *and* 98° *(Sun-Synchronous orbits), with the absolute peak at* 83°. *Values from Ref.[23].*

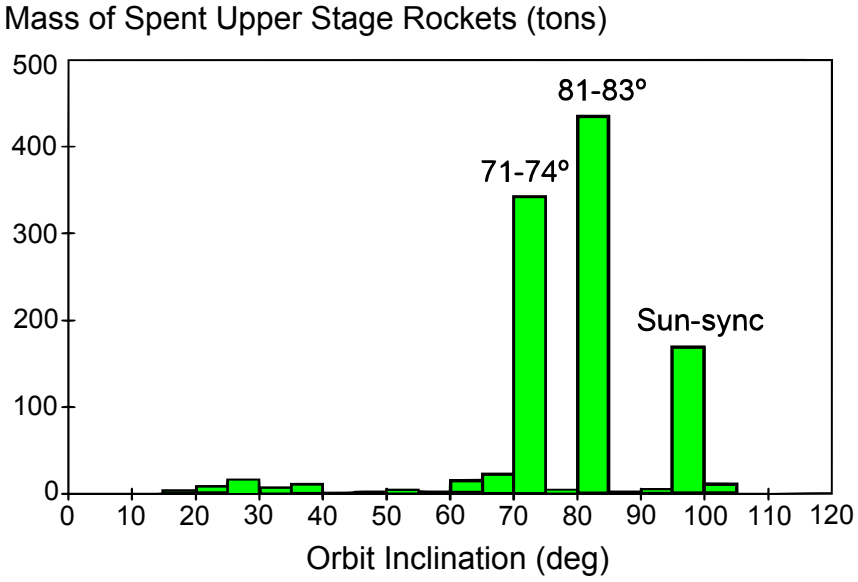

Figure 1.9: *Histogram reporting the number of spent upper stages with respect to orbital inclinations. Values from Ref.[24].*

Another very useful diagram is posted below, showing the density of objects with characteristic diameter higher than 10 km, only in the LEO region, with respect to both variable inclination and altitude.

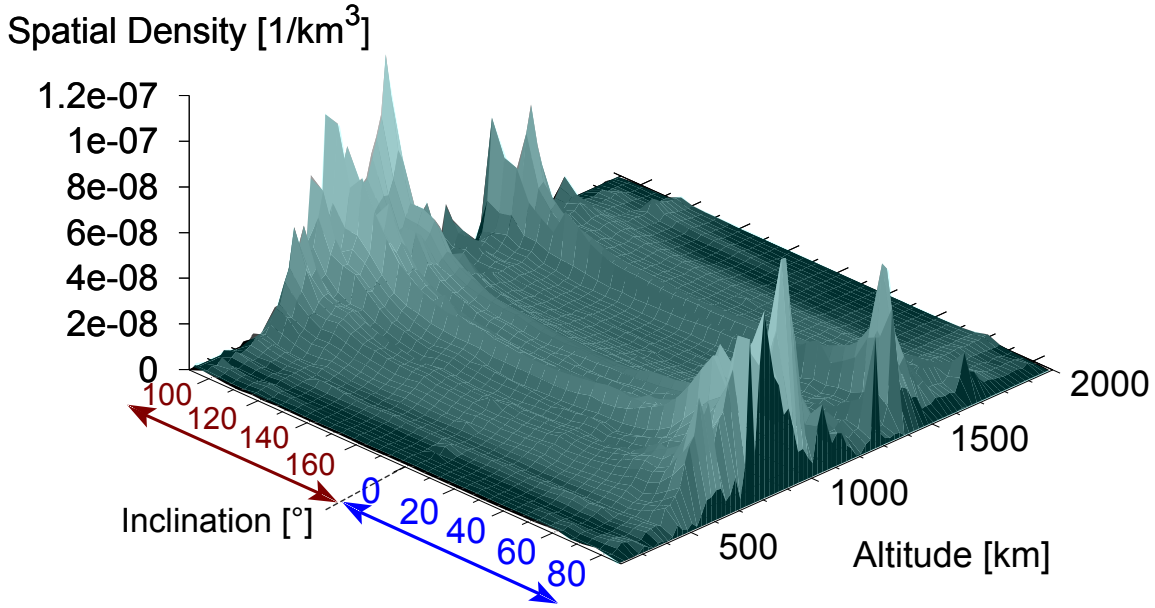

Figure 1.10: *3D diagram showing the spatial density, at different altitudes and inclinations, of objects in LEO with characteristic diameter* > 10 cm. *This threshold means that satellites and spent stages (targets for deorbit implementation) are all included in this diagram; instead, small to very small debris, for which deorbit procedures do not apply, are excluded from this diagram. Values from Ref.[23], according to the MASTER-2001 model, for May 2001.*

From the MASTER-2001 model, as displayed in the diagram above, it turns out that the peak densities in LEO region are found at inclinations of about $i = 82°$ and $i = 98°$ (with a secondary peak at 65°), combined with average altitudes $\bar{h} \approx 900$ km and $\bar{h} \approx 1400$ km.

1.2 Introduction to Debris Mitigation strategies

Two very different scenarios can be defined regarding procedures at the end of operational life of every artificial object launched to space:

- **Business-As-Usual** scenario, i.e. no implementation of any debris mitigation measure on future space missions.
- Scenario with **Implementation of Debris Mitigation Measures** on future space missions

Propagating the *Business-As-Usual* scenario for 100 years, starting from year 2000, the number of objects with diameter d larger than 1 m, in LEO orbits, would increase

fourfold. In the propagation, it is considered the annual trend of launches of new objects in LEO orbits, plus a typical annual rate of fragmentation occurrences in orbit. From approximately 2000 objects with $d > 1\,\mathrm{m}$ in year 2000, it would be reached a number of about 8000 objects with $d > 1\,\mathrm{m}$ in year 2100. Moreover, the expected number of catastrophic collisions in LEO orbits during the 100 years would be higher than 50. Consequently, in this scenario there will be a steep growth of massive objects and even higher increase of smaller debris, leading in year 2100 to a number of about 50000 objects in LEO with $d > 10\,\mathrm{cm}$ (with respect to the current 10000, hence a five-fold increase), and a number of about 1.6e+06 objects with $d > 1\,\mathrm{cm}$ (with respect to the current number of about 3e+05, thus again an approximately five-fold increase).

Mitigation strategies have been laid out with the aim of solving the debris problem in the long-term. These strategies are:

1. Collision avoidance and shielding technology
2. Reorbiting inactive satellites to storage orbits. For spacecrafts at altitudes higher than LEO, moving them into disposal orbits can be an effective measure, in the short term, to reduce risk of collision.
3. *Passivation* of spacecrafts and upper stages. End-of-Life *Passivation* consists in a series of measures aimed to prevent explosions on orbit: expulsion of residual propellants by burning or venting, discharge of electrical storage devices, release of pressurized fluids, unloading of momentum wheels or other attitude control devices. *Passivation* became a requirement only at the beginning of the '80s and therefore all upper stages and spacecrafts launched before then represent a significant explosion hazard, and their number is very significant. By mid 2004, there were 2780 rocket stages in LEO orbits: 25% of these (thus about 700 rocket bodies), they were launched before 1982 and therefore are surely not *passivated*. *Passivation* today is a standard procedure and it will lead to a reduction of critical-size objects with $d > 10\,\mathrm{cm}$ by almost 50% from year 2000 to year 2100. The same decrease, in percentage, will occur, through *passivation*, for all objects with $d > 1\,\mathrm{cm}$.
   Nonetheless, while the absolute growth of potentially hazardous objects is reduced, the increasing trend of objects in LEO is maintained, revealing the fact that End-of-Life *passivation* is a necessary but not sufficient condition to ensure a progressively safer space environment in the future.
4. It has been demonstrated that the most effective mitigation measure is the removal of mass, with priority for objects with mass higher than 100 kg (hence spent rocket bodies and inactive satellites), especially from orbital regions with high debris densities. Regulations from different space agencies all agree on 25 years as the maximum time for deorbit. In fact, even in the worst case of all deorbits lasting for 25 years, the debris problematic situation would be consistently healed over a 100 years time span, as shown in the graph below.

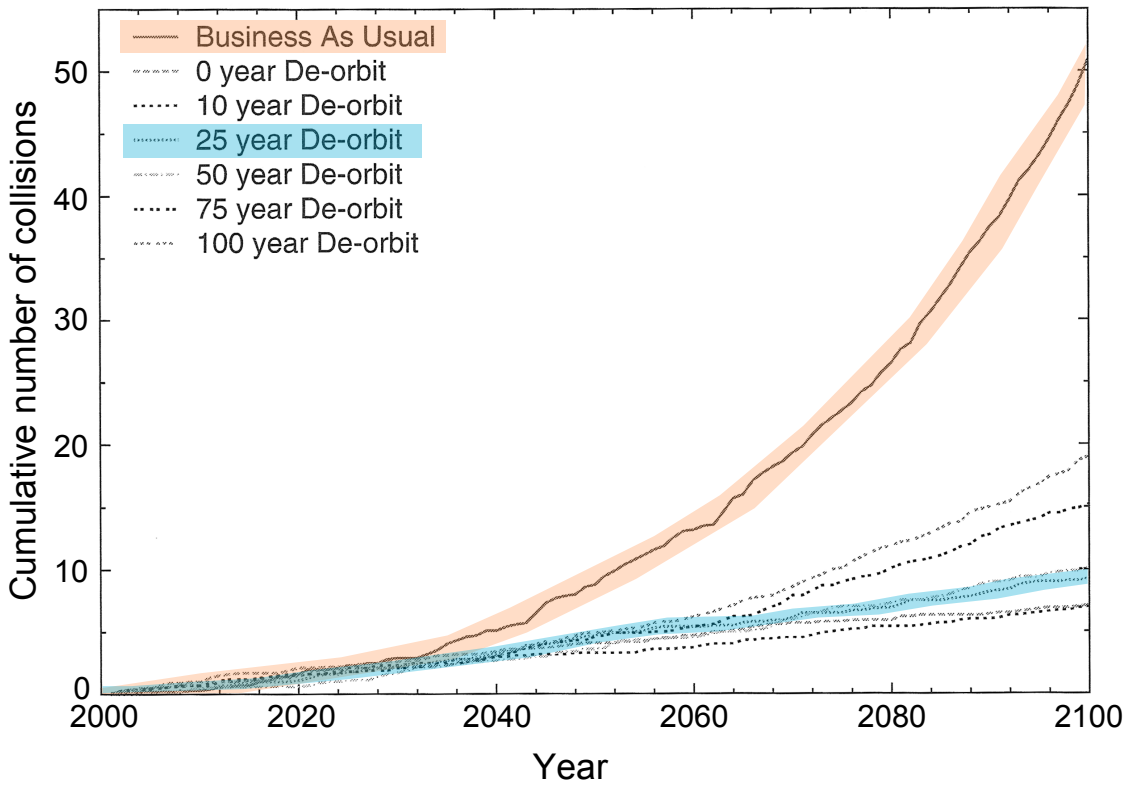

Figure 1.11: *Evolution of cumulative number of catastrophic collisions in LEO region, over 100 years starting from year 2000. Different curves allow comparison between* business-as-usual *scenario, and scenarios with mitigation measures plus deorbit of inactive payloads. Different curves are computed, in case of* debris mitigation *scenario, for different deorbit times.*

The diagram above underlines these important facts:

- In any *debris mitigation* scenario, even for extremely long deorbit times like 100 years, the number of collisions would significantly decrease over a 100 years time span
- For deorbit times lower than 25*years*, being the extreme case the direct deorbit (0 years curve in the picture), the cumulative number of collisions after 100 years is only very slightly minor than the cumulative number with a 25 years deorbit time. Between the *Business-as-Usual* scenario and the 100 years deorbit scenario, there is a difference in cumulative number of collisions, at the end of the 100 years time span, of more than 30. Instead, between the 25 years deorbit and 0 year deorbit, there is only a much smaller difference of about 3 collisions. This explains why 25 years has been selected as optimal maximum deorbit time by the major international regulations regarding debris mitigation. Choosing 25 years, instead of direct deorbit, allows to significantly reduce the cost burden and technological effort of deorbit, especially for satellites located at altitudes higher than 500 km. In fact, the LEO region above 500 km is the most densely populated region (approximately 90% of all LEO spacecrafts are orbiting above

500 km). Deorbit of satellites at initial altitudes lower than 500 km represents a much less challenging task: *direct* deorbit using *chemical propulsion* or even *natural decay* are expected to be the optimal choices. Actually, bodies orbiting with perigee altitudes below 500 km will generally always have *natural* orbit lifetimes lower than 25 years, i.e. only through dissipative aerodynamic drag they will decay in that maximum time and will, therefore, automatically satisfy the mitigation guideline. The 25 years guideline will have the greatest impact on programs with mission orbit perigee altitudes above 600–700 km, where objects may remain in orbit hundreds, or even thousands, of years if abandoned at the end of mission life. Refer to Fig.[2.1] and Section [2.1] for further description of deorbit by *natural decay*.

1.3 International Guidelines on Orbital Debris Mitigation

As reported in Ref.[23], [22], [1], the debris mitigation guidelines from *NASA*, *US Government*, *ESA*, *CNES*, *EDMS*, and *JAXA*, they all set **25 years** as maximum time for re-entry of any object in orbit, after its operational life, in case it is not economically convenient a direct retrieval, and in case it is chosen to avoid re-orbiting to orbits above the LEO region.

NASA Guidelines and Assessment Procedures for Limiting Orbital Debris (Ref. [1]) deals with "Postmission Disposal of Space Structures" from pg. 6-1 to pg. 6-9. Quoting the guideline:

> *"The 25-year removal time from LEO prevents the debris environment from growing over the next 100 years while limiting the cost burden to LEO programs. Spacecraft and upper stages in mission orbits with perigee altitudes below 600 km will usually have orbit lifetimes less than 25 years and will, therefore, automatically satisfy this guideline. This guideline will have the greatest impact on programs with mission orbit perigee altitudes above* 700 km*, where objects might remain in orbit hundreds of years if abandoned at the end of mission life"*

For more massive objects that might survive re-entry, the guidelines prescribe a *controlled re-entry*. The NASA guideline also sets 10 years as maximum allowed time in case of planned retrieval, i.e.in any case in which the satellite during deorbit is traveling across valuable regions of space. Consequently, the 25 years constraint must be interpreted as a general maximum constraint. However, it is highly desirable, in order to minimize risk of collision with other bodies, to reduce as much as possible the Are-Time Product of the object during deorbit. This means that the best deorbit system would be the one that leads to both minimum deorbit time and minimum collisional cross-sectional area; however, it also needs to limit as much as possible the additional mass and consequent cost of implementation.

Chapter 2

Description of different deorbit systems

2.1 Natural Decay

Natural decay of an object in orbit is is governed by *aerodynamic drag*, that is the only dissipative force constantly acting on the body.
As shown in the following picture, deorbit time, when opting for *natural decay*, depends mainly on the following parameters:

- initial deorbit altitude, i.e. altitude at the end-of-life of the orbiting body. The higher is the altitude the lower is atmospheric density, with exponential decrease: therefore, deorbit times rapidly diverge to extremely high values for initial altitudes higher than 500–600 km.
- ratio between a *characteristic drag area* and mass, A/m. The cross-sectional drag area of a satellite depends on the instantaneous attitude of the satellite: with deorbit by *natural decay* attitude cannot be controlled since satellites are generally completely inactive, therefore the attitude control system is normally not functioning anymore. Hence, an average drag area must be used for simulation of such type of deorbit. Of course the larger is the ratio between average drag area and mass, the lower is deorbit time.
- Solar Flux during deorbit time. In fact, a higher solar flux leads to higher local atmospheric density, at any altitude and inclination. As consequence, a denser atmosphere determines a greater drag force and lower deorbit time.

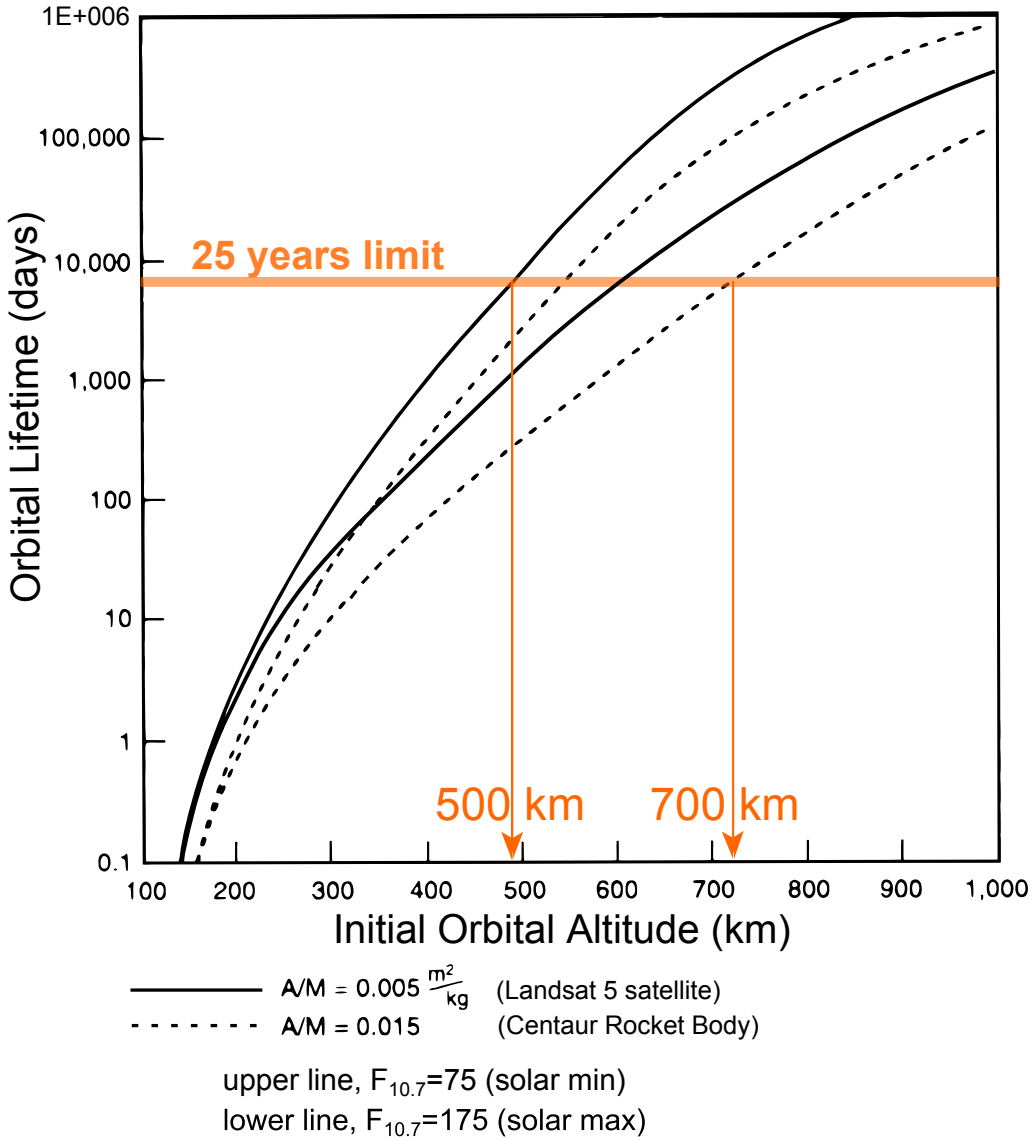

Figure 2.1: *Natural orbit decay time versus initial altitude. Two distinct curves, but with the same line type, are computed for maximum and minimum solar flux. Two extreme cases are shown for satellites: one with very low A/m ratio, i.e. drag area low with respect to mass (the worst condition for natural decay); the second with very high A/m ratio (best condition for natural decay). As shown in the diagram, natural decay exceeds the limit of* 25 *years, for initial altitudes in the range between about* 500 km *and* 700 km. *Data from Ref.[11].*

Natural decay is a viable option only when it is demonstrated that the features of the satellite and the initial orbital parameters are such that a deorbit time lower than the 25 years time constraint is surely achieved. From the diagram posted above, it is possible to conclude that, for initial orbits higher than 700 km, it is practically sure that a standard satellite will take more than 25 years for *natural decay*. Consequently, above 700 km *natural decay* is never an acceptable solution for deorbit. However, even for

orbits higher than 500 km, it is very improbable for *natural decay* to be a considerable option.

Only 10% , as rough estimate, of all cataloged objects have altitudes of perigee lower than 500 km (refer to Fig.[1.6]). *Natural decay* can then be an acceptable solution only for a very small portion of all satellites in LEO. However, it is important to note that *natural decay* can be used in sequence after a first deorbit phase with an active or passive deorbit system, mounted onboard, that lowers the orbit to an altitude from where *natural decay* ensures compliance with the 25 years guideline.

2.2 Deorbit with *Chemical Propulsion (CP)* system

Deorbit using *Chemical Propulsion* is classified as a *direct* deorbit method, inasmuch as the time of reentry is very short, the shortest among all the different deorbit solutions. *Direct deorbit* means that the satellite is inserted, through a single burn, with thrust exerted opposite to the satellite's orbital motion, into an elliptical *Hohmann transfer orbit*: a decrease in orbital velocity takes place in order to inject the spacecraft, from the initial circular orbit, into the transfer orbit. The insertion takes place at the apogee of the transfer orbit (point A in Fig.[2.2]) and the perigee of this transfer orbit is intentionally so low (normally at an altitude around 80 km, and with a reentry angle of about $-5°$) that no perigee burn is required. In fact, once the satellite reaches altitudes lower than 120 km, it encounters atmospheric densities so high that they rapidly decrease the velocity of the spacecraft, "capturing" it, and burning it out in the atmosphere. The absence of a perigee burn allows to consistently reduce the amount of propellant required for deorbit.
Chemical propulsion is expected to be an excellent solution for lower LEO orbits and for lower mass satellites. The higher is the mass of the satellite to deorbit and the initial deorbit altitude, the higher is the mass of propellant required to insert the satellite into the transfer orbit. For particularly massive bodies, that are expected not to burn out completely in the atmosphere, a *controlled reentry* is necessary.

One aspect that makes *Chemical Propulsion* a good competitor of other systems is that normally every spacecraft has already a chemical propulsion system onboard, e.g. the thruster used for the last orbit injection burn or thusters used for attitude control (see Ref.[38] pg.371). In particular these last ones generally use *Hydrazine monopropellant*, that is the ideal choice for deorbit, given that it is a propellant that can be stored for a long time. Consequently, the additional mass for deorbit, when using *chemical propulsion*, would be only the additional propellant (and extra tanks or larger tanks), not the "dry" hardware mass, since it is already part of the mission payload.

A potential negative aspect of deorbit via CP is that a very large mass of propellant has to remain onboard during the entire operational life. This means that, in case of

impact with meteoroids or debris, the outcome is devastating if the impact involves the propellant tank, causing the generation of thousands of new debris. On the positive side, it has to be said that the risk of collision during deorbit is extremely low, due to the lowest ATP among all the different deorbit solutions (since the both deorbit time and collisional cross-sectional area are minimum using CP).

The major problem of CP, with respect to other systems, is expected to be the very high additional mass of propellant required, in case of orbits with higher initial altitudes. Above a certain altitude, the additional mass might become unsustainable, and make the CP a non optimal solution.

In literature, it was proposed to alleviate the problem of high additional mass by performing a *partial* deorbit, instead of a *full direct* deorbit. This means to implement, instead of direct re-entry with a Hohmann transfer orbit to an altitude of about 80 km, to lower the spacecraft to a final higher altitude, e.g between 200 to 500 km. In any case, it must be an altitude such that the satellite would surely complete its re-entry, by *natural decay*, in a time lower than the 25 years maximum. This solution, anyhow, shows problems too, as will be described in Sec.[3.9.3], with results from analysis at hand.

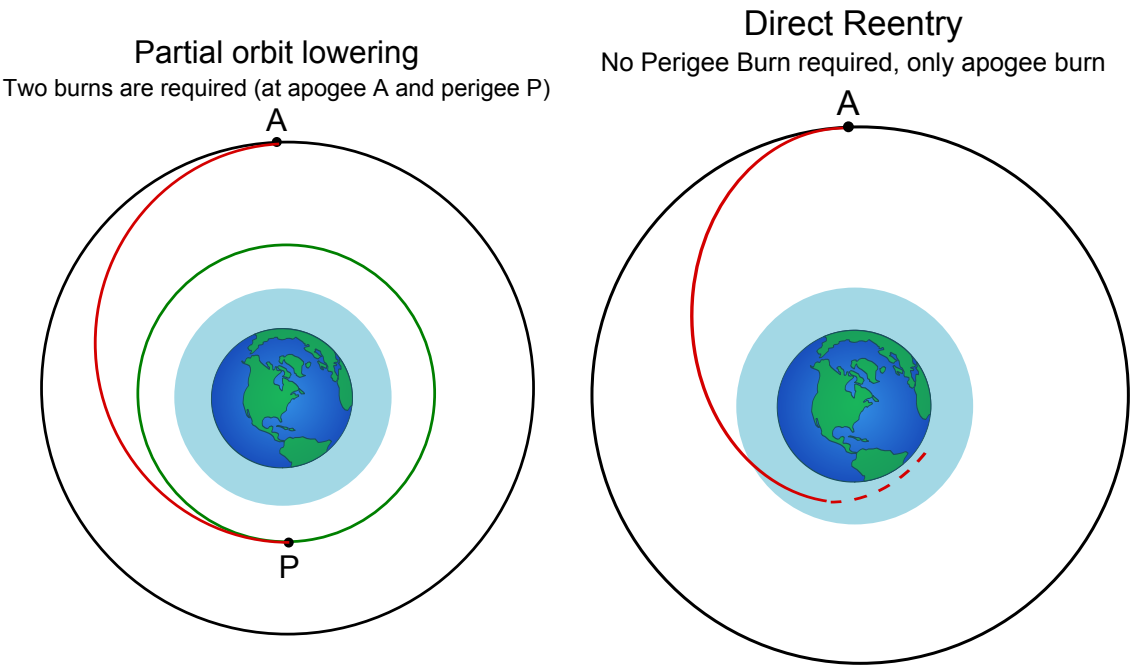

Figure 2.2: *Types of re-entry with* Chemical Propulsion *deorbit system. On the left:* partial *deorbit along an Hohmann transfer orbit with perigee higher than about* 130 km*. In this case the orbit is only partially lowered, therefore both apogee burn and perigee burn are required unless it is left the satellite orbiting in the Hohmann transfer orbit. On the right:* direct *deorbit, along an Hohmann transfer with perigee normally between* 80 *to* 100 km *and angle of reentry of about* $-5°$ *in order to ensure the "seizure" of the satellite by Earth's atmosphere without need of a perigee burn.*

H [km]	Δv [m/ s]	$\Delta m_p/m_0$ [%] for chemical propulsion systems			
		N_2H_4	solid motors	N_2H_4/ N_2O_4	LOX/ LH
200	35.9	1.65	1.30	1.17	0.83
300	65.0	2.97	2.34	2.11	1.49
400	93.3	4.23	3.34	3.02	2.14
500	120.8	5.44	4.30	3.90	2.76
600	147.7	6.61	5.23	4.74	3.36
700	173.9	7.74	6.13	5.56	3.95
800	199.4	8.83	7.00	6.35	4.51
900	224.3	9.87	7.84	7.11	5.06
1000	248.6	10.88	8.65	7.85	5.60
1100	272.3	11.85	9.44	8.56	6.11
1200	295.4	12.79	10.20	9.26	6.61
1300	317.9	13.70	10.93	9.93	7.10
1400	339.9	14.57	11.64	10.58	7.57
1500	361.5	15.42	12.33	11.21	8.03
1600	382.5	16.24	13.00	11.82	8.48
1700	403.0	17.03	13.65	12.41	8.91
1800	423.0	17.80	14.27	12.99	9.34
1900	442.6	18.54	14.88	13.55	9.75
2000	461.8	19.26	15.47	14.09	10.15
I_{sp} [s]		220.0	280.0	310.0	440.0
u_e [m/ s]		2,158	2,747	3,041	4,316

Figure 2.3: *Table with requirements for direct deorbit using different chemical propulsion systems. Deorbit starts from an initial circular orbit at altitude H, reported in the first column, and takes place along an elliptical transfer orbit with apogee at the initial altitude, and perigee at altitude $H_{pe} = 80\,\text{km}$. In the second column it is reported the required difference of velocity Δv at initial deorbit altitude (the apogee burn opposite to direction of motion). For every initial altitude, properties of different CP systems are posted: specific impulse I_{sp}, exhaust velocity u_e, propellant mass fractions (in percentage) $\Delta m_p/m_0$ where m_0 is the spacecraft's initial mass (including propellant mass Δm_p used for deorbit). Data of the table from Ref.[23]*

Referring to the table above, these important facts are to be highlighted:

- the best performing CP system would be the *Liquid Oxigen/Liquid Hydrogen* system (LOX/LH). The problem is that such propellants must be stored at cryogenic temperatures. Therefore, this system could never be used onboard a spacecraft, at its end-of-life, after years of operation. This solution has then to be removed as a non feasible option. This is why the values in the last column are crossed.
- A second option is the *Hypergolic Bi-propellant* system, with Hydrazine (N2H4) and Dinitrogen Tetroxide (N2O4) that form a self-igniting mixture. The bi-propellant system provides better performance that the monopropellant, but would imply an increased complexity of the hardware and higher inert mass (for example, at least one additional storage tank would be necessary). This choice would be then considerably more expensive, and consequently not optimal for deorbit.

- *Solid Propulsion* system is another considerable option, but it has a much lower reliability for deorbit application after years of onboard storage. In fact, combustion of a solid grain, after ignition, cannot be controlled; moreover, the grain would remain stored in the harsh space environment for years, so its performance and integrity might be compromised. In case of any problem with combustion, there is no possibility to turn the motor off other than venting the combustion chamber, losing then the possibility of deorbiting since the combustion cannot be restarted. There is of course also the risk of explosion, that would lead to thousands of new debris.
- Eventually, the best option, were CP used for deorbit, appears to be the *Hydrazine monopropellant* system (the yellowed column in the table). In fact, this system has a very strong heritage onboard spacecrafts during their entire operational life, and is then surely proven to be reliable for long term storage and usage in space. For instance, it is normally used for onboard attitude control thrusters. Unfortunately, this is also the solution that requires the highest propellant mass fraction. For example, in order to directly deorbit a 1000 kg satellite, from an initial altitude of 1000 km, about 122 kg of hydrazine would be required.

It is important to point out that the mass fraction f in the table is expressed in percentage, and that $m_0 = m_p + m_{sc}$. m_{sc} is the "dry" mass of the spacecraft, and m_p is the mass of propellant required for direct deorbit, i.e. for the single apogee burn. The propellant mass fraction $f = \Delta m_p/m_0$ from the table, divided by 100, is then:

$$f = \frac{m_p}{m_{sc} + m_p} \tag{2.1}$$

and consequently m_p can be computed as:

$$m_p = m_{sc}\frac{f}{1-f} \tag{2.2}$$

In the previous equation, the inert mass (i.e. the hardware) of the propulsion system is already included in m_{sc}, inasmuch as it is part of the spacecraft's payload used during operational life. To be precise, the only inert mass that should not be included in m_{sc} is the extra mass of the larger (or additional) propellant tanks to store the surplus of propellant required for deorbit. Anyhow, this inert mass is extremely lower than the additional mass of propellant, so it can surely be neglected in the analysis.

For comparison with the values of the table in Fig.[2.3], it is also reported below a diagram from Ref.[11] (pg.146).

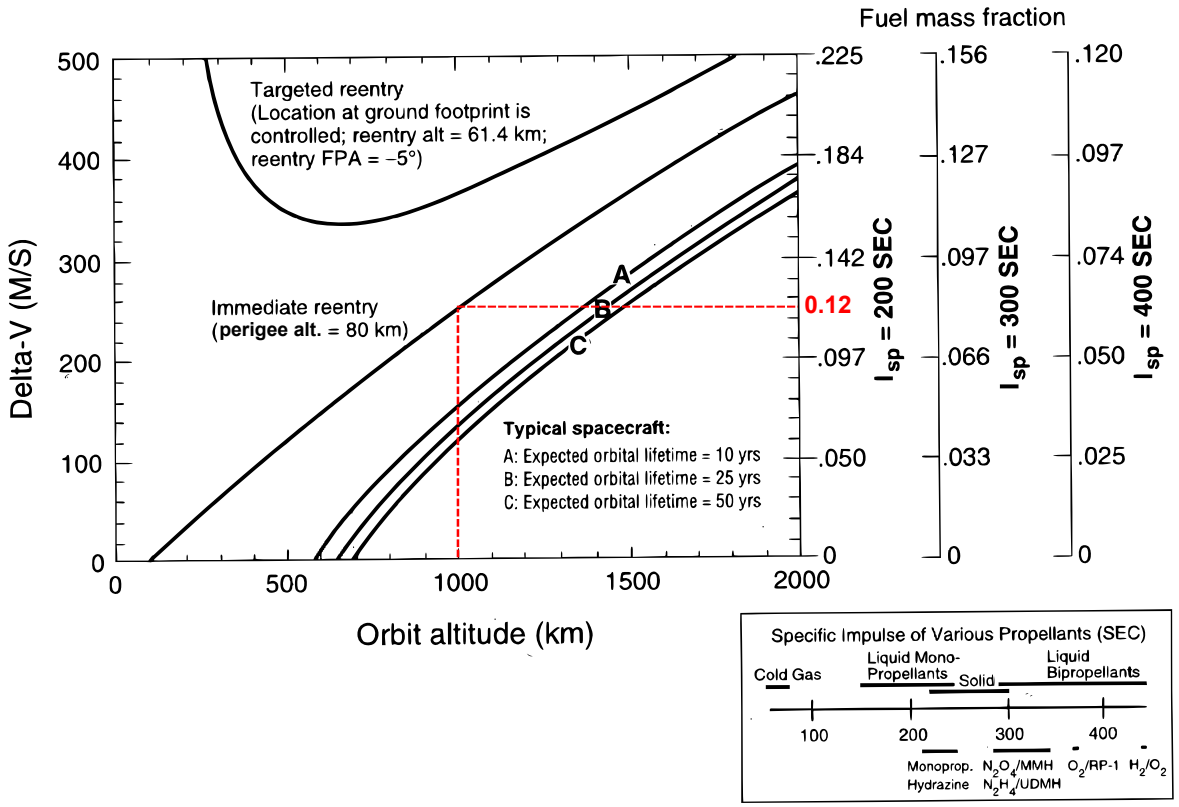

Figure 2.4: *Delta-V requirements and propellant mass fraction for disposal using Chemical Propulsion from initial circular orbits. Curves are computed for a satellite of cross-sectional area to mass ratio equal to* $0.01\,\frac{\mathrm{m}^2}{\mathrm{kg}}$ *and Solar activity index* $=$ $130\,\mathrm{SFU}$. *Source of data:* NASA/Reynolds. *For comparison with values from the previous table in Fig.[2.3], consider the curve for immediate reentry (with elliptical orbit with perigee altitude of* $80\,\mathrm{km}$*), initial altitude of* $1000\,\mathrm{km}$*, and Liquid Monopropellant with* $I_{sp} = 200\,\mathrm{s}$. *With these conditions, the diagram returns a value of approximately* 0.12 *for propellant mass fraction, value that is absolutely comparable with the propellant mass fraction of* 0.1088*, from the previous table, with the same deorbit conditions.*

The burning time of the *chemical propulsion* system, used at the apogee of the transfer orbit, is very short with respect to deorbit time. Therefore, it must be ensured the correct attitude of the satellite only during this very short initial time, not for the entire deorbit (that is, anyhow, very fast, being a direct deorbit). When deorbit starts, the satellite is at its end-of-life; consequently, there might be problems of attitude control system not functioning anymore, or without power to work, in case of active control systems. Each case must be then evaluated specifically: in the worst (unprobable) case of both no power sources available anymore and failed attitude control components, in the mass for deorbit also additional attitude control components and a battery to provide the required power (for a short time) must be included.

2.3 Deorbit with *Electrical Propulsion (EP)* system

Historically, *Electrical Propulsion* has been used, as reported in Ref.[19] at pg. 3, mainly for deep-space missions or for station keeping of Geostationary satellites. This last category is generally made of communications satellites whose antennas must be constantly pointed towards a specific ground station: hence, they need a continuous attitude control during their operational life.

This implies that LEO satellites generally do not have an EP system onboard. Therefore, the additional mass of the deorbit system, when using EP, is not only the mass of propellant, but also the mass of every hardware component of the EP system (such as mass of propellant tanks, mass of the thruster, mass of the power unit for the thruster, etc.). This inert mass will then be accounted as additional mass required for deorbit, when comparing different deorbit systems in Section [3.9].

Typical features of EP are much longer time of re-entry with respect to chemical propulsion, high I_{sp}, but very low thrust levels (again with respect to chemical propulsion). In fact the longer times to deorbit are specifically due to the low thrust, exerted by these systems against the satellite's motion, in order to progressively decrease its orbital velocity and consequently its altitude. The satellite would then re-enter along a "spiral" path.

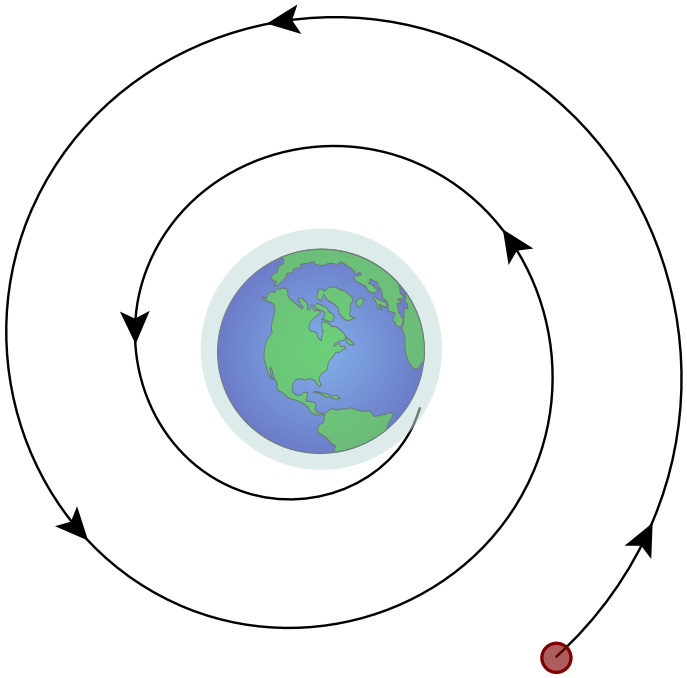

Figure 2.5: *View of a typical deorbit path of a satellite, when using* Electrical Propulsion *for deorbit*

Ion and *Plasma Thrusters* are the best performing solutions, but they should be avoided since they are generally too expensive to be used for deorbit. *Hall Thrusters* are, instead, the best option among the family of EP systems. They represent the optimum compromise between minimizing cost and achieving sufficient performance. More specifically, the Russian *SPT Hall Thrusters* are considered, whose features are listed below (further description at Ref. [34], [19] pg. 441, [26] pg.14).

Parameter	SPT-50	SPT-70	SPT-100	SPT-140
Slot diameter (cm)	5	7	10	14
Thruster input power (W)	350	700	1350	5000
Average Isp (s)	1100	1500	1600	1750
Thrust (mN)	20	40	80	300
Total efficiency (%)	35	45	50	>55
Status	Flight	Flight	Flight	Qualified

Figure 2.6: *Technical specifications of* SPT Hall Thrusters. *From Ref. [19]*

A major issue, associated with the use of *Electrical Propulsion* for deorbit, are the high values of power required by any EP thuster, as shown in the table above for the specific case of *SPT Hall Thrusters*. A crucial aspect is whether the satellite, at the start of deorbit, is completely defunct, on the power standpoint, or not, i.e. how much power it can still provide with the solar panels used during mission life. It appears as a very remote scenario that a satellite can still provide, at its end of life, enough power for the EP system during the entire deorbit, since normally a satellite is employed, either for scientific or commercial purposes, "until the last drop". Consequently, it will be much reasonably assumed, in this analysis, that the power required during deorbit must be provided by dedicated solar panels to be deployed only at the satellite's end of life, just before activating the thruster and starting the deorbit phase. Therefore, the additional mass for deorbit must also account for the mass of the dedicated solar panels used to sustain the electrical propulsion system.

In order to have an EP system that requires a reasonable power, i.e. a power such that additional solar panels do not need to be too large, it is chosen, among the SPT series reported in the table above, the *Hall Thruster SPT-70* as ideal candidate for deorbit application. It requires a power of 700 W, much lower than the power required by larger thrusters SPT-100 and SPT-140, and with consistently better performance than the smallest SPT-50 thruster.

Another important aspect regarding the use of EP for deorbit is that the correct attitude of the satellite must be granted, in order to have the drag thrust vector constantly pointed in the right direction. The case of EP is indeed more critical, from this standpoint, with respect to the *chemical propulsion* option, due to the fact that attitude

control must be ensured throughout the entire and much longer deorbit time. In case the attitude control hardware is not functioning anymore, an additional control system must be inserted only for deorbit, leading to an increase of deorbit system mass. In case of active attitude control system, additional power must be provided for it to work: also this power must come from solar panels deployed at the end of life, that shall be then larger and more massive.

Lifetime of the thruster should also be considered: for very high initial altitudes (as a rough value, higher than 1200 km), and more massive satellites, the usage of a Hall Thruster, like the *SPT-70*, can possibly lead to problems, since the deorbit time becomes comparable or even higher than the expected lifetime of the smaller and cheaper Hall thrusters, or the time during which the nominal performance is granted. For example, deorbiting a 3000 kg satellite, instead of the default 1000 kg satellite used for the analyses in Chapter [3], from an initial altitude of 1200 km, with the SPT-70 Hall thruster, it takes about 1.6 years. The lifetime of an Hall thruster, as accurately described on Ref. [19], is primarily determined by erosion of the channel wall and the life of the hollow cathode. Hollow cathode life seems to be of less concern. Instead, after a number of hours lower than 10000 (i.e. about 417 days equal to 1.14 years), the erosion of the channel wall due to ion bombardment reaches a level at which the magnetic circuit is exposed and eroded too, ultimately leading to a constantly higher decrease in thruster performance. Therefore, for a deorbit theoretically lasting 1.6 years, the last part of deorbit will take place with a thruster with decreasing performance, potentially causing much higher deorbit times than the expected 1.6 years. Other factors that can progressively compromise the thruster performance are: deposited material build-up on the electrodes, conductive-flake production, electrical shorting.

2.4 Deorbit with *Drag Augmentation devices*

This deorbit option comprises inflatable devices, i.e. *Drag Balloons*, and non-inflated thin devices, supported by rigid booms, i.e. *Drag Sails*. Using these systems poses two problems:

- in order to achieve deorbit times lower than 25 years, the drag area must be generally very large for any orbit higher than 500 km. As a consequence, the collisional area is large too, as well as the associated risk (related to the ATP, as described in detail in Sec.[3.2]).
- this solution is expected to be very hardly applicable for orbits higher than 800 km, above which the atmospheric density is so low that, in order to be effective, incredibly large drag areas would be required, making this solution technologically unfeasible, or anyhow economically not convenient since a too high mass would have to be carried onboard

The re-entry with this system will be simulated, in this work, with the software *Stela*® by CNES (see Appendix G). Details about the simulations are discussed in Sec.[3.4].

NASA Guideline (Ref. [1]), in section 6-1a, emphasize the limitations of using drag enhancement devices to reduce orbit lifetime. Quoting the exact words:

> *"Drag enhancement will increase the total area of the spacecraft or upper stage and may do little to reduce the probability of hitting large objects in the environment even though the orbit lifetime is reduced. It is, therefore, essential to demonstrate that drag enhancement does not in fact represent an increased risk to other users of space."*

and also

> *"If drag-enhancement devices are to be used to reduce the orbit lifetime, it should be demonstrated that such devices will significantly reduce the area-time product of the system or will not cause spacecraft or large debris to fragment if a collision occurs while the system is decaying from orbit."*

2.5 Deorbit with *Bare Electro-Dynamic Tether (EDT) system*

The EDT system employs a bare conductive tether of length L, deployed from the spacecraft towards space, followed by an optional inert segment of tether attached to it in sequence, of length L_{inert}. The function of the inert segment will be discussed later in Sec.[2.5.4]. Lengths of conductive tether between 3 km and 5 km are considered as an optimal compromise between deorbit performance, ATP and mass. Higher lengths would improve deorbit performance (lower times) but increase risk of tether being severed and extra mass to be carried onboard. The tether is deployed upwards or downwards from the satellite, at the end of mission life. The direction of deployment depends on the orbital inclination, as will be discussed later in Sec.[2.5.4].
In addition, an endmass is attached to the "free" end of the tether. Parts of the system are a deployment mechanism and a spool around which the tether is reeled and stored until deployment. For example, in the TSS mission, the deploying equipment consisted of a *Spacelab* pallet, a reel for tether deployment, an extendible/retractable boom for initial deployment and final retrieval of the satellite, and electrical power and distribution subsystem.

Deorbit using EDT is achieved exploiting the *Lorentz drag force* generated by an electrodynamic process that occurs due to the combination of relative motion of the tether with respect to the geomagnetic field, and the collection of electrons from the ambient plasma to the tether generating a current. The tether, in LEO orbits, is traveling either in the *ionosphere F-Layer*, for altitudes lower than about 1000 km, or in the *plasmasphere* for higher altitudes. The two phenomena mentioned earlier create a Lorentz force acting on every segment of the tether, and therefore transmitted to the entire system. This results to be a force against the orbital motion, i.e. a dissipative drag force that progressively decreases the orbital velocity, lowering the satellite's orbit.

One advantage of this system is that the current flowing along the tether can be employed, as it reaches the spacecraft (hence after having been "used" for the Lorentz force generation), for onboard power generation to sustain active components such as the deployment mechanism (except for the first phase of deployment when the current is still too low).

Another advantage of the EDT is that it is a *passive* deorbit system. A low amount of energy is only required during deployment phase. As already mentioned, there can be a load attached to the satellite using the current generated along the tether to provide enough power for deploying the tether. In the initial phase of deployment, since only a small portion of the tether is deployed, the generated current is too low: therefore it is necessary an auxiliary source of energy. This initial energy can be provided by using a battery that is kept fully charged until the end of life of the mission, using the *trickle charging* strategy, i.e. charging a fully charged battery under no-load at a rate equal to its self-discharge rate, thus enabling the battery to constantly remain at its fully charged level.

Differently from a deorbit system based on *electrical propulsion*, the EDT does not need an active attitude control during deorbit. In fact, the tether, if the system is well designed (e.g. using an inert segment of tether, as will be discussed later), is capable of achieving a stable, or at least controlled, attitude using only passive control. Nominally, the tether should be aligned along the local vertical direction: this desired configuration can be reached by *gravity gradient stabilization*, that tends to keep the tether straight along the local vertical, thanks to the presence of an endmass at the "free" end of the tether. In order to enhance the tether's stability along the vertical several solutions have been proposed, in addition to passive control by *gravity gradient*. For example, it has been investigated the possibility of using passive viscous oscillation dampers applied at the tether's end attached to the spacecraft. A possible design for this device could be a rod rotating about hinges, generating friction that dampens the oscillations of the tether in space. The use of an inert segment of tether is another effective way to significantly enhance stability of the system.

The NASA Guideline (Ref. [1], pg. 3-3, 3-4) provides specific instructions about tethered systems, regarding segments of tether released in orbit as operational debris. In case of a tether used for deorbit, it is not planned to be released since the tether is kept attached to the satellite until complete deorbit. When the satellite, plus attached tether reaches altitudes below 200 km it is not a problem anymore since the tether, being so thin, will burn out very soon due to exponentially increasing atmospheric drag during re-entry. Therefore, it is a very "clean" deorbit method since no operational debris will be intentionally left in space.

The only concern might come from the possibility of tether being severed during deorbit. The guideline defines a maximum length L_{max} as:

$$L_{max}[km] = \frac{1}{T[yr]} \tag{2.3}$$

where T is the orbital lifetime of the tether in years. If the mission plan is to abandon the entire tether after its usage, then the guidelines constrains the tether's length L to be lower than L_{max}. Instead if the tether is eventually retracted, or if it burns out in the atmosphere (like in the case of this work), then the expected length of tether that can statistically be cut off during deorbit, L_{cut}, must be lower than L_{max}. L_{cut} is computed using the procedure described step-by-step at pg. 3-4 of Ref.[1]. L_{cut} and L_{max} will be computed for all cases, when using the EDT as deorbit system, in order to verify compliance with this guideline. Refer to Appendix [B] for additional details.

2.5.1 History of Space Missions with Tethered Systems

20 sub-orbital and orbital flights have been made with tethered systems. Among all these missions, 8 of them used an *Electro-Dynamic Tether*. A table is reported below with concise information about all these missions. An extensive bibliography is available for more details (Ref.[10], [18], [32], Web Ref.15).

Mission	Date	Orbit	Tether Length	Additional Details
Gemini 11	1967	LEO	30 m	Spin Stabilized (0.15 rpm)
Gemini 12	1967	LEO	30 m	Gravity Gradient Stabilized, local vertical, stable swing
H-9M-69 [a]	1980	Sub-Orbital	500 m	Partial Deployment
S-520-2 [a]	1981	Sub-Orbital	500 m	Partial Deployment
Charge-1 [a]	1983	Sub-Orbital	500 m	Full Deployment
Charge-2 [a]	1984	Sub-Orbital	500 m	Full Deployment
Echo-7	1988	Sub-Orbital	–	Magnetic Field Alignment
Oedipus-A	1989	Sub-Orbital	958 m	Spin Stabilized (0.7 rpm), Magnetic Field Aligned
Charge-2B [a]	1992	Sub-Orbital	500 m	Full Deployment
TSS-1 [a]	1992	LEO	20 km, only 260 m deployed	Partially Deployed, Retrieved
SEDS-1	1993	LEO	20 km	Downward full deployment, swing and cut
PMG [a]	1993	LEO	500 m	Conductive, Upward Deployment
SEDS-2	1994	LEO	20 km	Downward full deployment, local vertical stabilized
Oedipus-C	1995	Sub-Orbital	1 km	Spin Stabilized (0.7 rpm), magnetic field aligned
TSS-1R [a]	1996	LEO	19.6 km	Close to full deployment, severed after 4 days by arcing
TiPS	1996	LEO	4 km	At 1022 km/63° since 1996, longest life tether on orbit (survived 12 years)
ATEx	1999	LEO	6 km	Partial deployment
ProSEDS [a]	2003	LEO	15 km	Hardware Built but not flown
MAST	2007	LEO	1 km	Did not deploy
YES2	2007	LEO	30 + km	Full deployment

[a] Electrodynamic Tether Mission

Table 2.1: *Table reporting all tethered satellite missions to date.* SOURCES OF DATA: Ref.[32], [23]

2.5.2 Technical Features of EDT Deorbit System

Tether

It has been demonstrated that the optimal design for a tether to be used for deorbit is a *tape-like* shape, with width w of about 2–3 cm and thickness $h_t = 50\,\mu$m. In fact, this geometry minimizes the risk of tether being severed by impacts with meteoroids or other debris. A detailed explanation can be found in Appendix [B]. The tether has a constant cross section of area A with constant perimeter p. The dimensions of the cross-section are such that the electron collection from ambient plasma can be analyzed using the *Orbital Motion Limited (OML)* theory. The tether behaves, substantially, like a giant *Langmuir probe* in a plasma. *Langmuir probes* are small metal wires used to gauge density of surrounding plasma and its temperature.

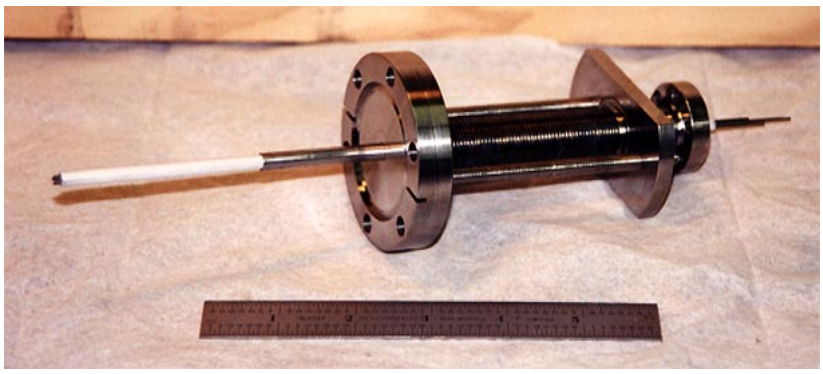

Figure 2.7: *Photo of a* Langmuir probe. *From Web Ref.[11].*

Figure 2.8: *Image of Aluminum Tape Tether like the one considered in this work. Courtesy of* Tether Applications Inc.

The tether is made of conductive material of density ρ and electrical conductivity σ_{el}, which is a function of temperature. Studies have been performed to find an optimal

material. The material that has been chosen is **Al 1100-H19**, i.e. an Aluminum Alloy made of 99% of Aluminum, plus very low percentages of other metals, including Copper. The presence of Cu enhances the electrical conductivity of the tether. Al has been chosen as principal material since it provides higher thermal and mechanical resistance, and at the same time has a lower density than materials with higher conductivity, such as pure copper (resulting in a much lower mass than a tether made of pure Cu). The selected material then represents an optimal compromise between electrical properties, and specific mechanical properties (i.e. properties divided by the material density). The *electrical conductivity* σ_{el} of the Aluminum alloy is the reciprocal of its *electrical resistivity* ρ_{el}:

$$\sigma_{el} = \frac{1}{\rho_{el}} \tag{2.4}$$

Another important feature of the tether is that it is *bare*, i.e. there is no insulating outer layer wrapping the tether. This feature has been proven as the optimal choice in order to maximize electron collection from ambient plasma. A *bare* tether, in fact, reaches the most efficient electrical contact with ambient plasma. Historically, the original solution was an entirely insulated tether with a conductive sphere at one end that functioned as the electron collection anode and another cathodic component mounted on the other end of the tether to expel the electrons back into space. Instead, with the new design, the conductive tether itself works as a positively polarized anode attracting electrons from space plasma, for almost its entire length. The number of electrons collected, and then the generated current, increases steeply with a bare tether, because of the much larger collecting area with respect to a spherical end collector. Higher current leads to higher Lorentz drag force and lower deorbit time. In addition to the high increase in electron current, and consequent decrease of deorbit time, the choice of a *bare* tether also brings a considerable mass saving, since only a cathodic emitter is necessary, not also an additional anodic component, since the anode is the tether itself.

A very short portion of the tether becomes negatively charged and works then as a cathode, emitting electrons. This will be described in Sec.[2.5.5]. Moreover, the very last segment of conductive tether attached to the spacecraft should be insulated, in order to prevent electrical arcing (see Ref.[6]).

Cathode and Endmass

At the end of the tether attached to the spacecraft there is a cathode, i.e. a component that maximizes electrical contact with ambient plasma, allowing a regular and continuous ejection of the electrons flowing along the tether, from the anodic part towards the cathode, back into space. Before the cathode, an additional load of impedance Z_l can be inserted in case power generation is needed.
The technology of cathodic emitter that has been most widely used and flight proven during tethered missions, is the *Xenon hollow cathode*.

This *hollow cathode* emits electrons from the tether by first ionizing a gas: Xenon is an optimal choice since it has a low specific ionization energy. This ionization process creates a high density plasma plume that generates contact with the surrounding plasma. In this plasma plume, the electron density is approximately equal to the ion density. However, the much higher electron velocities lead to electron currents much greater than Xenon ion currents. For each ion that exits the cathode an incredibly higher number of electrons is emitted. This number is approximately equal to the square root of the ratio between Xenon ion mass and electron mass m_e. The cathode requires a voltage bias of tens of volts only, determining a negligible contact impedance. The mass flow rate of Xenon required for this cathode is extremely low, i.e. between 0.05 to 0.1 $\frac{\text{mg}}{\text{s}}$ depending on the value of current coming from the tether.

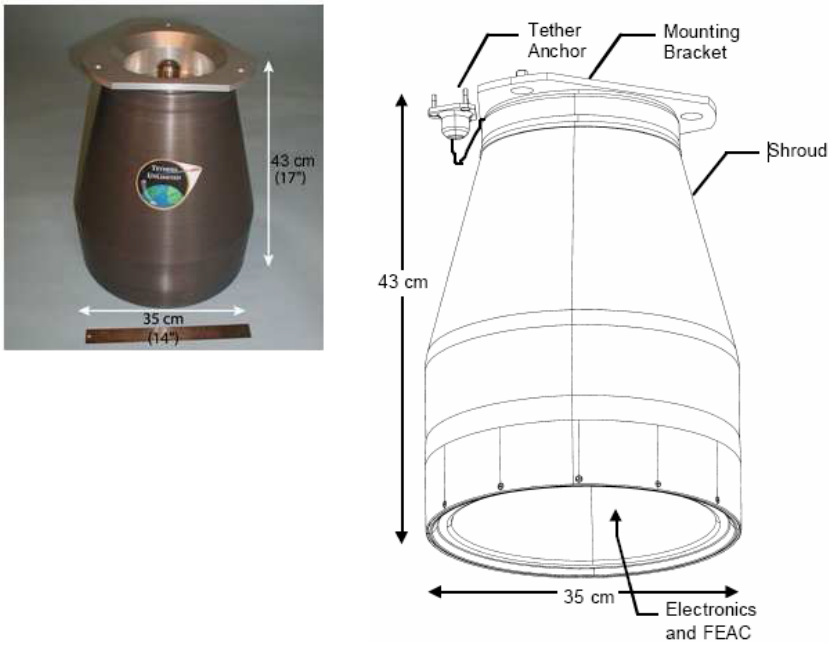

Figure 2.9: *Photograph and schematic view of cathode for EDT by* Tethers Unlimited^{TM}. *From Ref. [22]*

The cathode size, and consequently the Xenon mass flow rate, is strictly related to the altitude at which deorbit starts. For increasing altitudes, after reaching the peak at about 300 km, the electron density N_e constantly decreases. Consequently, the current generated along the tether decreases with increasing altitudes above 300 km. When the tether current, in the first phase of deorbit, is lower, then smaller cathodes shall be used, leading to a lower Xenon consumption.

It is posted below a picture showing an approximated electron density profile with respect to altitude (averaged over all longitudes and latitudes).

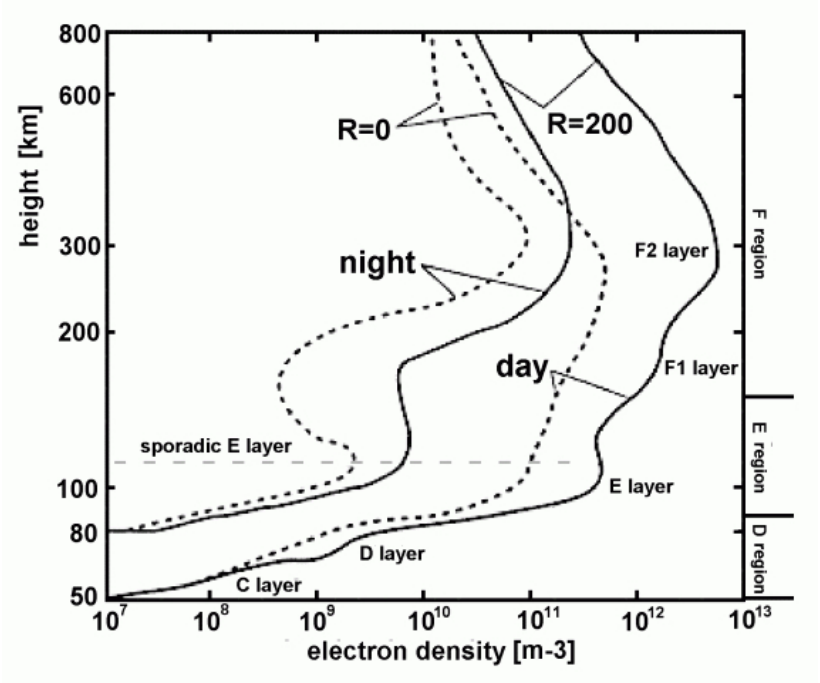

Figure 2.10: *Electron density N_e (in m^{-3}) profile versus altitude, showing its peak at about* 300 km. *Picture from Web Ref.[20]*

It is important to mention that recent research is investigating and developing new technologies for cathodic emitters that do not require propellant, leading to a very consistent mass saving. The most promising technology appears to be the *Field Emitter Array Cathode (FEAC)*, that is essentially a grid with millions of miniature low-biased tips that individually emit a very low electron current (on the order of micro-ampere). The ensemble of all these emitters creates a total current emission of the order of amperes. Of course the larger is the array, the higher is the maximum current that can be emitted. All these tiny tips are cost-effectively built using semiconductor fabrication technology. Electron emission takes place without heating or the need for an ionizable gas supply.

As of today, this technology has not been used yet in space. Recently, important developments have been reached, ensuring compliance with several requisites dictated by the space environment, such as capability of working in a vacuum environment and of enduring harsh temperatures. A major issue under investigation is the capability of working efficiently even after contamination of the array tips (or, as alternative, ways to prevent contamination). It seems in fact that contamination, e.g. due to outgassing from spacecraft components, affects significantly the performance of this emitter. Anyhow, there are all the elements to consider this technology a future asset for space application with EDT systems. More details about the FEAC can be found at Web Ref. [17].

Attached at the "free end" of the tether, released towards space, there is a tipmass, or endmass. This mass is fundamental for stability of the whole system since, as

already described, it permits gravity-gradient stabilization of the tether, helping the maintenance of alignment along the vertical direction.

2.5.3 Physical description of Electrodynamic Drag Force generation

Let us call x the direction transverse to the tether's length, i.e. going from the tether's surface towards the plasma in direction perpendicular to the tether's surface. Additionally, let us call s a parametric curvilinear system along the tether's length. Assuming the tether to be aligned along the local vertical $s = r$, where r is the axis parallel to the current radial location of the spacecraft from the Earth's center. $r = 0$ at the end of the tether attached to the spacecraft; $r = L$ at the other end of the tether where the tipmass is attached (or $r = L + L_{inert}$ if an inert segment is used too).

Two phenomena drive the current generation along the tether:

1. ***Potential Bias***, i.e. the difference of electrical potential along x direction. In other words, it is the difference of electrical potential between plasma and tether, at every point along the tether. The electrical potential along x will vary only inside a thin region called *sheath*, a layer surrounding the tether with thickness of the order of a *Debye length* λ_d. Outside the *sheath* the plasma is globally neutral, whereas inside the *sheath* it is non neutral. Refer to Appendix [A] and Ref.[5] for more details.

   This local difference of potential, at every point along the tether, is what determines the collection of electrons from ambient plasma towards every point of the tether. Electrons are collected by the tether, i.e. they move from space plasma towards the tether, at every point where the plasma potential is lower than the tether potential. This means in the *anodic* part of the tether, that extends for almost the entire bare conductive tether. However, in a very limited part of the tether, i.e. the cathodic segment, the opposite phenomenon occurs, since the plasma potential becomes higher than the tether potential. Therefore, electrons are emitted instead of collected, i.e. they go from the tether towards space.

   The potential outside the *sheath* (for $x > x_{sheath}$) is equal to the plasma potential, i.e. $V(x > x_{sheath}) = V_{pl}$. At the single point on the tether's surface ($x = 0$) the potential is instead $V(x = 0) = V_t$. At any x location between the tether and the sheath boundary, the potential has the generic value $V(x)$.

$$\Delta V(x) = V(x) - V_{pl} \tag{2.5}$$

$$\lim_{x \to 0} \Delta V(x) = V_t - V_{pl} = \Delta V \tag{2.6}$$

$$\lim_{|x| \gg \lambda_d} \Delta V(x) = 0 \tag{2.7}$$

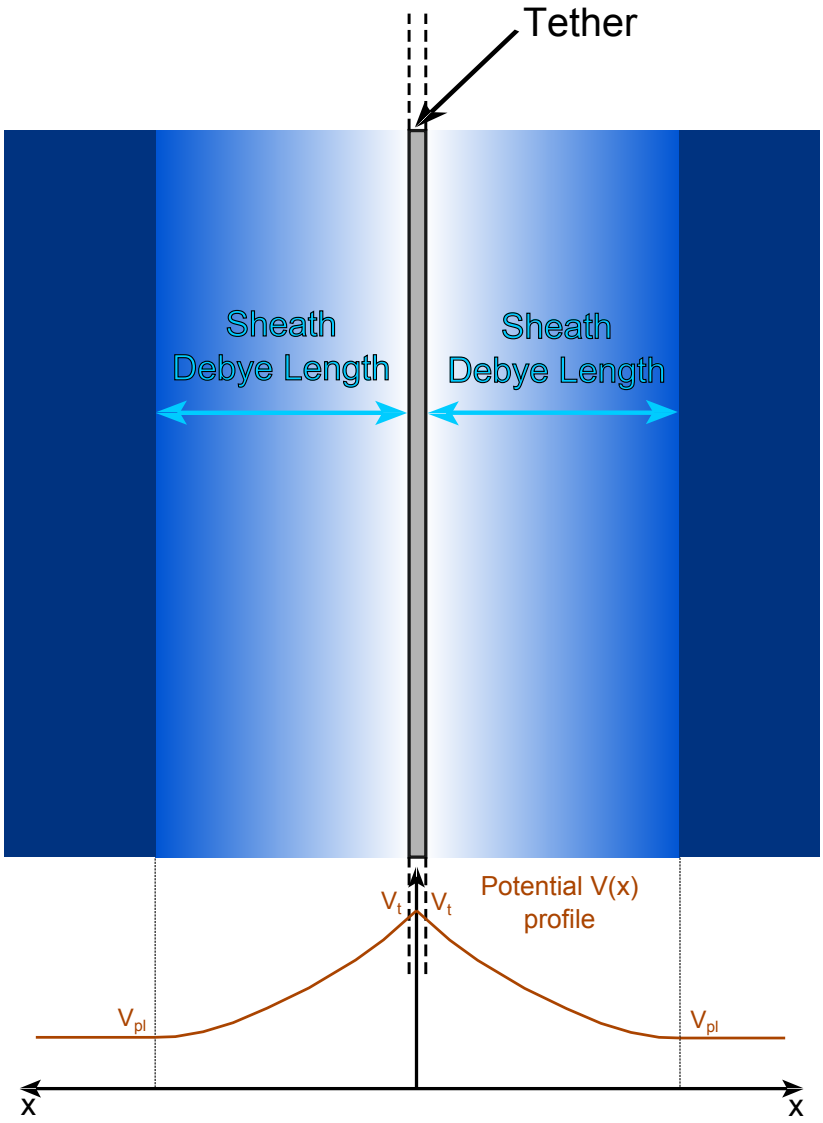

Figure 2.11: *Sketch of* sheath *surrounding the tether, with electrical potential variation profile along the x direction*

The potential of the tether is considerable constant on the single cross-section, i.e. it does not vary across the tether, but only along the tether (namely along the s direction).

2. **Difference of electrical potential along the tether, i.e. along r direction**: the relative motion of the tether, mounted on the spacecraft and orbiting with it at absolute velocity $\vec{v}_{sc}$, with respect to the geomagnetic field, moving with local absolute velocity $\vec{v}_B$, determines the generation of an induced electrical field $\vec{E}$. This electrical field is proportional to the relative velocity between spacecraft and magnetic field, i.e. $\vec{v}_{rel} = \vec{v}_{sc} - \vec{v}_B$. It is worth to note that in LEO orbits the velocity $\vec{v}_B$ of magnetic field at any specific satellite location is always much lower than the orbital velocity of the satellite $\vec{v}_{sc}$ at the same location. This is because the geomagnetic field can be reasonably assumed to be co-rotating with the Earth, and the linear velocity associated to Earth's rotation would equal the

spacecraft's velocity only at the much higher geostationary altitude. For orbits at any altitude lower than GEO, such as for LEO orbits, the orbital velocity is always higher than the linear velocity of Earth's rotation at that same radial location. The linear velocity of the magnetic field at the generic location of the satellite $r = R_E + h$, altitude h and orbital inclination i, can be computed as:

$$v_B = \Omega_E (R_E + h) sin(\frac{\pi}{2} - i) \tag{2.8}$$

where Ω_E is the spin rotation rate of the Earth. A sketch is reported below for a clearer understanding of the v_B computation.

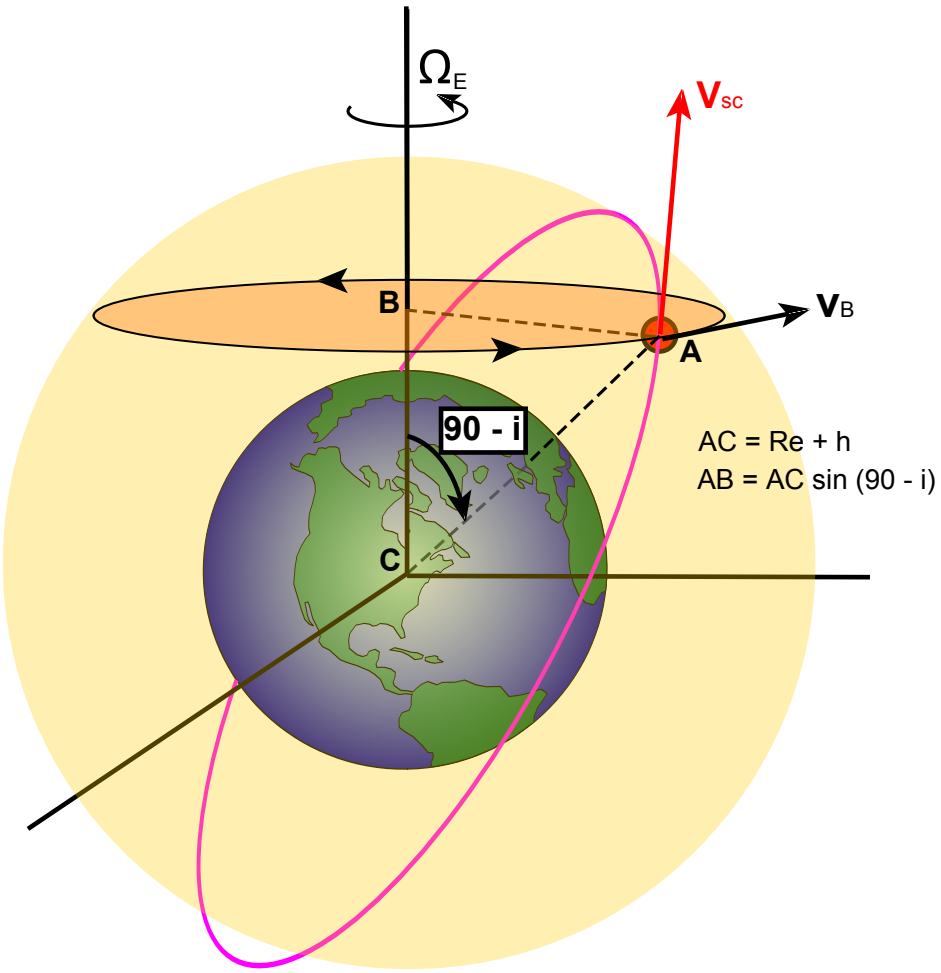

Figure 2.12: *Sketch showing the vectors of satellite's orbital velocity $\vec{v}_{sc}$ and velocity of magnetic field $\vec{v}_B$, at the same location in space.*

The induced electrical field $\vec{E}$ is computed with the following equation:

$$\vec{E} = \vec{v}_{rel} \times \vec{B} \tag{2.9}$$

where $\vec{B}$ is the local magnetic field vector. The component of $\vec{E}$ projected along the tether is responsible of the creation of a variable potential $V_t(s)$ along the

tether's length, i.e. along the parametric direction s, with $s = r$ when assuming the tether to be perfectly aligned along the local vertical.

The total difference of potential along the conductive tether's length, $\Delta V_{TETHER} = V_{t,A} - V_{t,C}$, i.e. between the anodic end of the tether and the cathodic end, can be computed as:

$$\Delta V_{TETHER} = \int_0^L \vec{E} \cdot \hat{u}_s ds = \int_0^L E_t ds \tag{2.10}$$

where E_t is the component of the electrical field $\vec{E}$ projected along the tether.

The simultaneous presence of electrons, collected inside the tether from the space plasma, and the difference of potential along the tether, triggers the generation of an electron current $I(s)$, variable in intensity along the tether (profile shown in Fig.[2.16] and Fig.[2.17]). The electron current flows in the direction opposite to $\vec{E}_t$ (instead positive conventional current flows in the same direction), given that electrons move from lower potential locations to higher potential locations (instead conventional positive charges move in the opposite way).

The current flowing through every infinitesimal segment ds of the tether interacts with the geomagnetic field generating infinitesimal Lorentz forces acting upon every segment ds. The sum of all these infinitesimal contributions, i.e. the integration over the entire length of the tether, gives the total Lorentz force acting on it, and therefore on the entire system. This force results to be opposite to the direction of orbital motion, in case of tether used in *passive mode* (i.e. the electrical field along the tether is not forced using external power, but it is has magnitude and direction of natural generation). Hence, it is a Lorentz *drag* force of electromagnetic origin. It can be calculated as:

$$\vec{F} = \int I(s) d\vec{s} \times \vec{B}(s) \tag{2.11}$$

Both the current $I(s)$ and the magnetic field $\vec{B}(s)$ vary along the tether. The variation of geomagnetic field $\vec{B}$ is surely low on a 3–5 km scale (i.e. typical lengths of the conductive tether). Hence, it can be reasonably neglected, assuming $\vec{B}$ constant along the tether. With this assumption, $\vec{B}$ can be pulled outside the integral.

The current $I(s)$ varies significantly along the tether, since, going from one end to the other, there is a continuous addition of new electrons collected from plasma at every segment of bare conductive tether. Hence, the number of electrons flowing in the tether constantly increases, leading to a current variation. In the analysis implemented in this work, it is used a value of electrical current, I_{av}, averaged over the entire tether's length. For the description of the *average current* computation refer to Sec.[3.7.2].

Lastly, in the analysis it is assumed to have the tether always perfectly straight and aligned along the local vertical. With all these assumption, the integral in Eq.[2.5.3] can be reduced to:

$$\vec{F} = I_{av} L \hat{u}_r \times \vec{B} \tag{2.12}$$

where $\hat{u}_r$ is the unit vector of the radial direction, from the Earth's center to the current spacecraft location. Considering I_{av} and L as positive values, for the correct computation this unit vector should be pointing in the same direction of the conventional current (not the electron current), i.e. the same direction of the electrical field along the tether $\vec{E}_t$.

The drag Lorentz force is higher, and as consequence the deorbit is faster, the higher is the average current I_{av} flowing in the tether. I_{av} depends on several parameters, in particular plasma density and geometry of the tether. In metallic solids (like the tether) current is made of electrons. Therefore only electrons will be collected from space plasma. For this reason only the electron density N_e is needed for computations, not the ion density. Refer to Appendix [F] for details.

2.5.4 ED Tether System configuration

Cathode, Inert Segment and Endmass configuration

There are two possible choices regarding the placement of the cathode: at the free tether's end, or at the end attached to the spacecraft. The cathode location is fundamental since the peak of tether's current is reached at the *zero-bias point* B that is very close to the cathodic end. This means that the segment of tether in proximity of the cathode is the part where the most of the distributed Lorentz drag force is concentrated. In fact, an infinitesimal Lorentz force acts on every infinitesimal segment of conductive tether. The distributed action of this force is equivalent to having the total Lorentz force acting on a specific point of the tether called *electrodynamic center of pressure (ECP).*

Given that, as previously stated, most of the Lorentz force is produced in the part of tether closer to the cathode, this means that the ECP will be much closer to the cathode than to the anodic end. In order to achieve the highest dynamic stability for the tether, the objective is to have this *electrodynamic center of pressure* as close as possible to the *center of mass (CM)* of the entire system. Since the satellite is much more massive than the tether's endmass, the *center of mass* is generally located very close to the satellite. If the cathode were placed at the other end, together with the endmass, and the conductive segment far from the spacecraft, the ECP would then be very close to the endmass, and very far from the center of mass of the system that is instead very close to the satellite. This configuration would then surely lead to stability problems. Consequently, improving stability of the system is the first reason

why the cathode should be placed attached to the spacecraft.

The farther is the ECP, where the resultant Lorentz force acts, from the CM, the higher is the "electrodynamic" force moment that causes a deflection of the tether, making it deviate from the stability condition that can be achieved by gravity gradient. Having the ECP perfectly coincident with the CM is an ideal case, so an electrodynamic moment will always be present: the objective of an accurate EDT system design is to make this distance minimum in order to attain a stable balance between gravitational moment and electrodynamic moment, reaching a stable configuration with straight tether at a certain angle (as small as possible) with respect to the local vertical. The assumption of tether constantly aligned with the local vertical is then an approximation since in reality this never occurs: however, the angle between the actual direction of the tether and local vertical is, for a well designed system, small.

Additionally, having the cathode attached to the satellite also means having available current arriving to the satellite, current that can be used for power generation if needed: e.g. power can be provided to the deployment system, or to an auxiliary active control system that enhances stability of the tether and spacecraft attitude over time.

From all these elements, it is now clear that the **optimal placement of the cathode is at the tether's end attached to the satellite**.

An additional strategy to make the ECP even closer to the CM, is to use an *inert* segment of tether attached in sequence to the bare conductive tether segment. An example of EDT design could be a 5 km Aluminum Alloy bare conductive segment, attached to the spacecraft, with cathode mounted on the spacecraft, and another 1 km of non-conductive inert tether attached at the end of the conductive segment. This non-conductive segment will then have the endmass attached at its "free end". This configuration is displayed in Fig.[2.15],[2.13],[2.14]. Adding an inert segment far from the spacecraft does not affect the location of the ECP, but it affects the location of the CM, "moving" it closer to the ECP. In fact, the ECP is not extremely close to the spacecraft, but it could be located, for a 5 km bare conductive tether, about 0.5 km away from the spacecraft along the tether (value reasonably assumed, not computed). Instead the CM is generally much closer to the spacecraft, being the mass of the system mostly concentrated at the satellite's body. Adding the inert tether would then increase the distance between the satellite body and the endmass. Consequently, the CM would be significantly shifted away from its original location (shifted away from the spacecraft body), and therefore it would approach the ECP. The additional mass burden, when using an *inert* segment, would be very limited, since low density materials like *Kevlar*® could be used (density of about 1440 kg/m^3, leading to only about 2.16 kg for a 1 km $\times$ 3 cm $\times$ 50 μm inert segment of tape tether).

Other references, such as Ref.[6], consider the configuration with cathode attached

to the "free" tether's end. This option has the advantage of using the cathode, and Xenon propellant in its tank, as part of the endmass, reducing the ballast mass (i.e. the mass added without having any function). Moreover, the tether's deployer is used too as part of the endmass. This configuration has the only advantage of saving some mass but from the stability standpoint, it is very critical, and it also does not allow power generation onboard the spacecraft.

This design will be then discarded in this thesis, opting instead for the previously described configuration, for all reasons already highlighted. The only variation that will be implemented is to use the tether's deployer, the spool assembly, ejection mechanism and battery for deployment as part of the endmass, since having these components attached to the spacecraft brings no advantage, instead having them as part of the endmass, allows for a significant reduction of the additional ballast mass (equal to the endmass subtracted of the mass of any component of the EDT system that is added to the endmass).

Direction of Deployment

Let us approximate the Earth's magnetic field as a perfect dipole, tilted of $\theta_m = 11.5°$ with respect to the Earth's spin axis. Then, *prograde* orbits with inclination i in the range $0° < i < 78.5° = 90° - \theta_m$, will be always characterized by an induced electrical field component along the tether, $\vec{E}_t$, pointing towards higher altitudes. This means that the electron current, flowing in direction opposite to $\vec{E}_t$, would go from higher altitudes to lower altitudes. Then the cathodic emitter must be located at the lowest altitude end of the tether. As described previously, it is preferred to have the cathode attached to the satellite. Consequently, this is the reason why, for *prograde* orbits with inclination i in the range $0° < i < 78.5°$, the tether should be deployed *upwards*. The alternative of deploying downwards, would force to have the cathode at the "free" end of the tether, not attached to the spacecraft. In conclusion, the optimal configuration in case of *prograde* orbits, with inclination i in the range $0° < i < 78.5°$, is: tether deployed upwards, cathode on the satellite attached to a first very short insulated part to prevent electrical arcing, then follows the long bare conductive segment, and finally the inert segment with attached tipmass at its end. This configuration is displayed in the following picture.

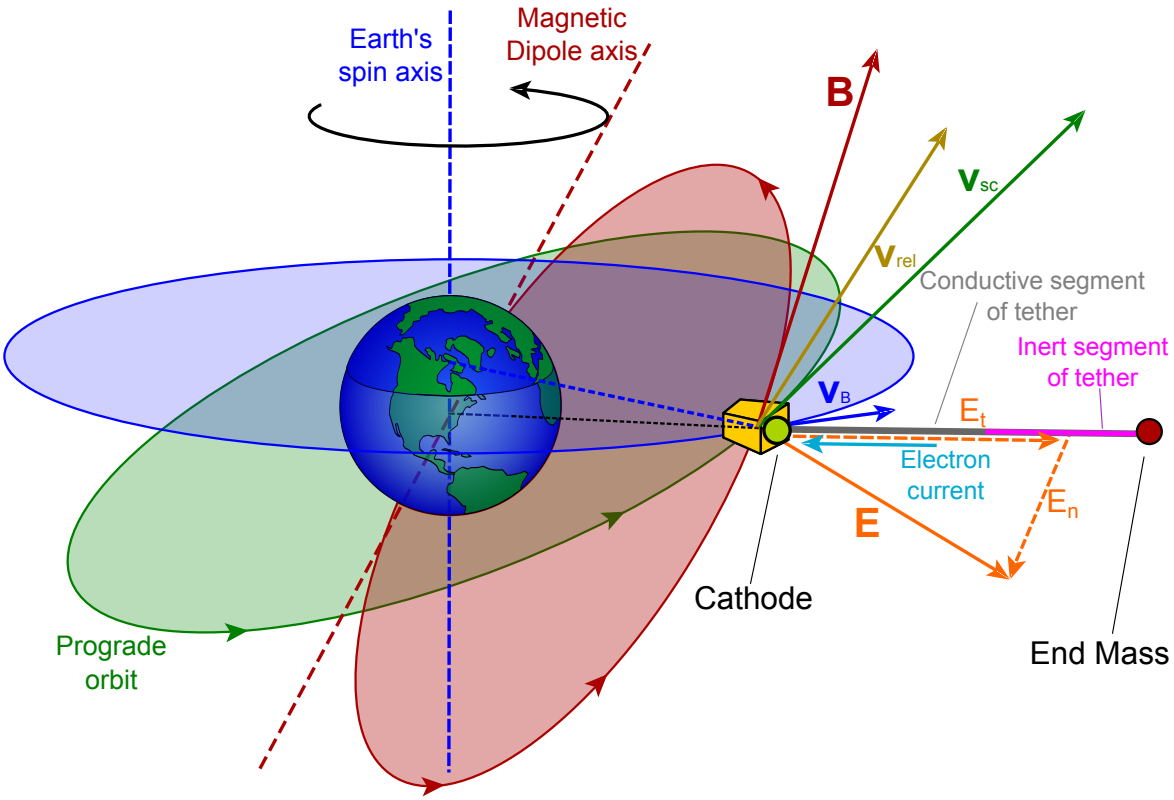

Figure 2.13: *3D sketch of satellite with EDT system, showing the specific configuration in case of a* prograde *orbit. Three planes are highlighted in the picture. The plane in green is the orbital plane, with the spacecraft velocity vector v_{sc} tangent to the orbit. The plane in blue is the plane parallel to equatorial plane but also passing through the satellite location: on this plane lies the vector of linear velocity $\vec{B}$ of magnetic field, that is co-rotating with the Earth. The plane in red is the plane where the local geomagnetic field line is lying, assuming an ideal dipolar model: the magnetic field vector $\vec{B}$ is then tangent to this line, and oriented in direction from North magnetic pole to South magnetic pole (that are placed opposite to the geographical poles location). The relative velocity vector $\vec{v}_{rel} = \vec{v}_{sc} - \vec{v}_B$ is displayed in yellow. The electrical field $\vec{E}$ is generated, not only with a component along the tether, $\vec{E}_t$, but also one orthogonal to the tether, $\vec{E}_n$. The electron current I is flowing along the tether in the opposite direction with respect to $\vec{E}_t$.*

Still considering a perfect dipolar model for the geomagnetic field, in case of *retrograde* orbits with inclination i in the range $90° + \theta_m = 101.5° < i < 180°$, the resulting electrical field along the tether $\vec{E}_t$ is always pointing towards lower altitudes. This means that the electron current, flowing in direction opposite to $\vec{E}_t$, would move from lower altitudes to higher altitudes. Then the cathodic emitter must be located at the highest altitude end of the tether. This fact, combined with the previously described constraint on cathode placement, implies that for *retrograde* orbits, with $101.5° < i < 180°$, the tether should be deployed *downwards*. In fact, the alternative of deploying upwards, would force to have the cathode at the "free" end of the tether, not attached to the spacecraft. In conclusion, the optimal configuration in case of

retrograde orbits, with inclination i in the range $101.5° < i < 180°$, is: tether deployed downwards, cathode on the satellite attached to a first very short insulated part to prevent electrical arcing, then follows the long bare conductive segment, and finally the inert segment with attached the tipmass at its end. This configuration is displayed in the following picture.

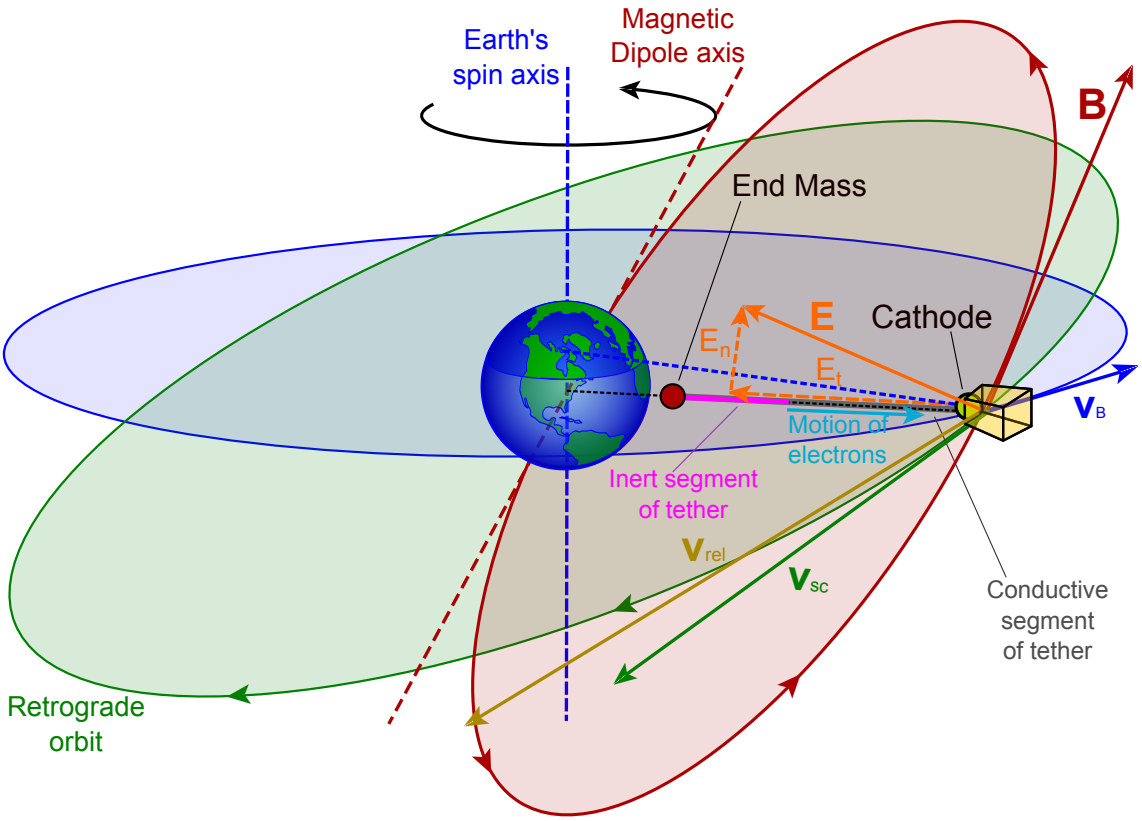

Figure 2.14: *3D sketch of satellite with EDT system, showing the specific configuration in case of a* retrograde *orbit. Three planes are highlighted in the picture. The plane in green is the orbital plane, with the spacecraft velocity vector v_{sc} tangent to the orbit. The plane in blue is the plane parallel to equatorial plane but also passing through the satellite location: on this plane lies the vector of linear velocity $\vec{B}$ of magnetic field, that is co-rotating with the Earth. With respect to Fig.[2.13], here the spacecraft is orbiting in opposition to Earth's spin rotation. The component of $\vec{v}_{sc}$ lying on the blue plane is opposite to $\vec{v}_B$: due to this fact, the relative velocity, $\vec{v}_{rel} = \vec{v}_{sc} - \vec{v}_B$, is higher for* retrograde *orbits than for* prograde*. The plane in red is the plane where the local geomagnetic field line is lying, assuming an ideal dipolar model: the magnetic field vector $\vec{B}$ is then tangent to this line, and oriented in direction from North magnetic pole to South magnetic pole (that are placed opposite to the geographical poles location). The electrical field $\vec{E}$ is generated, not only with a component along the tether, $\vec{E}_t$, but also one orthogonal to the tether, $\vec{E}_n$. The electron current I is flowing along the tether in the opposite direction with respect to $\vec{E}_t$.*

The most complex situation involves satellites with orbital inclination i in the range

$78.5° < i < 101.5°$, due to the fact that the Earth's spin will rotate the magnetic field too, being it co-rotating with the Earth. As a consequence, for satellites in this inclination range (that includes *prograde* orbits for $78.5° < i < 90°$ and *retrograde* orbits for $90° < i < 101.5°$), the satellite will experience, along its orbit, not only a different values of local magnetic field (as normally happens for any orbit), but also a different direction of the component of magnetic field vector orthogonal to spacecraft velocity vector, i.e. the component of $\vec{B}$ that is responsible for the generation of the electric field $\vec{E}_t$. This means that the electric field $\vec{E}_t$ will be, at the same inertial location along the orbit, pointing towards different directions at different times (in the numerical computations this means that, once the reference direction along the tether is set, the magnitude of E_t will show either positive or negative values at the same location in space, but at different times). Naturally, the orbiting direction is constant, i.e. a prograde orbit always remains prograde (same for retrograde orbits). Moreover, the configuration of the tether is of course fixed during the entire deorbit. These last two facts, combined with continuous changes in sign of E_t during the deorbit, imply that the electrodynamic Lorentz force would be sometime a drag force, and other times a boost force, during the deorbit phase for satellites with $78.5° < i < 101.5°$.

It is possible to say, as a "rule of thumb", that for orbits whose inclination is closer to 78.5° than to 101.5°, it is more convenient to deploy the tether upwards, i.e. to use the *prograde* configuration. In the fewer points along the deorbit when the electrical field changes direction, since there is no cathode at the other end of the tether, the current that develops opposite to the nominal direction is very small, and therefore the resulting unwanted boost force is absolutely negligible.
Instead, for orbits with i that is closer to 101.5° than to 78.5°, it can be considered more convenient to deploy downwards, i.e. to use the *retrograde* configuration. Also in this case, in the fewer points along the deorbit when the electrical field changes direction, since there is no cathode at the other end of the tether, the current that develops opposite to the nominal direction is very small, and therefore the resulting unwanted boost force is surely negligible.
The analysis code has then to account for all these facts. Further discussion about this problem, from the computational standpoint, is provided in Sec.[3.7].

Lastly, it is important to point out that the inclination range values of 78.5° and 101.5° are precise boundaries only when considering a perfect dipolar model for the geomagnetic field. In reality, this field is much more complex than a simple dipole model. Considering a higher number of spherical harmonics, such as it is done in the computational analysis of this work, these values are not strictly accurate anymore. To make this point clearer an example is useful. Let us consider a *prograde* orbit with $i = 77°$: if the model were a perfect dipole, along the entire deorbit, since $i < 78.5°$, the value of E_t would always be positive. Therefore, the Lorentz force would always be a drag force. Instead, with a more realistic model for the geomagnetic field, it can happen that, at some points along the deorbit, with $i = 77° < 78.5°$, E_t becomes negative. This means that, once in a while, the Lorentz force becomes a boost force instead of a drag force, even if, as already stated, this occasional boost force is negligible, since an appreciable current cannot develop in the direction opposite to the nominal one.

Sketches of a generic satellite with EDT system configured for both *prograde* and *retrograde* orbit are posted below, displaying vectors of significant parameters. In the picture, it is assumed for simplicity to have the geomagnetic field vector $\vec{B}$ perfectly perpendicular to the relative velocity $\vec{v}_{rel}$, and tether perfectly aligned along the local vertical. The Lorentz drag force vector, related to the cross product between a vector aligned with the tether and the magnetic field vector, is orthogonal to both, as shown in the picture.

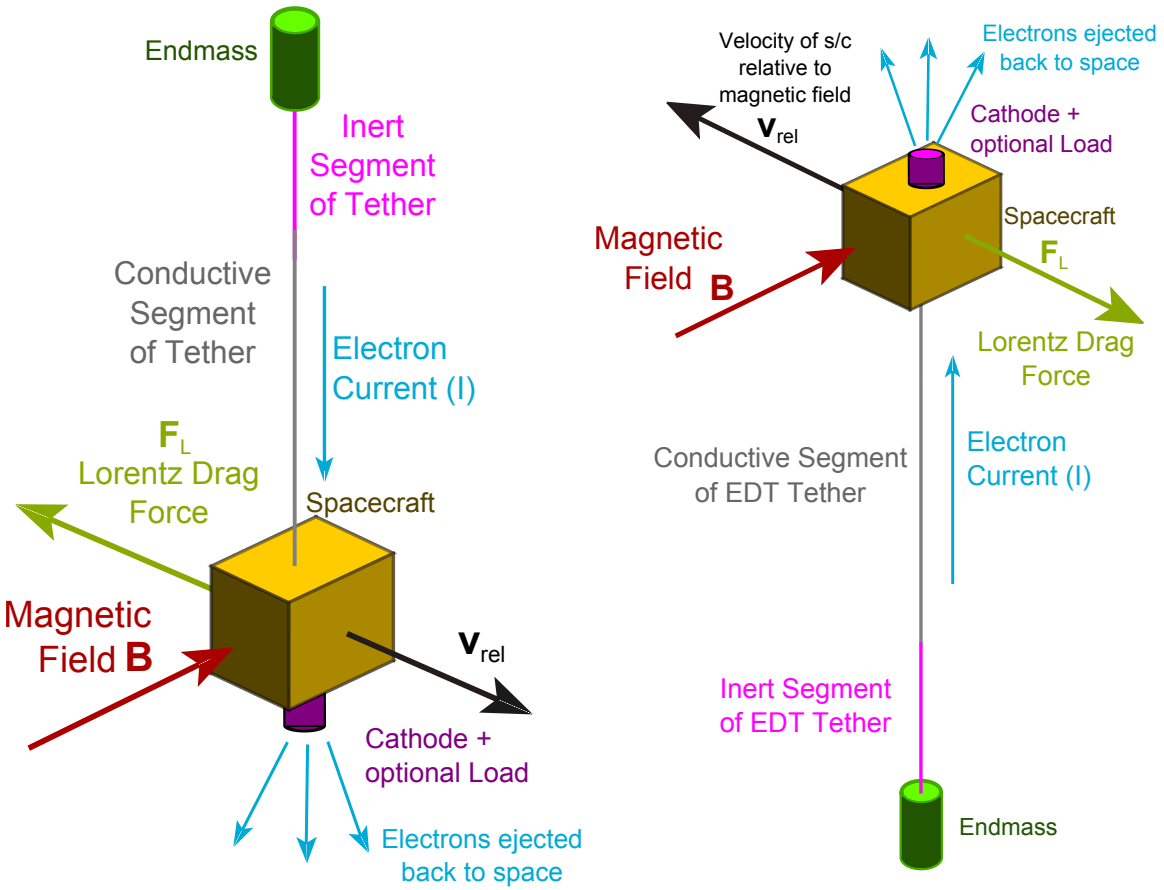

Figure 2.15: *Close view of EDT system, in the optimal case of magnetic field perfectly orthogonal to the relative velocity vector. On the left: case of* prograde *orbits. On the right: case of* retrograde *orbits.*

2.5.5 Potential and current profiles

The local bias between plasma potential outside the sheath and the potential of the tether, $\Delta V = V_t - V_{pl}$, varies depending on the variation of both V_t and V_{pl}. This variation is the difference between the two curves reported in the picture below, in the diagram of potential V profiles along s.
The plasma potential V_{pl}, that is initially lower than tether potential ($V_{pl,A} < V_{t,A}$, where $\Delta V_A = V_{t,A} - V_{pl,A}$), then constantly increases along s. It intersects the $V_t(s)$ profile at zero bias point B, located at $s = s_B$, such that $V_{pl,B} = V_{t,B}$. Then it becomes

higher than $V_t(s)$ in the very short final cathodic segment of tether.

As shown in the same picture, the current I, flowing along the tether, varies increasing from zero, at the anodic end A, to a maximum at the point B of zero-bias (i.e. $\Delta V_B = V_{t,B} - V_{pl,B} = 0$), and then slightly decreasing, due to a small loss of electrons in the short cathodic segment.

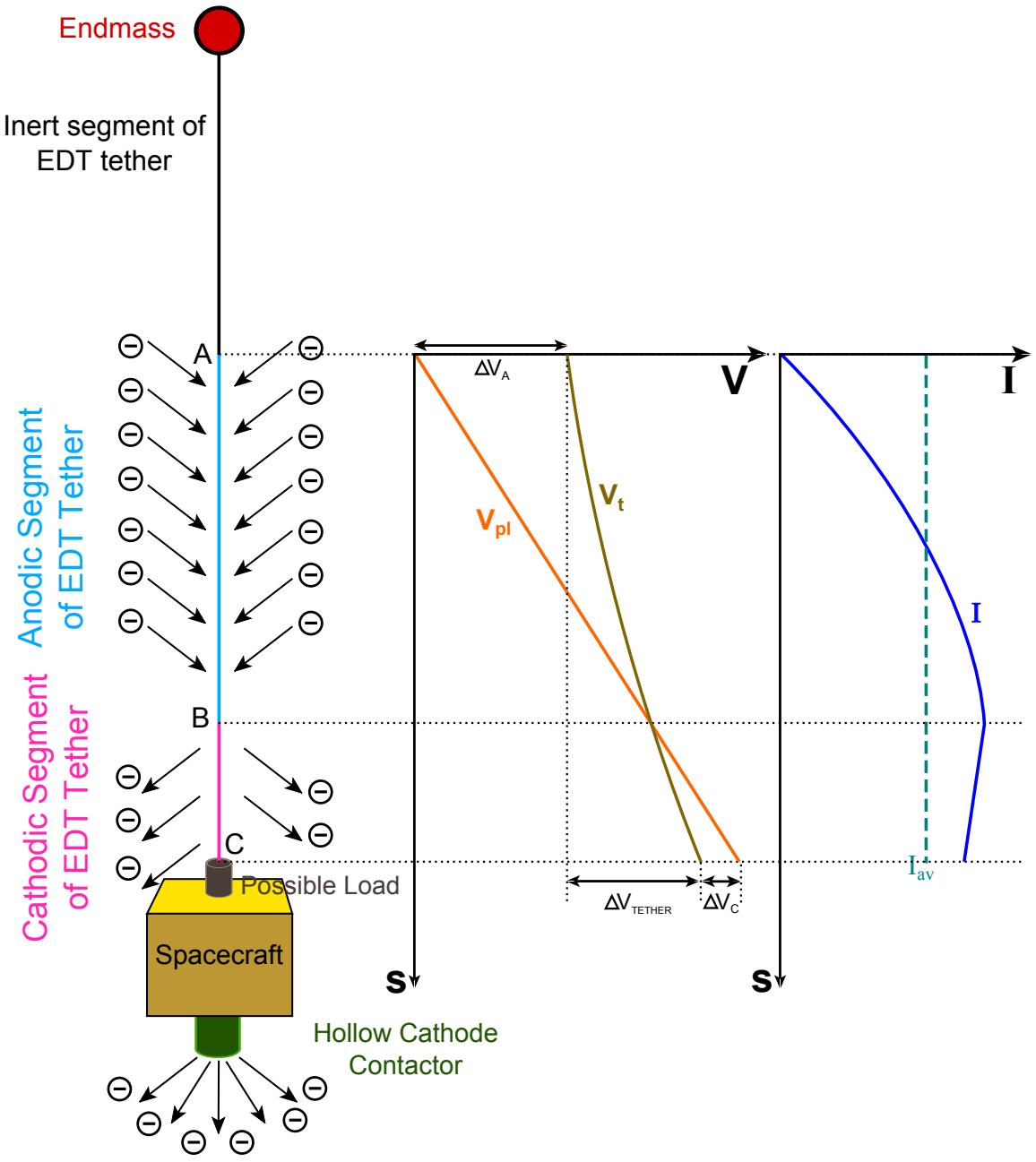

Figure 2.16: *Sketch of potential profiles and current profile along the ED tether, for* prograde *orbits*

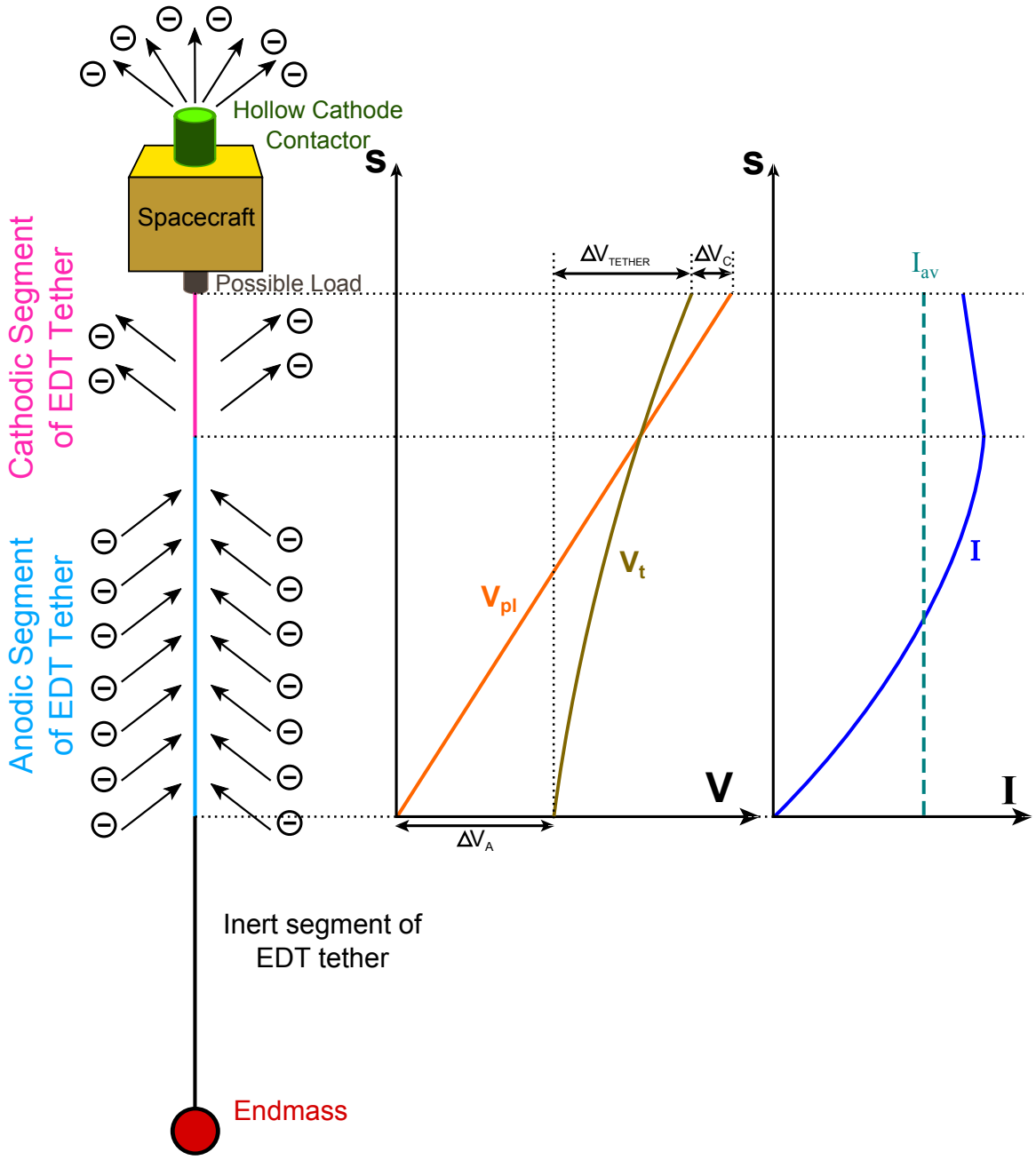

Figure 2.17: *Sketch of potential profiles and current profile along the ED tether for* retrograde *orbits*

Electrons flow from lower to higher electrical potential regions. This is why they are collected by the tether from surrounding plasma only in the segment of tether where $V_t > V_{pl}$. At every infinitesimal segment of the anodic part of the tether, ds, there is a corresponding "portion" of electrons flowing from plasma to that precise point of the tether (an opposite flow takes place in the cathodic part). This quantity of electrons depends on the local value of bias ΔV, variable along s. At the zero point bias electrons are not collected anymore since $V_{pl} = V_t$. And then, in segment BC, the tether potential is lower than plasma potential, so electrons flow from the tether to

the plasma.

The fact that electrons flow from lower to higher electrical potential regions also explains why, after being collected by the tether, electrons move, generating a current, from the anodic end A to the cathodic end C, given that $V_{t,C} > V_{t,A}$.

It is worth to remember that some references in literature deal with the *conventional current*, defined considering positive charges, that move opposite to the electrons flow. Consequently, the *conventional current* would flow from the cathodic end towards the anodic end. In this thesis it will always be considered the actual *electron current*, not the *conventional current*.

Chapter 3

Analysis and comparison of results

3.1 Parameters used for all simulations

Assumptions and inputs used for all simulations, regardless of the specific deorbit system, are listed below. The assumptions alleviate the computational burden of such complex analyses but, at the same time, they do not appreciably affect the accuracy of the comparison between different deorbit technologies. In fact, the purpose of this work is not to compute an extremely precise deorbit path and time, but to provide accurate enough results to implement an effective quantitative comparison between each deorbit technology.

1. The features of the satellite, without deorbit system, are set equal for all simulations: essentially, the required features for the analyses are the mass of the satellite and its geometry, from which drag area and collisional area are calculated, as described in Sec.[3.2].

2. It is set a reentry altitude, as final deorbit altitude for all simulations, of 120 km. The phase in which the mass experiences a fast decay can be neglected since it is a much shorter time in comparison to the time required to decelerate the satellite from its original orbit to an altitude at which reentry begins, and subsequent burn out in the atmosphere happens very rapidly. Therefore, the dry mass of the satellite (i.e. every hardware component, excluding only consumables) is considered always constant during deorbit.

3. *Keplerian* parameters are used to define the initial orbit:

   - *Eccentricity* e : **only initial circular orbits are considered in every analysis**. Therefore, e is always set to zero. The vast majority of LEO satellites actually lie in almost circular orbits, as shown in Fig.[1.7] at pg. 22. Consequently, the assumption of dealing with initial circular orbits only, it is a reasonable approximation for fulfilling the objectives of this thesis. Catalog objects data, updated to 2003, reports that about 54.5% of trackable objects reside on orbits with $e \leq 0.01$, and 32.0% on orbits with $0.01 < e \leq 0.1$.

- *Semi-major axis a*: equal to the initial orbit radius r, given the previously stated assumption of initial circular orbits.
- *Inclination i*
- *Right Ascension of the Ascending Node* (RAAN) Ω: assumed to be zero for all deorbit simulations. This parameter does not significantly affect the deorbit time. Any value could be chosen, without loss of generality nor accuracy.
- *Argument of perigee* ω: assumed to be zero. This parameter is not relevant in this case since only initial circular orbits are considered.
- *Mean Anomaly M* , or *True Anomaly* θ: both of them are always set to zero as initial value.

4. In all *Matlab*® codes, personally written for the analysis of deorbit with *EDT*, *electrical* and *chemical propulsion* systems, the deorbit is computed in a *quasi-circular* path, i.e. at every time step in the computation it is assumed that the satellite is lying on a circular orbit. Hence, at every computational step, the local velocity is computed as:

$$v = \sqrt{\frac{\mu_E}{r}} \tag{3.1}$$

where μ_E is the *gravitational parameter* of the Earth and r is the radius from the center of the Earth to the current spacecraft location.

5. In all *Matlab*® codes, the **orbital inclination is assumed constant during the entire deorbit**. Any perturbation that causes change in inclination is then neglected. This also implies the assumption that both Lorentz force, in case of the EDT system, and propulsive force, in case of EP and CP systems, are acting along the tangent and on the plane of the orbital path, without any component perpendicular to the orbital plane.

6. Orbits at LEO altitudes are mainly perturbed by the non-spherical geopotential, lunisolar attraction, solar radiation pressure, and by aerodynamic forces. Of these, only the aerodynamic drag, acting always opposite to the direction of motion, is a non-conservative, energy-dissipating perturbation. In case of reentry through *natural decay*, only the *aerodynamic drag* perturbation is considered. The cross-sectional drag area is computed as the surface area of the spacecraft, projected on the plane orthogonal to the velocity vector.
   In simulations with EP system, any perturbation to the orbit other than propulsive thrust is neglected (no aidrag perturbation, no third-body perturbation, no perturbation J_{22} due to non-spherical Earth, no solar pressure).
   In simulations with EDT system, any perturbation other than Lorentz drag force is neglected (no aidrag perturbation, no third-body perturbation, no perturbation J_{22} due to non-spherical Earth, no solar pressure).

7. for all simulations, a *mean Solar Activity* is used, i.e. it is considered a solar flux index F10.7 averaged over a full solar cycle, typically lasting for about 11 years. In simulations made with *Stela*® it is sufficient to select the option "Mean

Constant" in the *Solar Activity* field. This is a very relevant parameter, since both *atmospheric density* and *electron density* are strictly related to the solar flux.
For EDT simulations, it is found the Julian Day when the F10.7 index is as close as possible to an average value over a typical solar cycle. Using a *Fortran* routine that extracts ionospheric data from the IRI model, this Julian Day is input, as date at which to compute the values of *electron density* that are required for EDT simulations. Consequently, this set of values of *electron density* can be considered as a *mean ionosphere* over a solar cycle. This *mean ionosphere* data will be kept constant throughout the simulation of deorbit with EDT. For more details about ionospheric data computation, refer to Appendix [F].

3.2 Risk estimation using the Area-Time Product

The risk of collision with other objects, during deorbit of a satellite, is proportional to a certain characteristic area A of the spacecraft (including the deorbit device) and to the deorbit time t. Therefore, the risk evaluation is performed by estimating the *Area-Time Product (ATP)* of every deorbit solution. The lower is the ATP the lower is the risk of collision associated to a specific deorbit solution. This is, in fact, one of the most important drivers for the optimal selection of the best system for deorbit.

In most of scientific literature, it is generally considered, for the ATP calculation, the *drag area* of the object. Guidelines too normally refer to the *drag area* for ATP calculation, i.e. the area of the system projected onto the plane orthogonal to the instantaneous velocity vector (that means orthogonal in every instant to the orbital path). This is the cross-sectional area facing the *aerodynamic drag* force exerted by the atmosphere.

In this thesis, it is instead proposed and used an innovative calculation of the ATP, regarding what area to consider in the ATP and how to accurately calculate its value. This solution is completely original, and developed starting from what was reported in Ref.[28].

This new solution starts from the fact that the use of *drag area* is a too rough approximation in the ATP calculation of satellites, essentially for two reasons:

1. the cross-sectional area that can be potentially interested by a collision is higher than the *drag area*, and defined as *Collisional Cross-Sectional Area (CCSA)*. In the following section, Sec.[3.2.1], this concept will be thoroughly described.
2. not all *collisional areas* "behave" in the same way, regarding the potential of new debris generation, when hit by a meteoroid or debris with a certain characteristic size. *Risk Factors* need to be defined, with different values depending on specific *area types*. This topic will be developed in detail in Sec.[3.2.2].

3.2.1 Collisional Cross-Sectional Area (CCSA)

Let us consider a random debris or meteoroid, with generic irregular shape, that is impacting the system during deorbit. It is defined the circumscribed circle, enclosing the debris projected area, with radius R_{ch}, called *characteristic radius*, and center in point C. Refer to the picture posted below.

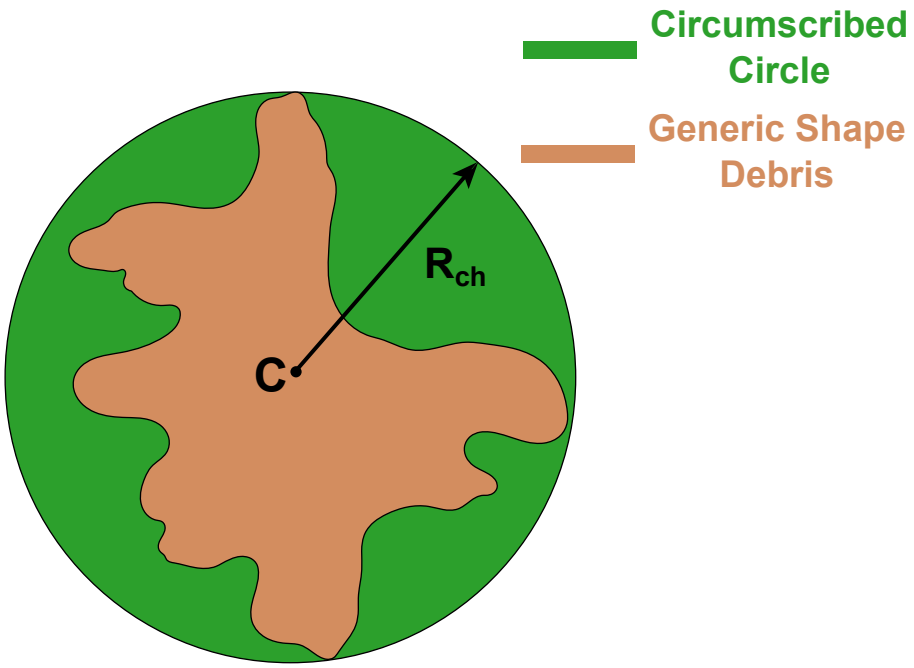

Figure 3.1: *Sketch of debris or meteoroid of generic shape, showing the circumscribed circle and the characteristic radius R_{ch}*

A collision event occurs anytime there is contact, at least in one single point, between the spacecraft and the generic debris or meteoroid. The limit condition occurs when the two bodies touch themselves. The *Collisional Cross-Sectional Area (CCSA)* is defined as the area such that, if the point C of the impactor falls inside it (or as limit situation falls on its boundary), then the two bodies *might* intersect themselves (or as limit situation they touch each other), and a collision takes place. The CCSA is not only composed of the area of the satellite projected on the plane orthogonal to the impact direction: in fact, this projected area must be augmented, extending it of a length R_{ch}. The additional area is the area defined by "sweeping" a segment of length R_{ch} all along the perimeter of the projected area, maintaining it always perpendicular to every point of the perimeter. At sharp corners of the perimeter this sweeping path corresponds to an arc of circumference of radius R_{ch}. This procedure becomes clearer by looking at Fig.[3.3].

It is reported, in the picture below, the model of spacecraft used in all analyses, with projected geometry and dimensions. Of course it is used a simple geometry: precise

geometric features are not required for the analyses of this thesis work. The main body is represented, on the 2D plane, as a rectangle (colored in yellow in Fig.[3.2]). Two identical solar panels are considered in the design, placed symmetrically with respect to the main body. Their projected area results as other two rectangles (colored in blue in Fig.[3.2]).

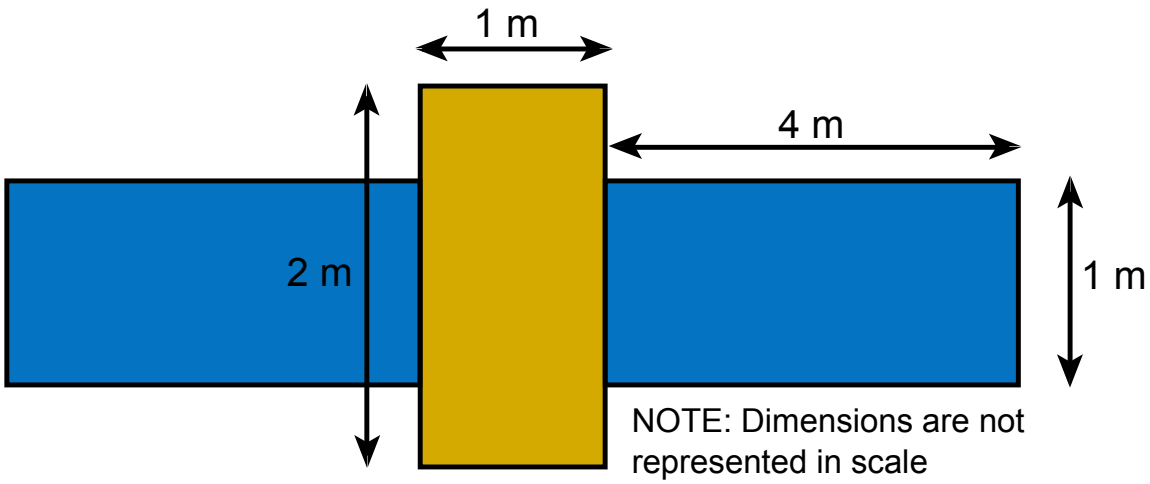

Figure 3.2: Drag area *of the generic spacecraft, considered in all analyses. For the* CCSA *computation the* drag area *is assumed equal to the projected area on the plane orthogonal to the direction of impact.*

The following image represents instead the *CCSA*.

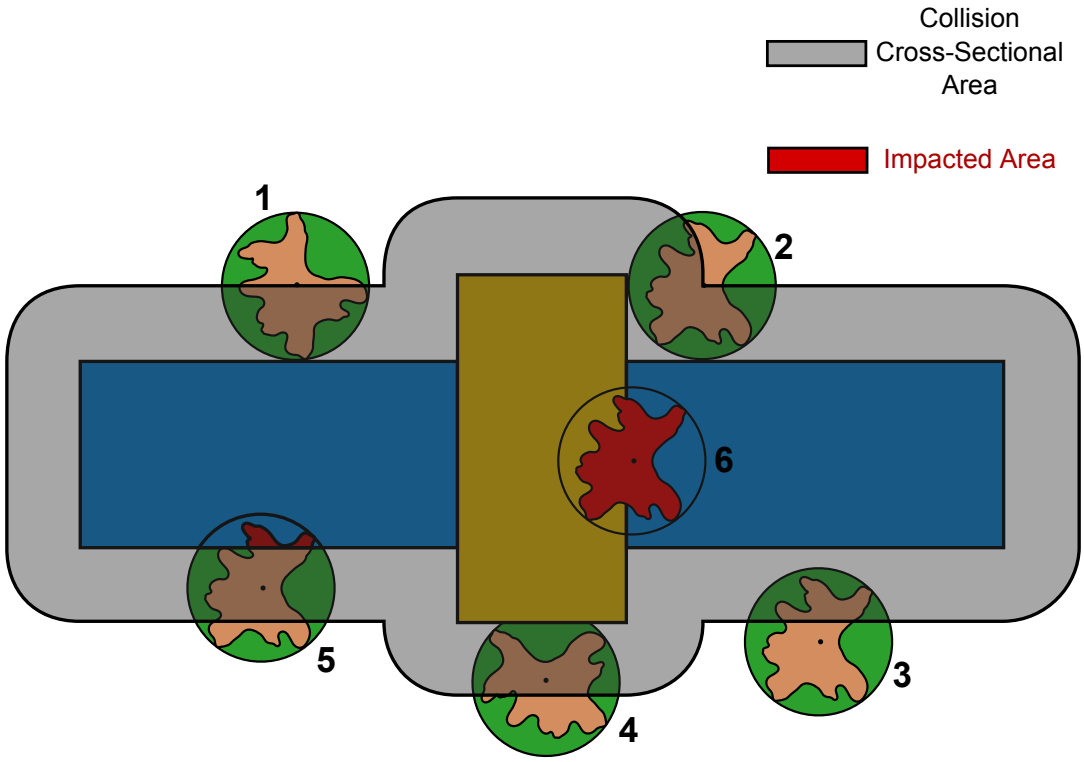

Figure 3.3: Collisional Cross-Sectional Area *associated to an impacting object of generic shape. Several cases are portrayed.* Case 1*: the debris touches the edge of the spacecraft in one single point. This is a limit condition.* Case 2*: the circle touches the spacecraft in two points and the point C lies on the boundary of the CCSA. This is another limit condition.* Case 3*: the point C falls outside the CCSA, hence the two bodies do not intersect, nor touch, each other.* Case 4*: even if C falls inside the CCSA the two bodies do not intersect.* Case 5*: the point C falls inside the CCSA and the two bodies partially intersect. Therefore, a partial collision takes place.* Case 6*: the point C falls inside the CCSA and the two bodies completely intersect. A complete collision takes place.*

An impact will occur if the projected areas of the two bodies intersect, even if only partially. However, it is important to emphasize that the CCSA does not necessarily represent an area where, if the point C falls inside, a collision surely takes place. In fact, if the debris portrayed in the picture is oriented like in Case 4, collision does not occur even if the center point C falls inside the collision area. The CCSA is an area of *potential* collision not of sure collision. Instead, what is sure is that if C falls outside the CCSA, whatever is the orientation of the impacting object, collision will never happen.

The value of CCSA varies depending on the size and shape of the impacting object, i.e. depending on its R_{ch}. For the comparison between different deorbit system, it is considered a generic debris with $R_{ch} = 5\,\text{cm}$, and maintained the same value for all simulations and for all deorbit systems. In fact, since the objective is a comparison between values of CCSA for different deorbit solutions, it is only important to use

always the same value of R_{ch}, not which precise value will be chosen. Hence, the ATP comparison will not be related to the specific impacting object size or shape; different CCSA values will be found not due to different impacting object size, but only due to different projected areas for each deorbit system.

It is presented below an analytical equation, part of the original material of this thesis work (i.e. not taken from any reference in literature), that allows an accurate estimation of the CCSA:

$$CCSA = A_{sc,proj} + p_{proj} R_{ch} + N_{convex} \frac{1}{4} \pi R_{ch}^2 - \sum_i A_{rep,i} \tag{3.2}$$

where $A_{sc,proj}$ is the cross-sectional area of the spacecraft projected on the plane orthogonal to the velocity vector of the colliding object. In all analyses, this area is assumed equal to the maximum drag cross-sectional area of the spacecraft, i.e. $A_{sc,proj} = A_{drag,max}$; then p_{proj} is the perimeter of the projected cross-sectional area of the spacecraft; N_{convex} is the number of convex sharp corners along the perimeter; $A_{rep,i}$ is every portion of area that is repeated, i.e. that is counted twice in the sum of the previous terms, and that must be consequently subtracted to make it counted only once.

For computation of the CCSA, the 3D surface of the two bodies should be projected on the 2D plane that is perpendicular to the velocity vector of the impacting object. Moreover, for an accurate CCSA calculations, an average on all 3D directions should be made since the debris can hit the spacecraft on all spatial directions, and the projected area, depending on the specific direction, is different. However, since the objective of the thesis is to make a comparison, it is not necessary to compute CCSA values averaged on all directions. It is sufficient to decide one specific direction along which impacts would occur and then calculate the CCSA in all cases, and for all systems, preserving always this same direction. In this work, as already mentioned, it will be assumed that the impact velocity vector, in all cases and for all deorbit solutions, is always perpendicular to the plane where the projected area of the system is maximum (i.e. the worst case). In turn, this maximum projected area is assumed equal to the *drag area* of the body. For example, in case of the EDT system with the tape tether, it will be used, as projected area of the tether, the rectangle where the length $L + L_{inert}$ ($= 6\,\text{km}$) is one side, and the other side is the width of 3 cm, not the thickness of $50\,\mu\text{m}$.

3.2.2 Risk Factors

Not all *collisional cross-sectional areas* have the same "weight" in an accurate risk estimation. This is due to the fact that, if collision occurs, it leads to very different outcomes depending on where specifically the collision takes place. For instance, if a large debris collides with the massive body of a spacecraft, a very high-energy impact

occurs causing the complete destruction of both bodies and the generation of a cloud of thousands of new orbital debris. Instead, if a very thin surface is impacted (e.g. a tether or an inflatable balloon) the local mass involved in the collision is so small that there is not enough energy to cause a catastrophic event. The tether could be cut or a thin balloon could be pierced, and only very few fragments would be generated. For example, in case an ED tether is cut by a meteoroid, it is very probable that only one additional debris is generated, i.e. the part of tether that was cut.

Therefore, it is necessary to distinguish between different categories of CCSA. Three main CCSA types are defined, each one leading, when impacted, to significantly different results in terms of new debris. The number of new debris, that are potentially generated by different types of area, is expressed, in the CCSA calculation, using *Risk Factors*. These factors, ranging from 0 to 1, each multiplied by the corresponding CCSA areas of distinct types, allow the calculation of a total "weighted" CCSA.

1. ***High Energy* CCSA, or *Type 1* CCSA**: CCSA that, when impacted, determines the generation of a cloud of thousands of new debris. To this area type, it is associated the maximum *risk factor* $RF_1 = 1$. This is the projected areas of the most massive ("thickest") parts of the system, such as the satellite's main body.

2. ***Medium Energy* CCSA, or *Type 2* CCSA**: CCSA of components that are thicker than few millimeters up to 2-3 cm. These parts cause, when impacted, generation of many additional debris, but in quantity much lower than the previous category. Parts that fall into this category are, for example, solar panels or appendages like rigid booms to support drag augmentation sails. For these areas it is used a *risk factor* value of $RF_2 = 0.1$. This value of risk factor means that if an impact occurs to this type of area, the number of new released debris is 10% of the number that would be created if an impact with same object were occurred in an equal area of *Type 1*.

3. ***Low Energy* CCSA, or *Type 3* CCSA**: CCSA that is very thin (like a sheet or foil) so that, when impacted, it is pierced or cut but it does not lead to significant generation of new debris. At worst, only very few debris would be released. Typical elements falling into this category are thin tethers and thin surfaces of drag augmentation devices. For these areas it is used a *risk factor* value of $RF_3 = 0.001$. This value of *risk factor* means that if an impact occurs to this type of area, the number of new released debris is 0.1% of the number that would be created if an impact with same object were occurred in an equal area of *Type 1*.

The *risk factors* used in all analyses are reasonably assumed, but they are not derived experimentally. Therefore, the values of "weighted" CCSA are not intended to be extremely precise, but at least very reasonable for implementing an effective comparison between the different deorbit solutions. Moreover, it has to be pointed out that the outcome of a collision event, in terms of absolute number of newly generated debris, strongly depends on the size of the impacting debris or meteoroid. An example to make this point clearer is presented.

If a satellite is impacted on its main body by another satellite, i.e. the most catastrophic collision event possible, the number of new debris can reach numbers as high as ten thousands. But if the satellite's body, i.e. a collision area of type 1 (high energy area), is impacted by a very small meteoroid, e.g. with diameter of 1 cm, then an extremely lower number of debris is generated.

For the objective of this thesis, i.e. the comparison between deorbit systems, this is not a problem, since it is used the same impacting object characteristic size R_{ch} and it is chosen a size such that it is expected to create approximately 1000 new debris when impacting a CCSA of *Type 1*, about 100 new debris when impacting a CCSA of *Type 2*, and about only 1 new debris when impacting a CCSA of *Type 3*. The *characteristic radius* R_{ch}, of such impacting object, is reasonably assumed to be $R_{ch} = 5\,\text{cm} = 0.05\,\text{m}$.

For ATP calculation, it is derived a *"Weighted" Collisional Cross-Sectional Area (WCCSA)* for all the different deorbit solutions considered in this work.
The equation used to compute the WCCSA is:

$$WCCSA = RF_1 \cdot CCSA_1 + RF_2 \cdot CCSA_2 + RF_3 \cdot CCSA_3 \tag{3.3}$$

where $CCSA_1$ is the total CCSA of *Type 1* (i.e. total projected area of type 1, augmented using the method described in Eq.[3.2.1]); similarly, also $CCSA_2$ and $CCSA_3$ are defined.

The WCCSA is finally multiplied by the total deorbit time, in order to calculate the ATP of each deorbit system. These ATP values allow the user to implement an effective collision risk comparison. As already stated, the lower is the ATP the lower is the collision risk associated to the use of a certain deorbit system.

3.3 Deorbit using Natural Decay

Software *Stela*® will be employed to model the *natural*, uncontrolled re-entry of the satellite without any deorbit device (i.e. reentry forced only by aerodynamic drag).

It is set a reentry altitude of 120 km for *Stela*® computations. This means that *Stela*® will end its calculations as soon as the altitude of the satellite reaches 120 km. In fact, at this altitude, burn-out of the object rapidly begins and the satellite is progressively destroyed in the atmosphere. For most massive satellites, a controlled reentry must be planned, since they would not be completely consumed during reentry and surviving parts can hit the ground.

The objective of the *Stela*® simulation is to derive the total time required for a satellite to reach 120 km from its initial altitude, with only *aerodynamic drag* as dissipative force acting on it.

The cross-sectional area is set to be constant since the very last phase when burn out begins (and cross-sectional area changes) is not considered in the simulation.

3.3.1 *Stela*® parameters for the LEO simulations

Stela® computes a long-term propagation of the *natural decay* orbit that a generic spacecraft will undergo. The following "General Parameters" are used for all simulations. Between different simulations, only the initial altitude is changed.

- "Single Extrapolation" mode is used. Iterative mode is not required since it performs an iterative search of an initial orbit once set the desired orbit lifetime; instead, in this analysis the initial orbit is already set. Simulations with iterative mode can be useful to compute the initial orbit that a satellite with specific characteristics must have in order to decay in 25 years (maximum deorbit time allowed by guidelines).
- Mass of the spacecraft without deorbit system: 1000 kg.
- The value of *Drag Area* of the spacecraft, used for all simulations, is derived from calculations based on the geometry described in Sec.[3.2]), and shown in Fig.[3.2]. It results a value of $10\,m^2$. For the Drag Coefficient the *Variable(file)* option is chosen, which means that the Drag Coefficient is considered variable with the altitude, following a profile given from a *Stela*® file, based on an empirical equation. The atmospheric density is computed using the empirical model *NRLMSISE-00*.
- The Solar Activity is set to *Mean Constant*. This choice follows what is done in the analysis of deorbit with EDT system, where values for of *electron density* approximately averaged over one complete solar cycle are used.
- Initial orbit parameters are chosen as: (*Mean Parameters*, *Keplerian* type, *Celestial Mean of Date* frame. The only parameter that changes between different simulations is the semi-major axis a of the initial orbit, where $a = h + R_E$ since the eccentricity is always set to zero ($e = 0$ given that in this work only initial circular orbits are considered). All the other parameters, including the orbital inclination, are negligibly influential towards deorbit time via natural decay, so any value could be inserted. In all simulations, they are simply set to zero.
- The simulation duration must be set for a number of years long enough to make sure that the final altitude of 120 km is reached in that maximum orbit propagation time. It could be set 25 years as simulation duration, since 25 years is the maximum time allowed for deorbit by the guideline. It is instead chosen to use 100 years, in order to detect the exact deorbit time also for initial conditions such that the limit of 25 years is surpassed. When initial conditions are such that the final altitude of 120 km is not reached, not even in 100 years, then

the computations stop, returning the message that the object, in the selected simulation time, did not arrive to the final altitude.

- Number of integration steps for each ephemeris step: 1.

The following Advanced Parameters are used:

- Integration step of 24 hours, i.e. the reentry orbit is computed in steps of one day each.
- Reentry altitude: 120 km
- The parameter *TT minus UT1* represents the delay between Terrestrial Dynamic Time (TT or TDT) and the Universal Time (UT1). The default value of 67.184 s is used.
- Only the *Atmospheric Drag* is enabled, all the other perturbations are unchecked (no solar pressure, no third body perturbations, no Earth tesseral perturbation). This is done in order to comply with the absence of those perturbations in computations for the other deorbit systems. The objective of this work is the comparison between different deorbit systems: therefore, the "boundary conditions" should be the same, or as close as possible, in order to reach the most effective comparison.

3.3.2 Results from *Stela*® for Natural Decay

Various simulations are launched with initial altitudes between 300 km and 700 km, with an altitude step between each case of 50 km. The deorbit time, i.e. the time elapsed from the initial altitude until the final altitude of 120 km is reached, is collected for every case and an *Excel*® spreadsheet and diagram is created with the results. Below, it is posted the resulting diagram, showing that for initial altitudes higher than approximately 670 km, with the specific satellite mass and drag area used in these computations, the deorbit time exceeds the maximum of 25 years.

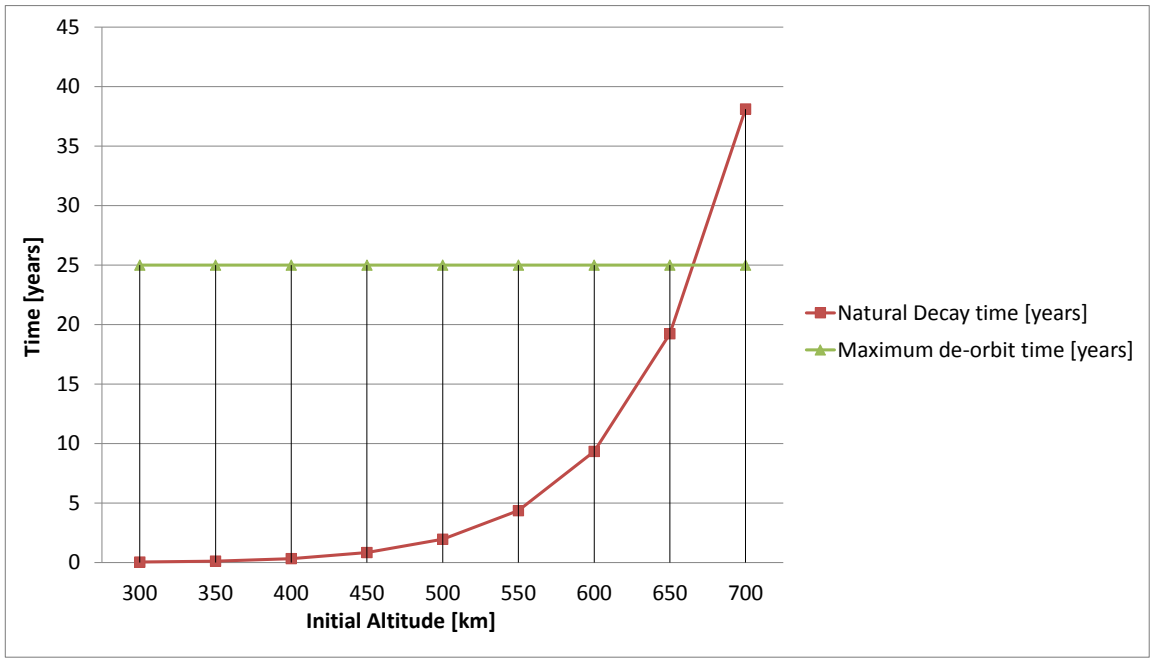

Figure 3.4: *Diagram showing the deorbit time via* Natural Decay *VS initial altitude at which decay starts. Values computed with* Stela®.

Unfortunately, the vast majority of LEO satellites is orbiting above 600 km. Consequently, *natural decay* has a very limited field of application. It is also important to point out that a major competitor of the *natural decay* option, for altitudes lower than 600 km, is the *Chemical Propulsion* deorbit system, due to the extremely lower deorbit times and ATP, the only problem being that it is not cost-free as *natural decay*. More details will be provided in Sec.[3.9].

3.4 Deorbit using Drag Augmentation devices

As already described in Sec.[2.4], two main categories of drag augmentation devices exist, i.e. *inflatable balloons* and *drag sails* supported by rigid booms. Both solutions are analyzed using *Stela*®, with the same identical parameters that were used for the previous case of *natural decay* deorbit. This means that also in this case only the dissipative *aerodynamic drag* is considered in the orbit propagation; all other perturbations are neglected.

The only changes, with respect to the *natural decay* computations, are obviously in the mass (that in this case includes also the additional mass of deorbit system) and the drag area.

A separate *Matlab*® code called 'ATPDragDevices.m' is written in order to compute a good estimate of the added mass due to the drag augmentation system, and the

resulting augmented drag area. This was one by setting in the code the precise dimensions of both the balloon and the drag sail, and the density of materials used for every part of these systems. It is considered, as shape of the main body of the spacecraft projected orthogonal to the drag direction, the one portrayed in Sec.[3.2], with the same identical dimensions. This means to have a drag area for the spacecraft, without deorbit devices, of $10\,\mathrm{m}^2$ and a mass of $1000\,\mathrm{kg}$ (still without deorbit device).

For stability reasons, two balloons or two drag sails are used, placed symmetrically with respect to the spacecraft's body, as shown in Fig.[3.5] and Fig.[3.6].

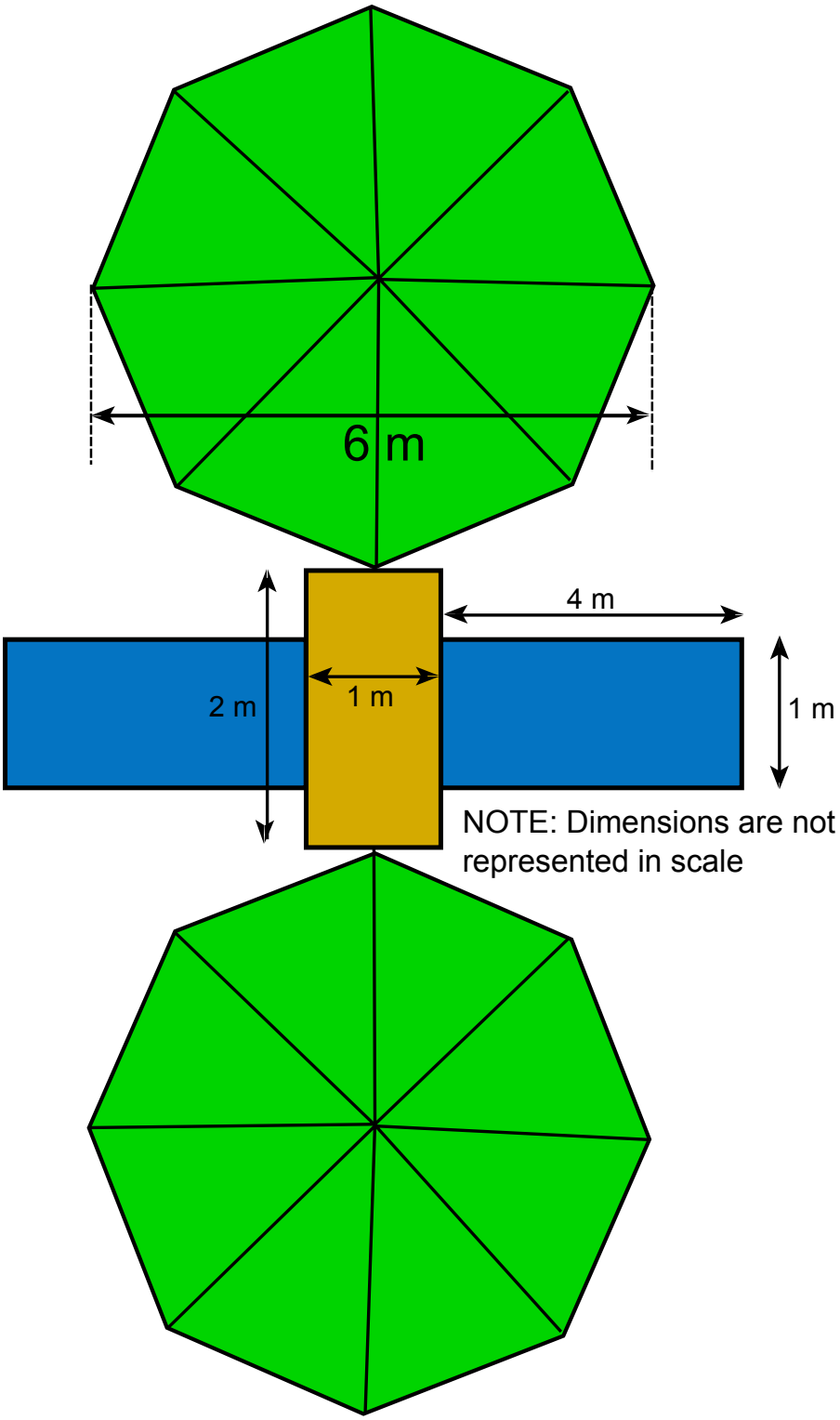

Figure 3.5: *Sketch showing the satellite with* drag sails *mounted on it. Dimensions are specified. Each drag sail is supported by booms and each boom is* 3 m *long; therefore, the characteristic dimension of the sail is* 6 m.

From calculations, it turns out that, when using two octagonal *drag sails* like shown

in the picture above, of characteristic dimension of 6 m (it can be approximately regarded as a diameter), the total drag area of the system (including spacecraft's body drag area) is about 35.93 m^2. This value is then inserted in *Stela*®. The mass of sail plus booms, i.e. the added mass to the spacecraft, is estimated to be about 60 kg, assuming them made of pure Aluminum. A more conservative value of 100 kg is used in *Stela*®, i.e. the total mass of the system is set to 1100 kg. With these values, different *Stela*® simulations are launched varying only the initial altitude. An *Excel*® spreadsheet is created with deorbit time results (time to reach 120 km starting from the initial altitude).

Regarding drag augmentation achieved with a system using two spherical inflated balloons, the configuration shown in the picture below is considered.

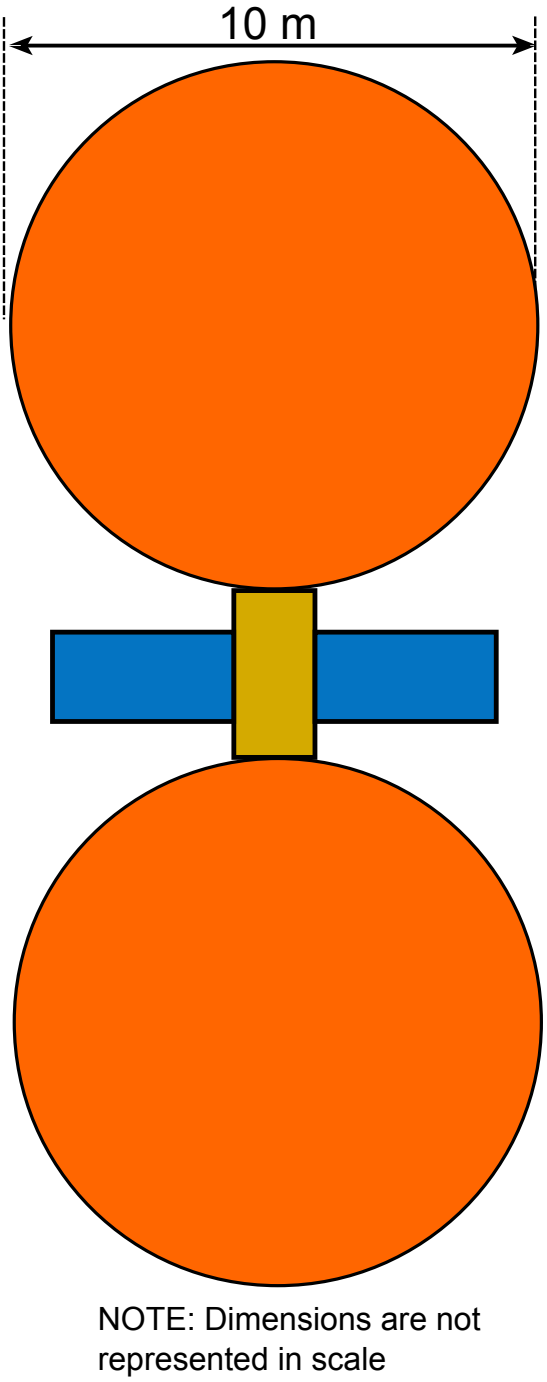

Figure 3.6: *Sketch showing the satellite with* drag balloons *mounted on it. Each spherical balloon, when completely inflated, has a diameter of* 10 m.

This configuration is an extreme configuration, i.e. with a balloon size, with respect to the 1000 kg spacecraft that is extremely large. This size is specifically chosen in order to detect how much influence this consistent augmentation of drag area exerts on deorbit time. It has to be pointed out that the first problem of this system is the very large added mass that such a large balloon, e.g made of Aluminum foil, would imply.

Moreover, there is a considerable mass of compressed gas that is required onboard to inflate the balloon. Additionally, the balloon, if pierced by an impact with a meteoroid or debris, loses internal pressure and progressively crumples up, and as consequence the drag augmentation function is permanently compromised. For all these reasons, the *drag balloon* already starts as a very questionable choice with respect to *drag sails*.

From computation with *Matlab*® code 'ATPDragDevices.m', it is output a total drag area, with this system, of about $167\,m^2$. The added mass, accounting for balloon mass and inflating gas mass (plus related tanks) can be easily around 500 kg, or even more. With such values it is run a series of *Stela*® computations with variable initial altitude, leading to the results displayed in the plot below, together with results for deorbit with *Drag Sail*.

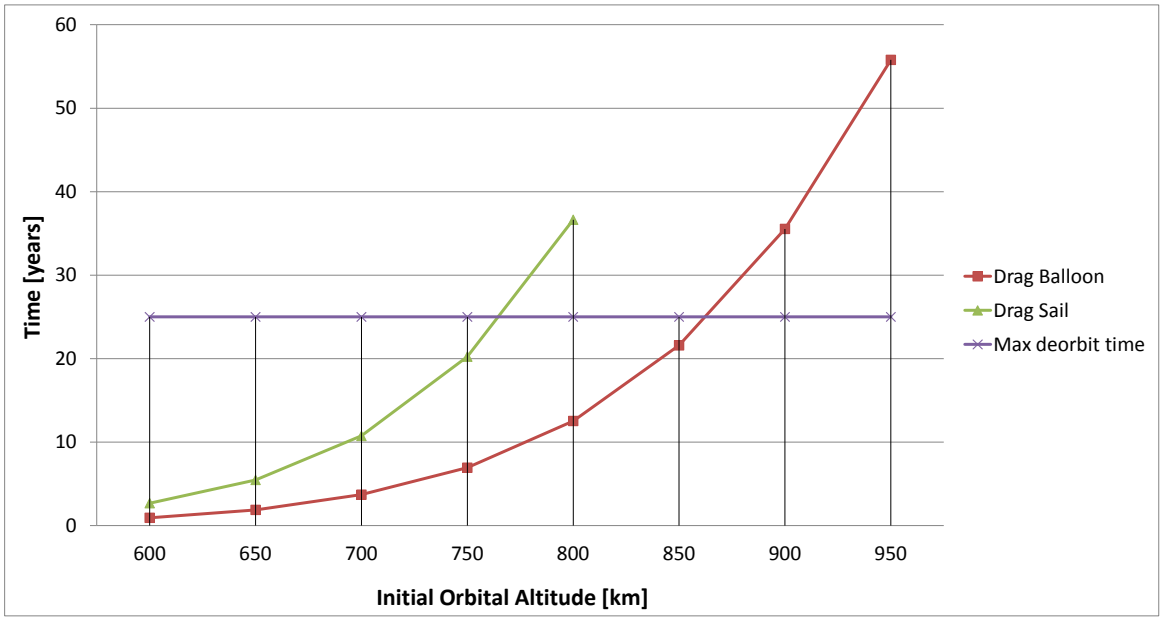

Figure 3.7: *Diagram showing the deorbit time via* Drag Sail *and via* Inflated Balloon *VS initial altitude at which deorbit begins. This* Drag Sail *curve is referred to the configuration with two drag sails for a total drag area of about* $35.93\,m^2$*, as shown in Fig.[3.5]. The* Drag Balloon *curve is referred to the configuration with two balloons for a total drag area of about* $167\,m^2$*, as shown in Fig.[3.6]. The maximum deorbit time allowed by the guidelines, i.e. 25 years, is displayed too. Values of deorbit time computed with* Stela®.

Facts to be highlighted from the previous diagram are:

- for initial altitudes higher than about 770 km, the deorbit time with *drag sail* exceeds the 25 years maximum. Therefore, above this altitude, *drag sail* cannot be used.
- for initial altitudes higher than about 870 km, the deorbit time with *drag balloon* exceeds the 25 years maximum. Therefore, above this altitude, *drag balloon* cannot be used.

- even with a very consistent augmentation of drag area, from *drag sail* to *drag balloon* (i.e. from about $35\,m^2$, for the first, to about $167\,m^2$ for the second) there is not much difference in deorbit times, that are always very high, in both cases, for altitudes above 700 km. Also the difference in altitude, above which the 25 years constraint is violated, is limited. All of this suggests the fact that even by augmenting the drag area to the maximum technologically feasible values, the deorbit performance does not change so much.

3.5 Deorbit using Electrical Propulsion (EP)

The additional hardware mass that is required to sustain the EP system is estimated as about 30 kg, including additional attitude control hardware and additional solar panels, plus deployment mechanism, since the satellite at its end of life is almost surely completely defunct both from the power and the attitude control standpoints, as already mentioned in Sec.[2.3]. This mass is then added to the mass of the EP system itself, and to the Xenon propellant mass, in order to compute the total additional mass that would be required to implement deorbit with an EP system, based on the chosen *SPT-70 Hall Thruster*.

In the calculation of CCSA (see Sec.[3.2.1]), the exposed area of additional solar panels, deployed at the end of life, is considered too. This area is a *Type 2* area, and will be therefore associated to a *risk factor* $RF_2 = 0.1$. Refer to Sec.[3.2.2] for description of *risk factors*.

3.6 Deorbit using Chemical Propulsion

Chemical Propulsion is, from the deorbit time and ATP point of views, always the best option for deorbit, since it is a *direct* deorbit method. Consequently:

- it ensures the shortest deorbit time possible
- no additional device that causes augmentation of collisional area (CCSA) is used. Therefore also the CCSA is minimum (equal to the CCSA of the satellite without deorbit system).

From these two features, it obviously turns out that also the ATP is the minimum possible among all deorbit systems. Moreover, as previously mentioned in Sec.[2.2], a CP system is generally always present onboard a LEO satellite. Hence, the dry mass of the system normally has not to be accounted as additional mass for deorbit.

In the comparison plots presented in Sec.[3.9], the *Chemical Propulsion* is added only in additional mass plots. In deorbit time and ATP plots it would not make sense to add it since it is already known that it has a much lower deorbit time and ATP than all the other systems.

The biggest problem of CP for deorbit is the very large mass of additional propellant to carry onboard, as already mentioned in Sec.[2.2]. This added mass, above a certain initial altitude, can be much higher than the added mass using other deorbit systems.

It is also worth to note that there is a considerable risk associated to the onboard storage of such a large mass of propellant for many years, until the end of life of the vehicle when deorbit starts. Rules of debris mitigation set by the guidelines strongly suggest the depletion of any remaining stored propellant after the end of life of the mission: a procedure called *passivation*. This should be done in order to minimize the risk of explosions in space due to impacts with meteoroids or debris, even of very small size, piercing the propellant tanks. A *passivated* satellite, if impacted by a very small meteoroid or debris, would generate only a few additional debris; conversely, a satellite with a large mass of propellant onboard can easily be subjected to a catastrophic explosion generating thousands of new debris. Deorbit phase, with *chemical propulsion*, lasts for a very short time; consequently, the probability of impacts during deorbit is extremely low with respect to other solutions. However, the major problem is that a large mass of propellant (normally always higher than 150 kg) has to be stored onboard for years, i.e. for the entire lifetime of the satellite. Hence, the major risk is associated to the period of mission life, not to the very short deorbit time.

3.7 Deorbit using ED Tether system

The analysis (with *Matlab*® personal codes) of the reentry using an Electro-Dynamic Tether system is performed using these specific assumptions:

1. The tether's length given in input for electrodynamic computations is the length of the bare conductive segment of tether. An inert segment is considered too, for dynamic stability, but is accounted only in mass calculations being it uninfluential in the electrodynamic process.
2. As already described in Sec. [2.5.3], the magnetic field is assumed to be co-rotating with the Earth, i.e. the magnetic field velocity vector $\vec{v}_B$ is tangent to a circle whose radius is the local distance between spacecraft location and Earth's spin axis and whose plane is parallel to the equatorial plane. See Fig. [2.12] at pg. 50.
3. The tether geometry is such that the Orbital Motion Limited (OML) theory can be applied with sufficient accuracy. As from Ref.[7], in LEO orbits the plasma Debye length λ_d reaches a minimum value of 3 mm in daytime conditions. For a thin tape tether the equivalent radius is about one-fourth of the tape width. OML current collection theory is valid for tethers whose equivalent radius is lower than λ_d. Tape tethers of up to 1.2 cm of width would then comply with the OML regime. In the present analysis it is considered a tether 2 cm or 3 cm wide, hence an approximation is made by considering electron collection in OML regime. However, this approximation is surely legitimate and does not affect significantly the precision of the analysis or, anyhow, it does not affect the analysis more than

other assumptions that were already taken.

4. The tether is assumed to be already completely deployed when deorbit simulation begins, and constantly aligned along the local vertical direction, stabilized and kept straight by *gravitational gradient*. Transient phases (such as tether deployment) and in general the tether's lateral dynamics, such as bowing of the tether and tether oscillations, will not be considered in this work.

5. The EDT system is modeled as a *rigid dumbbell*: this means that the tether is considered as a rigid (non-extensible and non-flexible) structure. In reality, the dynamics of the tether are indeed complex and will not be described in detail in this work. In this work the tether is treated as a rigid body: the name "rigid dumbbell" is used simply due to the fact that the tether plus the two masses at each end make the system looking similar to a dumbbell.

6. As already described, the tether interacts with the environment plasma with local electron density N_e, with the local magnetic field $\vec{B}$, and moves with relative velocity $\vec{v}_{rel}$ with respect to the magnetic field. N_e, $\vec{B}$ and $\vec{v}_{rel}$ are considered constant all along the tether. Generally, this is an optimal approximation since these parameters do not vary significantly along a tether of length 3–5 km.

7. The *electron density* N_e, at every location in space, is dependent on *solar flux*. It is decided to use the values of N_e correspondent to a Julian Day when solar flux is as close as possible to the average value over a typical solar cycle, lasting approximately 11 years. Further details are reported in Appendix [F].

8. Deorbit is assumed to occur in a *quasi-circular* path. This means that between one computational time step and the subsequent, the orbit radius decreases, but at the single specific time step the current orbit is assumed to be circular. Circular initial orbits are assumed for every case, as already stated in Sec.[3.1].

9. No impedance Z_l for power generation purposes is applied at the cathodic end, i.e. $Z_l = 0$.

10. A reasonable value of 20 kg is used as endmass, with the 1000 kg satellite considered in all analyses. The endmass should be higher the greater is the satellite's mass. It is wise to use as part of the endmass the components of the EDT system that are not required to be kept attached to the satellite, e.g. the deployment system. Therefore, it is used a ballast mass that is obtained subtracting the mass of every component of the EDT that is used as endmass, from the endmass target value of 20 kg. This strategic choice would lead to mass savings, with the EDT system, up to 10 kg–15 kg.

11. *Small ohmic effects* are assumed along the tether, i.e. it is assumed that the ohmic impedance (electrical resistance) along the conductive tether, made of Aluminum alloy, is small compared to the impedance of the "electrical path" between the ambient plasma and the bare tether itself. This impedance regulates the amount of electrons per unit length that the tether is capable of collecting (the lower this impedance, the higher amount of electrons is collected, and higher current is generated along the tether).

12. The EDT system employs Xenon as ionization gas for ejection of electrons at the cathodic emitter (*hollow cathode*). It is known the mass flow rate of Xenon once the hollow cathode is chosen. Larger cathodes obviously use a higher mass flow rate of Xenon. After selecting the type of cathode, following the procedure described later in Sec.[3.7.1] (depending on the average current value at the first iteration), the mass flow rate is set. The total mass of Xenon required for deorbit is then simply calculated by multiplying the Xenon mass flow rate by the deorbit time computed by the 'MAIN_mod.m' code and returned in the core code 'DIAGRAMS.m'. This mass of Xenon is then added to the total additional mass due to the presence of the deorbit system onboard, used for the comparison described in Sec.[3.9.3].

A further improvement would be to consider a variable current along the tether, and therefore local contributions to the Lorentz drag force that vary along the tether's length. This would mean to compute at every point of the tether the *local potential bias*, i.e. the electrical potential difference between each point of the tether and the surrounding plasma, and the *current profile*, i.e. the current flowing at each specific point of the tether. For this work, such level of accuracy would be unnecessary with all the assumptions already taken; therefore, it is calculated directly the total Lorentz force acting on the entire system using a value of current averaged along the tether.

The code used for the EDT deorbit computation can accept any initial orbital altitude (limited to the LEO region) and inclination (that is assumed to remain constant throughout the deorbit). As from Ref. [12] at pg. 203, orbits are categorized as *prograde* when the orbit inclination is in the range $0° < i < 90°$, or *retrograde* when $90° < i < 180°$. An orbit with an exact inclination of $90°$ is called *polar* orbit. For *prograde* orbits, the satellite revolves in the same direction as the Earth; for *retrograde* orbits the satellites revolves in the opposite direction with respect to the Earth's spin rotation. In fact, the *Matlab*® code does accept inclinations in the range $0° \leq i \leq 180°$, i.e. the range that covers all the possible orbits. It is not necessary to tell the code whether the orbit is *prograde* or *retrograde*. Any orbit with input inclination $0° < i_0 < 90°$ is automatically treated as *prograde* by the code and the configuration of deployment for *prograde* orbits, described in Sec.[2.5.4], is used. Any orbit with input initial inclination $90° < i_0 < 180°$ is automatically treated as *retrograde* by the code, and the configuration of deployment for *retrograde* orbits, described in Sec.[2.5.4], is used.

The velocity vector in CGOR coordinates (see Appendix [C])will always be $[0, v, 0]$ both for *prograde* and *retrograde* orbits, since v is assumed to always be oriented following the right-hand rule with respect to the normal to the orbital plane.

As already mentioned in Sec. [2.5.4], the code for the EDT analysis has to account of two problems:

1. **$\mathbf{E_t}$ can change in sign during deorbit**, in a certain inclination range: this problem affects orbits with $68° \lessapprox i \lessapprox 96°$, as detected by analyzing several cases

with the code.
The code will overcome with this problem in this way:

- First of all, in the "problematic" inclination range $68° \lessapprox i \lessapprox 96°$, the configuration of the tether is chosen to be either *prograde* or *retrograde* according to the number of times E_t is positive or negative during the deorbit phase. If the number of times E_t is positive is higher than the number of times E_t is negative, then the *prograde* configuration, with upwards deployment, is selected. Viceversa, if the number of times E_t is positive is lower than the number of times E_t is negative, then the *retrograde* configuration is automatically selected.
  From computations, it also turn out that for *prograde* orbits with inclination in the range $86° \lessapprox i < 90°$ the number of times E_t is negative exceeds the number of times E_t is positive. This fact means that it is not strictly true that for every *prograde* orbit the most convenient option is to deploy the tether upwards. In fact, in the small inclination range reported above it is more convenient to deploy downwards, i.e. to use the *retrograde* EDT system configuration, even if the orbit is classified as *prograde*, being the inclination lower than 90°.

- Thereafter, once the tether configuration is chosen, and of course maintained for the entire deorbit, it is also set the only acceptable direction along which current can flow. In fact, it is reasonably assumed that current can develop and flow only in one way, since in the other way there is no cathode at the end, therefore the current would be so small that it can be surely neglected.
  Consequently, it is absolutely reasonable to set $E_t = 0$, at every computational step when E_t is opposite with respect to the nominal direction (i.e. direction that E_t should have according to the tether configuration). This is done in the code with an 'if' routine. For any iteration step when E_t is set to zero, no current (and therefore no Lorentz force) will be generated in that specific step of the deorbit phase.

2. **$\mathbf{E_t}$ has very low value in certain conditions**. The *asympotic solution* for the average current calculation, used in the code, (see Ref. [7] and Sec.[3.7.2] of this work) encounters problems when E_t has a very low value. The method uses the non-dimensional potential drop at the cathode $v_{HC} = \frac{\Delta V_{HC}}{E_t L}$, and is reported to provide enough accuracy for $v_{HC} < 0.1$. A reasonable estimate of the dimensional potential drop at the cathode is $\Delta V_{HC} = 10\,\mathrm{V}$.
   Given that E_t is at the denominator in the v_{HC} expression, when it has a very low value, v_{HC} as consequence exceeds 0.1, or even 1 in some cases. In all cases when $v_{HC} > 1$ the code gives computational problems since square roots of negative values appear: therefore, a dimensional computation should be performed instead of the non-dimensional one, described in Ref.[7] and used in this work. However, in all cases when E_t is so low that $v_{HC} > 1$, it means that the generated current, and consequent Lorentz force, is absolutely negligible. Eventually, for all these reasons, it is chosen to simply set $E_t = 0$ at every computational step

when $v_{HC} > 1$.
A routine is also implemented to count how many time steps, during a certain deorbit case, show a value of $v_{HC} > 1$. This occurs more and more frequently as the orbital inclination approaches the inclination of the magnetic dipole axis. For inclinations higher than 30°, depending also on the orbital altitude, this problem starts to occur. A longer tether would of course partially heal the problem: the longer is the tether, in fact, the higher is the product $E_t L$ and therefore the lower is v_{HC} (with fixed ΔV_{HC} and E_t).

Moreover, even if all cases with $v_{HC} > 1$ are "filtered out", another issue of the code is that for values of $v_{HC} < 1$ but close to 1, the calculation of the ξ_B location returns a value greater than 1 which is not acceptable since ξ_B is the non-dimensional location of the zero-bias point B, i.e. $\xi_B = \frac{x_B}{L}$ and of course x_B cannot be greater than L. Therefore, also in every computation step when $\xi_B > 1$, again due to low values of E_t, the code bypasses the problem by reasonably setting the $E_t = 0$ and non-dimensional current $i_{av} = 0$. Also in this case, the error introduced is very small since these bypassed steps are steps when the average current along the tether is so low, that the resulting Lorentz drag force is negligible.

For a thorough dynamics analysis of deorbit with EDT, an even more complex (and computationally "heavy") numerical model is required. This is beyond the scope of this work. Such model would include extension and flexural modes, i.e. it would use a tether modeled as an extensible and flexible structure. Studies about lateral dynamics of the tether and its stability are reported in Ref.[39] and [32].

As a "rule of thumb", the closer is the orbital inclination to the magnetic dipole axis inclination, the longer should the tether be in order to maintain the same deorbit time. Anyhow, for orbits with inclinations between about 70° and 110° excessively long tethers would be required in order to reach the same deorbit times as with lower inclinations. Having tethers longer than 6 km is not recommendable due to various factors, such as increase in risk of seizure and of generating new debris, and higher mass to carry onboard. Therefore, it has to be accepted a higher deorbit time, that is, however, not so high compared to the 25 years guideline (maximum deorbit time with EDT is about 1.3 years with the parameters used in this work). Refer to Sec.[3.9.1] for discussion about deorbit times resulting from computations.

In Appendix [B] it is also demonstrated the full compliance of tethers, that are maximum 6 km long, as considered in this thesis work, with the NASA guideline regarding debris potentially released in space, due to cut of the tether caused by impact with a debris or meteoroid.

3.7.1 Cathode Selection and consequent Current Limitation

The electrons flowing along the tether, generating the current, are emitted back to space once they reach the cathodic end, using a *hollow cathode* that employs Xenon as ionization gas (in very low mass flow rates), in order to exert its function. The Xenon consumption (i.e. its mass flow rate) strictly depends on the size of the cathode, that in turn depends on the average current that has to be ejected back to space (in terms of electrons flow rate). It is decided to use cathodes that support a maximum current of 2 A, since higher currents would lead to a more difficult current and tether's stability control, with more complex and massive components required. For the ProSEDS mission, already mentioned in Sec.[2.5.2], a cathode supporting a maximum current of 5 A was designed. However, this mission was designed for very low orbital altitudes (about 300 km) and mainly for scientific experiments, not for deorbit application. Such a high current would never be used for deorbit.

By running different computations, it is seen that, for higher altitudes, the generated current is almost always lower than 1 A. Only to give an idea, for a bare conductive tether of dimensions 5 km × 2 cm × 50 μm the current is lower than 1 A for initial altitudes higher than about 1100–1150 km. Conversely, for progressively lower altitude, due the electron density increase, the current constantly increases, reaching values even higher than 5 A in the lowest altitudes region.

It is then decided to implement in the code two different options for the cathode: either a smaller cathode, supporting a maximum current of 1 A, or a larger cathode, supporting a maximum current of 2 A. The choice is done in relation to the value of current generated along the tether at the initial altitude where deorbit starts (i.e. at the first iteration step of the code). If the current generated at the first deorbit time step is higher than 1 A, the choice is the larger cathode, supporting a maximum of 2 A as tether current. This larger cathode consumes a mass flow rate of Xenon of 0.098 mg/s. Instead, if the first iteration current is detected to be lower than 1 A, as happens for higher altitudes where the electron density is lower, then the smaller cathode is chosen by the code, that will then use a lower Xenon mass flow rate equal to 0.059 mg/s. Mass flow rate data were acquired from cathode manufacturers. Given that the cathode cannot vary its properties during deorbit, once the decision of what cathode to use is taken, the maximum current and the Xenon mass flow rate are maintained fixed for the entire deorbit.

Consequently, if the satellite starts to be deorbited at very high altitudes, such as 1450 km it will surely have a 1 A cathode; then, anytime the current along the tether becomes higher than 1 A during descent, it will be cut off to 1 A using a current limiter mounted on the EDT system. From the computational standpoint, the cathode selection and the current limit are implemented using a nested 'if' cycle and a nested 'switch' cycle (in the 'EDTCalculation.m' code).

The choice of the cathode is then a compromise between mass and deorbit performance:

choosing the smaller cathode would mean having lower Xenon mass, but higher deorbit times; the opposite happens choosing the larger cathode.

The code also enables the possibility of using a new technology of cathode without need of consumables: an example is the *Field Emitter Array Cathode (FEAC)* technology, described in Sec.[2.5.2]. In this case, there is no propellant mass to be added to the system, consequently leading to a significant mass saving.

3.7.2 Average current computation

The *Matlab*® code 'EDTCalculation.m' computes the *average current* I_{av}, at every time step, at every location along the deorbit path. The routine employs the *aysmptotic expansion method*, presented in Ref.[7], assuming *small ohmic effects* along the tether, as already mentioned above in Sec.[3.7].

The *average non-dimensional current* along the tether is given by:

$$i_{av} = \int_0^{\xi_B} i_a d\xi + \int_{\xi_B}^1 i_c d\xi \tag{3.4}$$

where i_a is the current flowing in the *anodic* part of the tether, and i_c is the current flowing in the *cathodic* part. ξ is the non-dimensional location along the tether, i.e.:

$$\xi = \frac{x}{L} \tag{3.5}$$

and then ξ_B is the non-dimensional location of the zero-bias point B.

The integral reported above, in case of *small ohmic effects*, can be effectively approximated with the asymptotic expansion:

$$i_{av}^S \approx i_{av0} + \epsilon i_{av1} + \epsilon^2 i_{av2} \tag{3.6}$$

where

$$\epsilon = \frac{I_{ch}}{I_{sc}} \tag{3.7}$$

being $I_{sc} = \sigma A E_t$ the *short circuit current* (σ is the electrical conductivity of the tether material, A the cross-sectional area, E_t the electrical field component along the tether). The *characteristic current* I_{ch} is defined as:

$$I_{ch} = \frac{2}{3}\frac{pN_e}{\pi}\sqrt{\frac{2E_t q_e^3 L^3}{m_e}} \tag{3.8}$$

and the other terms for the i_{av}^S equation are defined as:

$$i_{av0} = \frac{\xi_B^{3/2}(5 - 2\xi_B) - 2\mu(1 - \xi_B)^{5/2}}{5} \tag{3.9}$$

$$i_{av1} = \frac{1}{40}[7\xi_B^4 - 16\xi_B^3 + 8\mu\xi_B^{3/2}(1 - \xi_B)^{5/2} - \mu^2(1 - \xi_B)^4] \tag{3.10}$$

$$i_{av2} = \frac{1}{4400}[\xi_B^{9/2}(319 - 130\xi_B) - 132\mu\xi_B^3(1 - xi_B)^{5/2} + 2\mu^3(1 - xi_B)^{11/2}] \tag{3.11}$$

The non-dimensional location of zero-bias point B, with the assumption of *small ohmic effects*, can be estimated using another asymptotic expansion:

$$\xi_B^S \approx \xi_{B0} + \epsilon\xi_{B1} + \epsilon^2\xi_{B2} \tag{3.12}$$

where

$$\xi_{B0} = 1 - v_{HC} \tag{3.13}$$

$$\xi_{B1} = -v_{HC}(1 - v_{HC})^{3/2} + \frac{2}{5}\mu v_{HC}^{5/2} \tag{3.14}$$

$$\xi_{B2} = -\frac{3}{10}v_{HC}(1 - v_{HC})^2(2 - 7v_{HC}) + \frac{3}{5}\mu v_{HC}^{5/2}(2 - 3v_{HC})(1 - v_{HC})^{1/2} - \frac{3}{8}\mu^2 v_{HC}^4 \tag{3.15}$$

Lastly, the parameters μ (known as *mass ratio*)and v_{HC} (non-dimensional potential drop at the cathode) are defined.

$$\mu = \sqrt{\frac{m_e}{m_i}} \tag{3.16}$$

$$v_{HC} = \frac{\Delta V_{HC}}{E_t L} \tag{3.17}$$

m_i is the mass of the most abundant ion species at a certain altitude, and m_e is the electron mass. In the LEO region, over 1000 km the dominant species is H+ (atomic Hydrogen ions), whereas below 1000 km it is O+ (atomic Oxigen ions).
In the code, it is used a value of $\Delta V_{HC} = 10\,\mathrm{V}$ as dimensional potential drop at the cathode.

3.8 Output data validation

3.8.1 Validation of magnetic field data using NASA applet

It is used the applet found at Web Ref.[5] by NASA, in order to verify to correctness of the values of geomagnetic field used in the computations of this work, from the

personally written *Matlab*® code, called 'magnetGP.m'. This code loads the *Schmidt Quasi-Normalized* coefficients from the IGRF-2010 model and then computes the geomagnetic components, following the procedure described in detail in Appendix [E]. The personal code accounts for the highest number of harmonics available in the IGRF model (degree up to 13 and order up to 13). Therefore, results should be very accurate.

This code requires, as inputs, the altitude, the longitude (East from Greenwich), and the co-latitude (South from North Pole) of the location in space where it is desired to compute the magnetic field components. Different cases are computed with both the personal code and the NASA applet, for an exhaustive comparison. They are reported in the image below, together with the results.

Date	Altitude [km]	Longitude [deg]	Latitude [deg]	Magnitude of magnetic field [T] from NASA applet	Magnitude of magnetic field [T] from personal code 'magnetGP.m'
Jan 1st, 2010	600	0	0	2.2955E-05	2.3043E-05
Jan 1st, 2010	1100	0	0	1.8103E-05	1.8170E-05
Jan 1st, 2010	500	10	20	2.8503E-05	2.8612E-05
Jan 1st, 2010	1000	10	20	2.2541E-05	2.2627E-05
Jan 1st, 2010	700	60	40	3.6385E-05	3.6422E-05
Jan 1st, 2010	1200	60	40	2.9213E-05	2.9251E-05
Jan 1st, 2010	800	90	90	4.0991E-05	4.0776E-05
Jan 1st, 2010	1300	90	90	3.3896E-05	3.3734E-05

Figure 3.8: *Table reporting the magnitude of geomagnetic field in different cases, calculated with NASA applet and with personal* Matlab® *code, in order to validate this personal code. The inputs of each case are: date and location coordinates in terms of altitude, longitude and latitude (converted to co-latitude for the personal code input)*

As displayed in the table, values from NASA applet are very close to values output from the *Matlab*® code. The NASA applet did not allow to specify the date, instead the personal *Matlab*® code did support secular variations depending on the specific date after January 1st,2010. Here it was used January 1st, 2010 as date for all computations; consequently secular variations were not used since data of IGRF-2010 is computed precisely for January 1st 2010. It is normal to have a very small difference between results from the two sources, but this difference is absolutely negligible, and results from the personal code are then successfully validated.

In conclusion, the computation of geomagnetic field in the personal code 'magnetGP.m', used for the analysis of deorbit with EDT, is proven to be correct and very accurate.

3.8.2 Validation of Electron Density data

The personal *Matlab*® code, for EDT deorbit analysis, requires also the *electron density* N_e, that is loaded in the function 'EDTCalculation.m' that calls the ancillary function 'ElectronDensityGP.m' using the data from file 'IonosphereDataGP.m'. The file 'IonosphereData.m' (then renamed 'IonosphereDataGP.m') is computed extracting data from the IRI database, by compiling the *Fortran* routine 'Map.f90'. All of this is explained in detail in Appendix [D] and [F].

It is performed a verification check to ensure that data for N_e used in the code is correct. This check is based on the comparison between values of N_e output from the code, and from a NASA applet that implements calculations from the IRI database (see Web Ref.[7]).

The values of *electron density*, above 200 km of altitude, typically range between the order of 10^9 and $10^{12}\,\mathrm{m}^{-3}$, with a peak at about 300 km altitude, and values dependent on solar flux (in addition to night/day excursions). Refer to Fig.[2.10] pg. 47.

Several computations of N_e with the NASA applet and the *Matlab*® code are performed. There is often a difference between values at same date and location in space, but the order is usually always the same, or anyhow any value of N_e from the personal code is constrained in the range of orders between 10^9 and $10^{12}\,\mathrm{m}^{-3}$, as expected. Small differences in values are not important for validation purposes, since they are surely due to how the solar flux and other environmental variables are defined in the NASA applet with respect to the personal code. In fact, solar flux has a very strong influence on electron density.

In conclusion, also the *Matlab*® codes for *electron density* computation, from IRI database, are successfully validated.

3.8.3 Validation of deorbit times

Deorbit times with *Electrical Propulsion* are validated using data from literature about propulsion, such as Ref.[15]. Deorbit times for ED Tether are validated by comparison with data from Ref.[8]. Collisional cross-sectional areas are accurately computed and return perfectly reasonable values. Additional mass calculations are precisely performed too, and match with data from literature. Therefore, once all the previous quantities are validated, the entire set of personal *Matlab*® codes for single cases analysis, and for multiple cases analysis plus diagrams computation, can be considered fully validated.

Comparison of EDT deorbit times with data from Ref.[8]

The diagram in Fig.[4] of Ref.[8] is considered the most reliable reference for deorbit times with EDT system, for variable orbital inclination. Only the inclination range between 0° and 100° is considered in this thesis (the same is done in Ref.[8]), since in LEO region the number of satellites in *retrograde* orbits with $i > 100°$ is extremely low. Increasing inclination, the last large cluster of satellites that is encountered are satellites on Sun-Synchronous orbits, with inclination of about 98°. See Fig.[1.10] as useful reference.

Moreover, it has to be pointed out that the diagram for inclinations between 90° and 180°, i.e. for *retrograde* orbits, is symmetrically very similar, as first approximation, to the profile at inclinations between 0° and 90°, i.e. for *prograde* orbits. The situation is even more advantageous for *retrograde* orbits, due to higher relative velocities between the spacecraft and geomagnetic field. This is due to the fact that in *retrograde* orbits the spacecrafts is orbiting with a component that is opposite with respect to Earth's spin rotation, and consequently opposite to the local linear velocity vector v_B of the magnetic field. See Fig.[2.12] and [2.13], pg. 50 and 55, as references for the visualization of spacecraft velocity and magnetic field velocity vectors. This fact results in slightly lower deorbit times for *retrograde* orbits, with respect to the corresponding symmetrical *prograde* orbits.

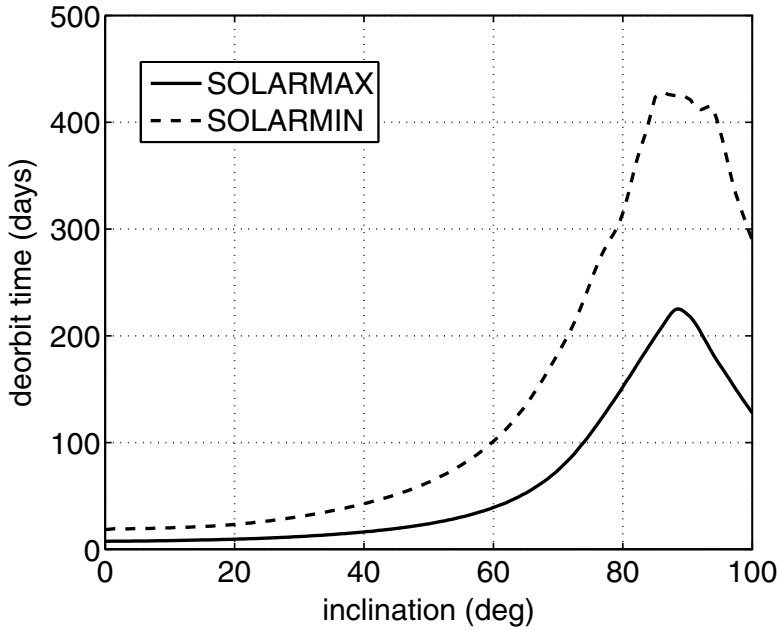

Figure 3.9: *Deorbit time VS Inclination, from* 1000 km *to* 500 km *with a* real *perfectly aligned tether of dimensions* $5\,\text{km} \times 2\,\text{cm} \times 50\,\mu\text{m}$. *From Ref. [8]*

A plot is created with both results from my code and results shown in Fig. [3.9]. Values from Fig.[3.9] are "visually" extracted and then manually inserted in the personal code, in order to plot them together, as shown below.

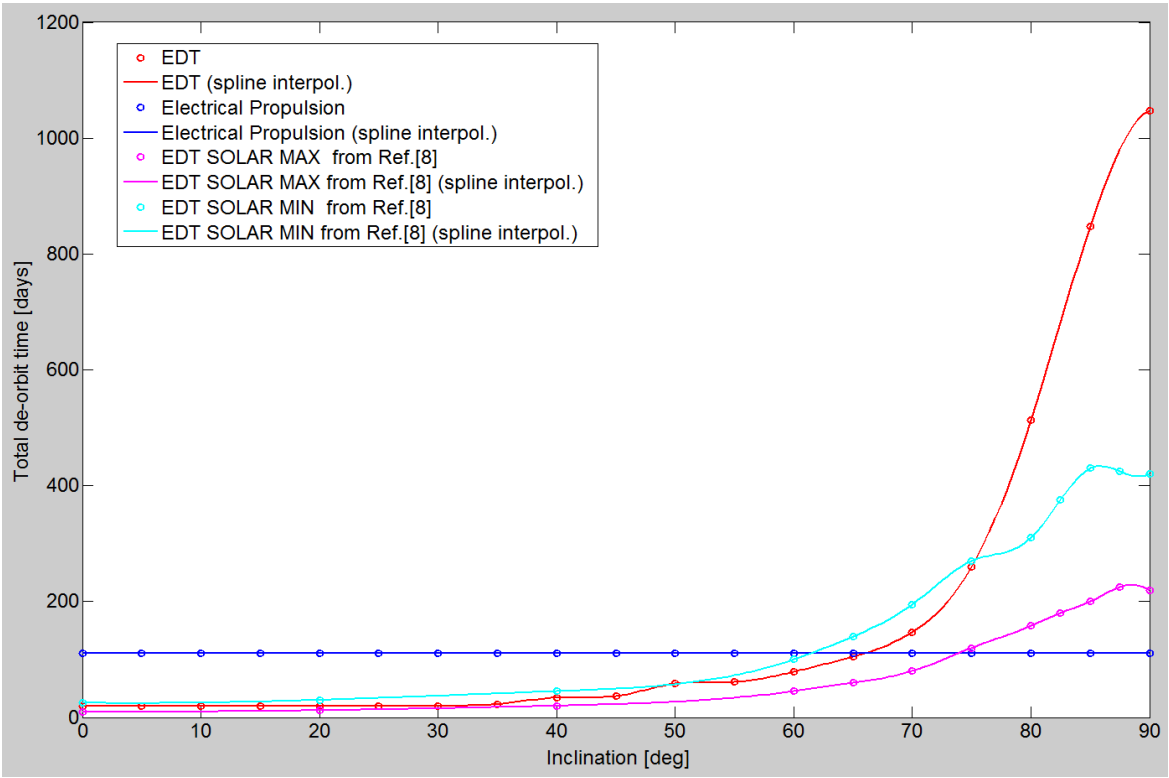

Figure 3.10: *Deorbit time VS Inclination, from* 1000 km *to* 500 km *with a* real *perfectly aligned tether of dimensions* 5 km × 2 cm × 50 μm. *In the diagrams different curves are plot: as shown in the legend, curves from both the personal code and Ref. [8] are present in order to allow a direct visual comparison*

The simulation with my code was performed using the same initial conditions and EDT system parameters as the ones used in Ref.[8]. Instead, different values are surely used for electron density and geomagnetic field. Therefore, small differences in the outputs are normal. In particular, the electron density, in my code, was considered constant throughout the deorbit and computed in a Julian Day at which solar flux has an average value over a complete solar cycle, as described in Appendix [F]. In fact, the curve from my code, for $i \lessapprox 75°$ is located in between the two curves from Ref.[8], that are calculated for either minimum and maximum solar flux. Therefore, for this reason, and also for the fact that all curves (from my code and from Ref.[8]) are very close, it is possible to conclude that my personal code is successfully validated for inclinations below 70°–75°.

For inclinations higher than 75° the values of deorbit time output from the personal code are higher with respect to the values from Ref.[8]. The fact that deorbit times are higher for high inclinations is discussed in Sec.[3.9.1]. Talking instead about the difference between the two codes, upon thorough investigation about this issue, it is found out that this difference in results is due partially to the assumptions taken in my analysis and partially to the method used for the average current computation. In the model from Ref.[8], the orbital inclination was considered variable during deorbit, not constant as in my model. Therefore, a satellite starting from high initial

inclinations might progressively drift towards more favorable lower inclinations. This of course results in a considerably lower deorbit time, since there is a very consistent increment in typical Lorentz force values, even just decreasing the orbital inclination of few degrees.
The other source of deviation at high inclinations is the *asymptotic expansion* method, used for the *average current* calculation. A proof of this fact is that also from computational analysis by D.Zanutto (see discussion in Ref.[39], [41], [40] where, however, results for high inclinations are not posted), using this same method, problems were detected at high inclinations.

Consequently, it is decided to consider results from the personal code for inclinations up to 70° and then to perform an extrapolation of results for higher inclinations, based on results reported in Ref.[8]), the most reliable reference, where the most complex and full model for EDT system analysis was implemented. The extrapolation was performed for inclinations between 70° and 100°, and in the range of initial altitudes between 600 km to 1500 km.

3.9 Results and comparison

The final objective of this work is to implement a thorough comparison between the different deorbit systems, that have been discussed in detail in Chapter [2] and in the sections above of the current chapter. The comparison, as already described, is based on these main drivers:

1. **Total time of deorbit**, remembering that the constraint of 25 years from guidelines must be, in any case, respected. Consequently, in case that, with a certain deorbit system, the deorbit time is higher than this time limit, that deorbit system must be automatically discarded as a non-acceptable solution, for the specific initial altitude and inclination at which deorbit starts.
2. **Additional mass due to deorbit**, including all components and consumables added in order to deorbit the spacecraft. In other words, this is the mass that, if deorbit were not implemented, would not be present onboard.
   The added mass of course should be as low as possible.
3. **Risk of collision** and consequent generation of new debris. This is evaluated using, as most significant parameter, the *"Weighted" Collisional Area Time Product (WCCSA)*, described in Section [3.2].
4. **Technology Readiness Level (TRL)**. This parameter, for all deorbit systems analyzed in this work, can be found in Ref.[22]. Both NASA and DoD (US Department of Defense) TRL levels are posted below.

Deorbiting Technology for LEO Satellites	Electrodynamic Tether *	Electrical Propulsion with SPT-70 Hall thruster	Non-Inflatable thin Drag Aumentation Device supported by booms **	Inflatable thin Drag Aumentation Device (balloon) **	Direct De-Orbit using Chemical Propulsion (monopropellant hydrazine) ***	Natural Decay **
NASA & DoD TRL Level	6-7	9	5	5	9	NA

Figure 3.11: TRL levels *are posted below for all the different deorbit systems considered in this work*

Results from analysis are related not only to the specific deorbit system, and to orbital initial parameters, but also to geometry and mass features of the spacecraft that is being deorbited. Therefore, for a correct comparison, it is considered for all the cases always the same "original" spacecraft (i.e. without deorbit system). This means that everything that is not added mass for deorbit, remains the same for all cases.
It is reported below a list of these features, used in all cases:

- Spacecraft mass (excluding added mass for deorbit): 1000 kg.
- Rough geometry and drag area: as explained more in detail in Sec.[3.2], the spacecraft is assumed to be made of two rectangular solar panels symmetrically placed with respect to a center cylindrical massive body. The resulting drag area can be then approximately represented as in Fig.[3.2] pg. 67, and the value of this drag area (of the satellite without deorbit system) is $10\,\mathrm{m}^2$.

From the values presented above, it turns out that the spacecraft, considered in all cases, has a *cross-sectional drag area-to-mass ratio* of $0.01\,\mathrm{m}^2/\mathrm{kg}$, that is a typical value often used in literature (see for example the diagram in Fig.[2.4] pg. 36, that is computed for a spacecraft with this same A/m ratio).

The computations consider, among the drivers listed earlier, the total deorbit time, ATP and additional mass. Regarding the ATP, it is always displayed the ATP in $m^2 * years$ calculated using the WCCSA area (see Sec.[3.2.2] for definition). TRL Levels, for each deorbit option, are already reported above in Fig.[3.11].

Results are presented in three ways:

- **2D plots** showing the profile of either deorbit time (in days), ATP (in $\mathrm{m}^2 * \mathrm{years}$), additional mass (in kg). For each of these parameters, two plots are created: one showing the profile for a constant inclination (set to 65°) and variable initial altitude between 600 km and 1500 km; the second showing the profile for a constant initial altitude (set to 1000 km) and variable inclination between 0° and 100°. Therefore, 6 bidimensional plots are created. Inside each plot, results for EDT system and electrical propulsion are always posted. The *chemical propulsion* option is posted only in plots showing the additional mass (for the reasons already stated in Sec.[3.6]).
- **3D plots** showing the profile of either deorbit time (in years), ATP (in $\mathrm{m}^2 * \mathrm{years}$), additional mass (in kg). The profile is plotted in relation to both initial altitudes, on the x axis, and inclinations, on the y axis. Therefore, 3 tridimensional plots are created. Inside each plot, results for *EDT* system and *electrical propul-*

sion are always posted. The *chemical propulsion* option is posted only in plots showing the additional mass (for the reasons already stated in Sec.[3.6]).

- An ***Excel*® spreadsheet** is automatically created by the code, reporting the numerical results for each case that is computed, and used for the 2D and 3D plots. One case means one single combination between an initial altitude from where deorbit starts, and a specific orbital inclination. Each row of the spreadsheets is referred to each case. Numerical values of selected cases, related to the most populated LEO regions, are posted in Sec.[3.9.4].

It is chosen, as optimal geometry for the tether, a conductive tether with dimensions $5\,\text{km} \times 3\,\text{cm} \times 50\,\mu\text{m}$, followed by an inert segment of $1\,\text{km} \times 3\,\text{cm} \times 50\,\mu\text{m}$ to enhance dynamic stability. In total, the tether is then 6 km long. This geometry will be used for all the analyses reported in the subsequent sections.

3.9.1 Comparison based on deorbit time

The first 2D plot, posted below, shows the fact that for a fixed inclination of 65° (where a high number of LEO satellites are placed) the EDT systems performs better than the EP system, at all initial altitudes. The gap in deorbit time increases, and the EDT becomes more advantageous, with increasing initial altitude.

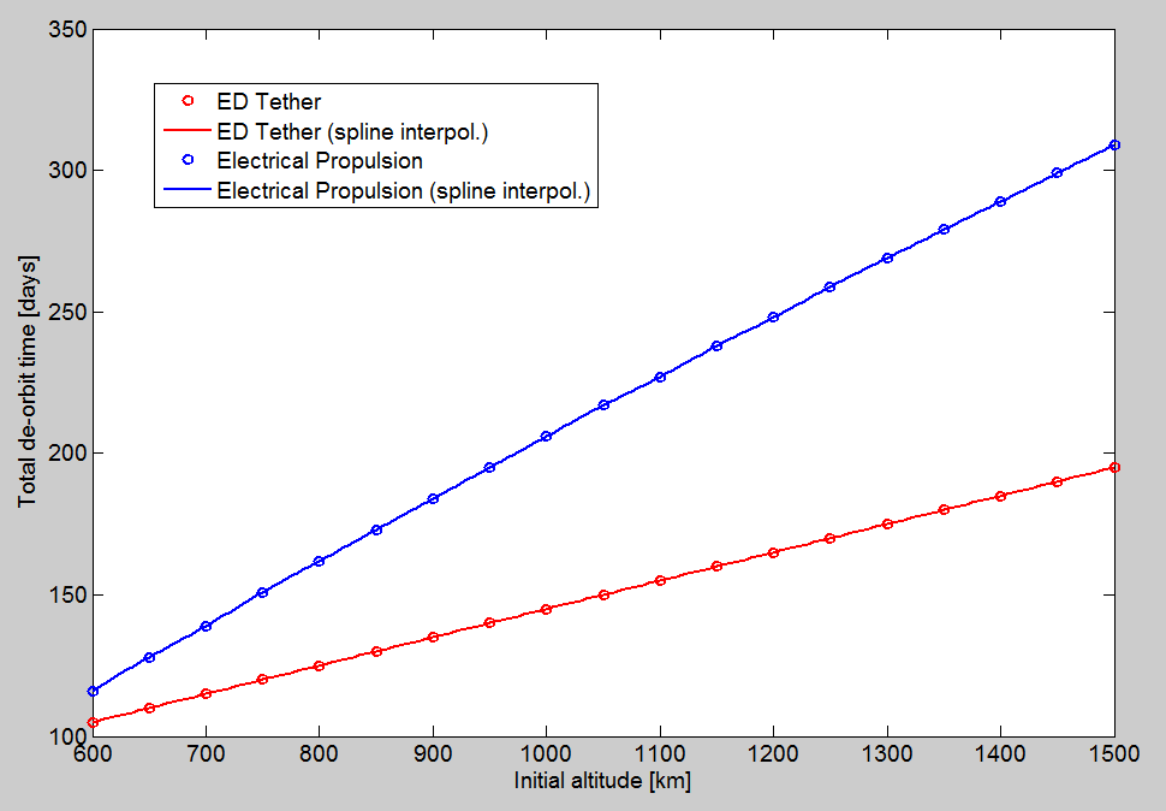

Figure 3.12: *Deorbit time VS Initial Altitude, for a constant inclination of* 65°. *Profile for EDT system with conductive tether of* $5\,\text{km} \times 3\,\text{cm} \times 50\,\mu\text{m}$ *followed by an inert tether of* $1\,\text{km} \times 3\,\text{cm} \times 50\,\mu\text{m}$. *An* average solar flux *is used (average electron density over a solar cycle) for the EDT system computations. Profile for* electrical propulsion *using the* SPT-70 Hall Thruster. *The final deorbit altitude is set to* 120 km.

The following diagram shows the profile of deorbit time with respect to increasing orbital inclination, for a fixed initial altitude of 1000 km. As expected, the deorbit time with EP does not vary with the inclination (it only depends on the initial altitude). The EDT system performs better than EP for all inclinations lower than about 72°. At higher inclinations, deorbit times become higher than with EP. The worst case for EDT is around an inclination of about 85°, where deorbit time becomes almost twice the corresponding deorbit time with EP.

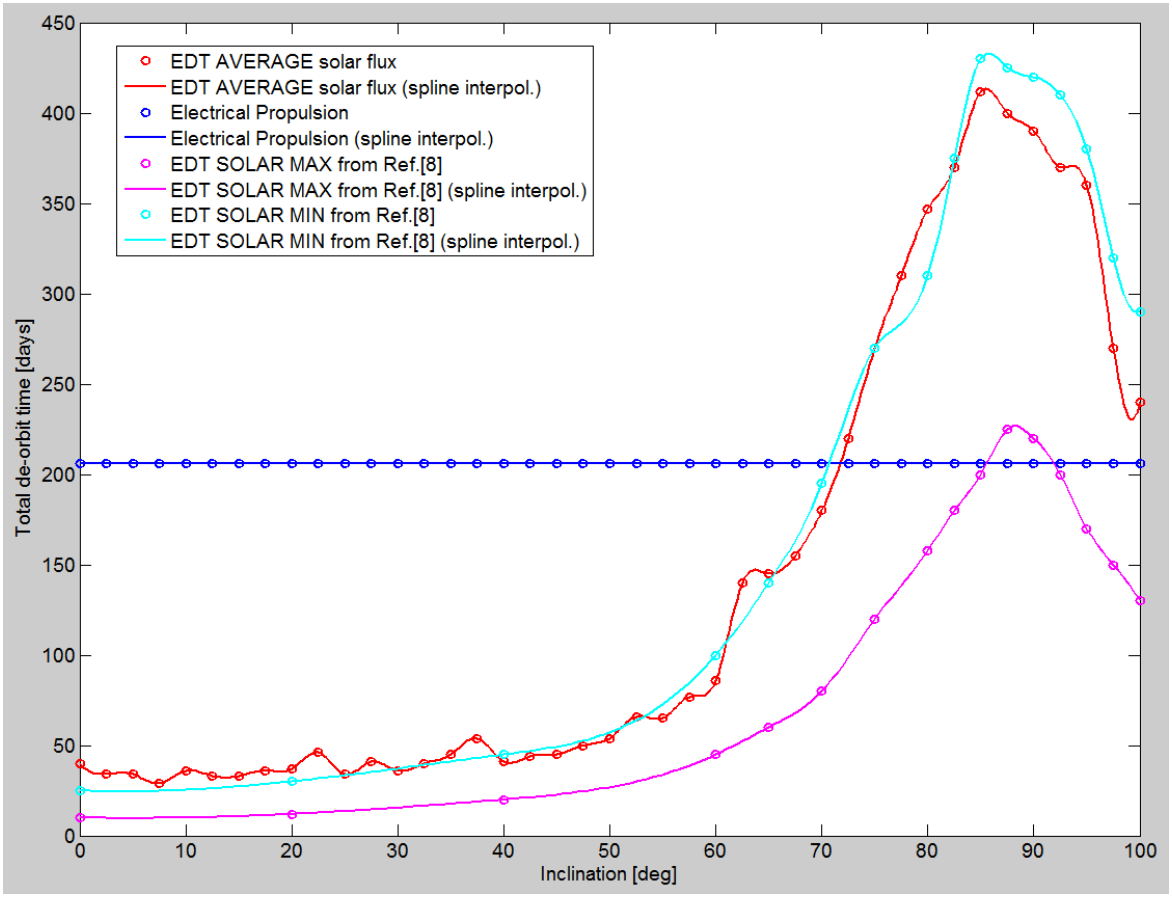

Figure 3.13: *Deorbit time VS orbital inclination, for a constant constant initial altitude of* 1000 km. *Profile for EDT system with conductive tether of* 5 km × 3 cm × 50 μm *followed by an inert tether of* 1 km × 3 cm × 50 μm. *An* average solar flux *is used (average electron density over a solar cycle) for the EDT system computations. Profile for* electrical propulsion *using the* SPT-70 Hall Thruster. *The final deorbit altitude is set to* 120 km. *In this diagram also values for EDT from Ref.[8] are plotted.*

The fact that at high inclinations the deorbit time, with the EDT, becomes higher is due to the fact that the geomagnetic field vector is often, during the deorbit phase, nearly parallel to the tether. Recalling Eq.[2.5.3], for the Lorentz drag force acting on the EDT system:

$$\vec{F} = I_{av} L \hat{u}_r \times \vec{B} \tag{3.18}$$

the tether is assumed to be aligned on the local vertical direction of unit vector $\hat{u}_r$ (that is the the direction of current flow). Since $\vec{B}$ is often nearly parallel to $\hat{u}_r$, it turns out from the vector product that the generated Lorentz drag force, averaged during the entire deorbit, is significantly lower than the average value obtained at low inclinations. Lower drag force causes, in turn, the higher deorbit times detected in the diagram above.
If the geomagnetic field were a perfect dipole, the most critical inclination would be

at $i = 78.5° = 90° - 11.5°$ where $11.5°$ is the approximate tilt angle of the magnetic dipole axis with respect to the Earth's spin axis. In this case, were the LEO orbit at $i = 78.5°$, it is possible to find the satellite exactly above the magnetic axis, such that the tether is aligned with it. In this worst case, portrayed in the picture below, $\vec{B}$ would be perfectly parallel to the tether, and as consequence the Lorentz force would be zero. It is important not to forget that the magnetic field is constantly rotating with the Earth: hence, this drastic situation can happen only in specific instants of time.

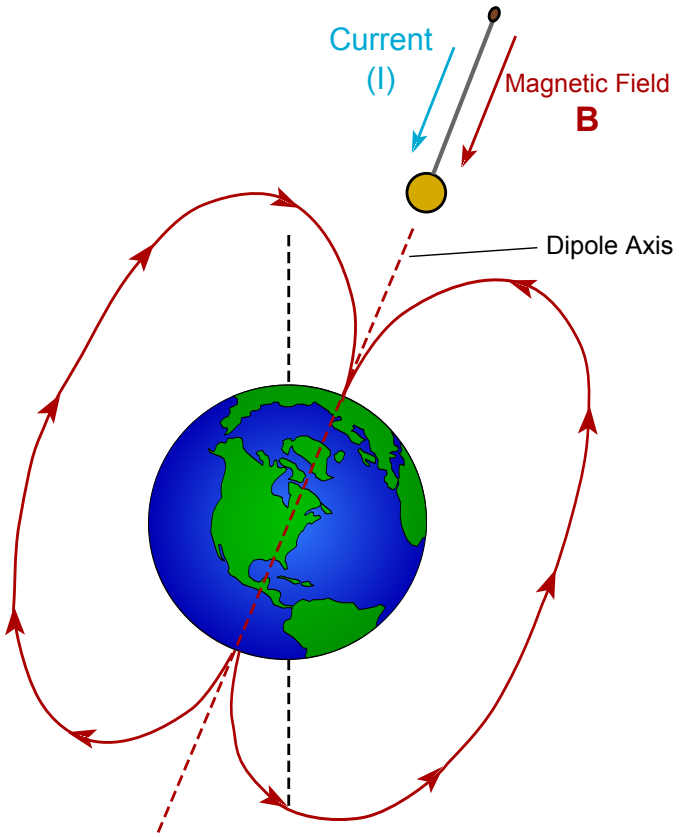

Figure 3.14: *Sketch showing the worst situation of tether perfectly aligned with axis of magnetic dipole. In this case the Lorentz force is zero.*

In reality, the geomagnetic field is much more complex than a simple dipole. This leads to the fact that the most critical inclinations, from the deorbit time standpoint, are observed at $i \approx 85°$, not around $78.5°$ as expected considering the dipole model.

It is then posted, in the following page, the 3D plot showing deorbit time with respect to both initial altitudes and inclinations. This plot has the aim of showing immediately when the most convenient system is the EDT or the EP, from the deorbit time standpoint. These aspects can be noticed from the plot:

- the lower is the initial altitude, the lower is the inclination at which deorbit time with EP becomes lower than with EDT. For initial altitude of 600 km, the EP

becomes more convenient for $i \gtrapprox 67.5°$; for initial altitude of 1500 km, the EP becomes more convenient for $i \gtrapprox 75°$.

- as expected, the deorbit time for the EP is constant at the same inclination, whereas it increases with increasing altitude. For the EDT, deorbit time increases with both initial altitude and inclination from 0° to about 85° where the peak in deorbit time is detected.
- deorbit time for EDT system in the range $85° < i < 100°$ is nearly symmetric with respect to the profile for $70° < i < 85°$.

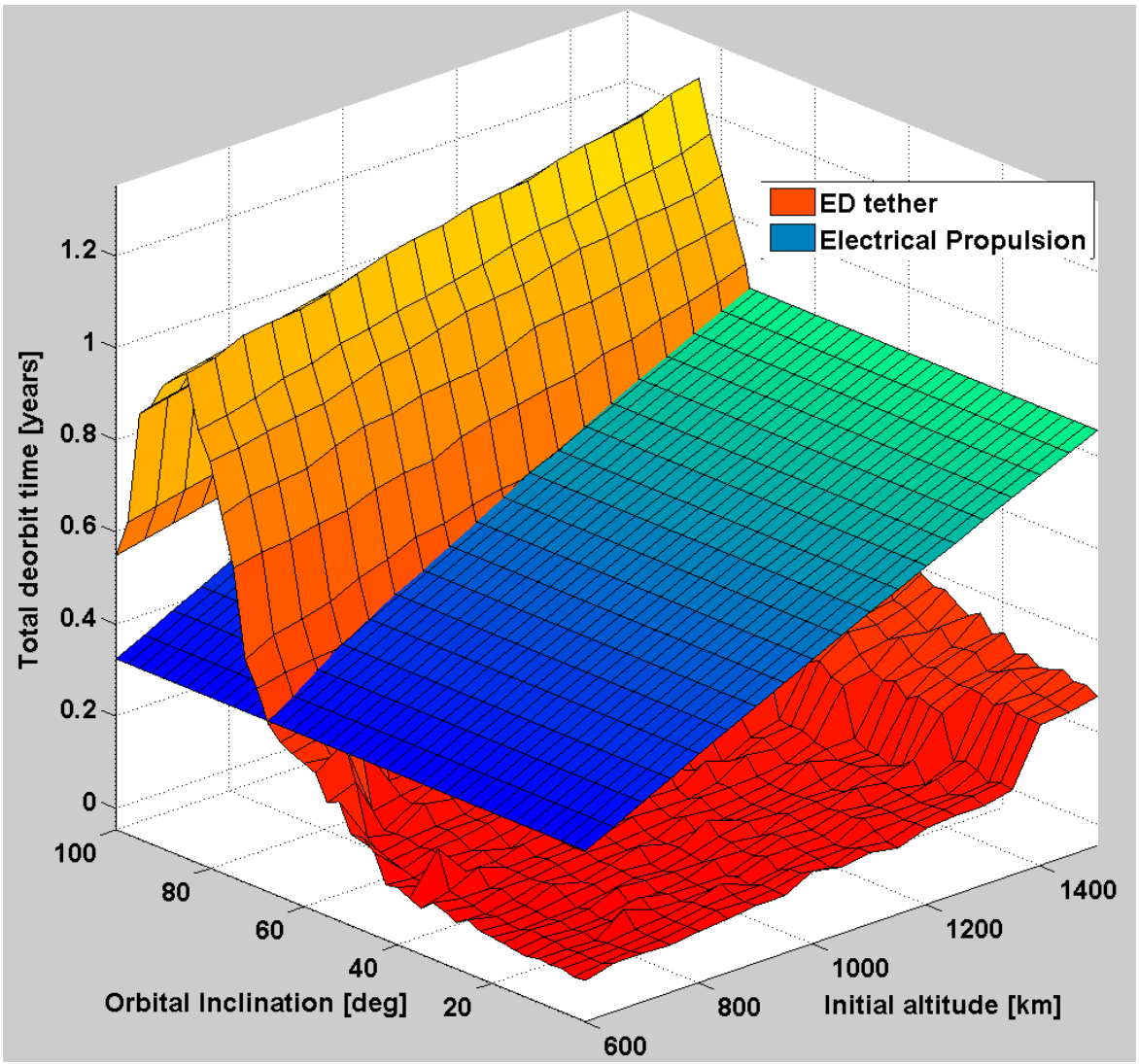

Figure 3.15: *3D Plot showing deorbit time with respect to both initial altitudes and inclinations*

3.9.2 Comparison based on ATP

It is important to point out that the absolute value of the ATP is dependent on the *characteristic radius* R_{ch} of impacting debris or meteoroid, used to calculate the

WCCSA. Refer to Sec.[3.2] for details. Since the objective is to perform a comparison, it is only important to always use the same R_{ch} for every deorbit system compared, not what value of R_{ch} is used (in the computations of this work a *characteristic radius* of 5 cm was used, as already described in Sec.[3.2]).

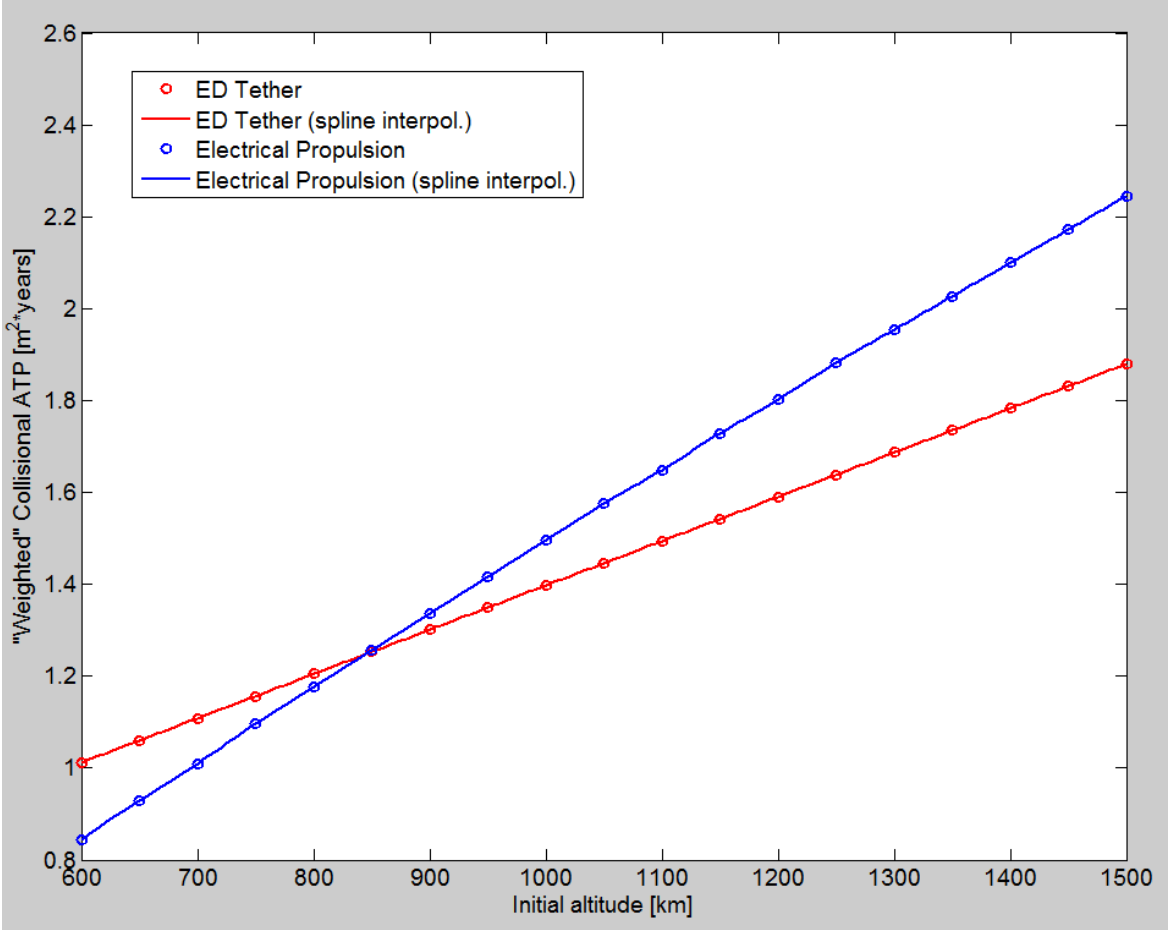

Figure 3.16: *Area-Time Product VS Initial Altitude, for a constant inclination of* 65°. *Profile for EDT system with conductive tether of* 5 km × 3 cm × 50 μm *followed by an inert tether of* 1 km × 3 cm × 50 μm. *An* average solar flux *is used (average electron density over a solar cycle) for the EDT system computations. Profile for* electrical propulsion *using the* SPT-70 Hall Thruster. *The final deorbit altitude is set to* 120 km.

On Fig.[3.16], it is interesting to note that the EDT becomes the best option, i.e. has a lower ATP, at altitudes higher than about 850 km (constant inclination of 65° at all initial altitudes). This is due to steeper increase of deorbit time with EP than with EDT, for increasing initial altitudes (as shown in Fig.[3.12]).

The following plot emphasizes another very important point, i.e. the fact that the EDT system performs better, on the ATP standpoint, than the EP up to an inclination of about 67.5°. This plot is for an initial altitude of 1000 km.

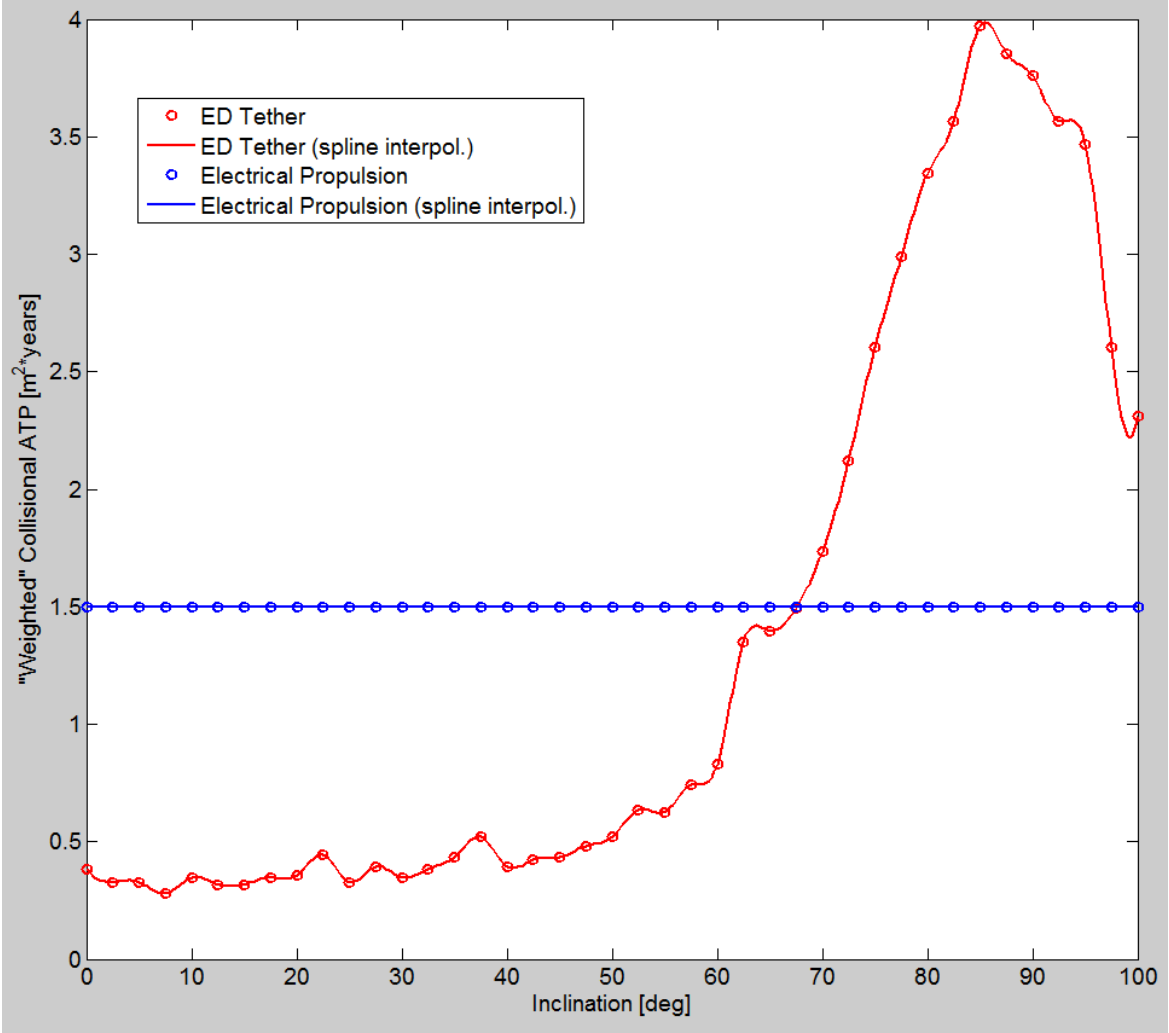

Figure 3.17: *Area-Time Product VS orbital inclination, for a constant constant initial altitude of* 1000 km. *Profile for EDT system with conductive tether of* 5 km × 3 cm × 50 μm *followed by an inert tether of* 1 km × 3 cm × 50 μm. *An* average solar flux *is used (average electron density over a solar cycle) for the EDT system computations. Profile for* electrical propulsion *using the* SPT-70 Hall Thruster. *The final deorbit altitude is set to* 120 km.

The ATP tridimensional plot substantially confirms the information already stated for the deorbit time 3D plot. Regarding the ATP, the inclination threshold at which the EP becomes better than the EDT system is lower, at all altitudes, with respect to what was seen on the deorbit time plot. This is due, as already mentioned, to the considerably higher WCCSA of the EDT system with respect to the EP system. At an initial altitude of 600 km, the EP becomes more convenient for $i \gtrapprox 60°$; at an initial altitude of 1500 km, the EP becomes more convenient for $i \gtrapprox 70°$.

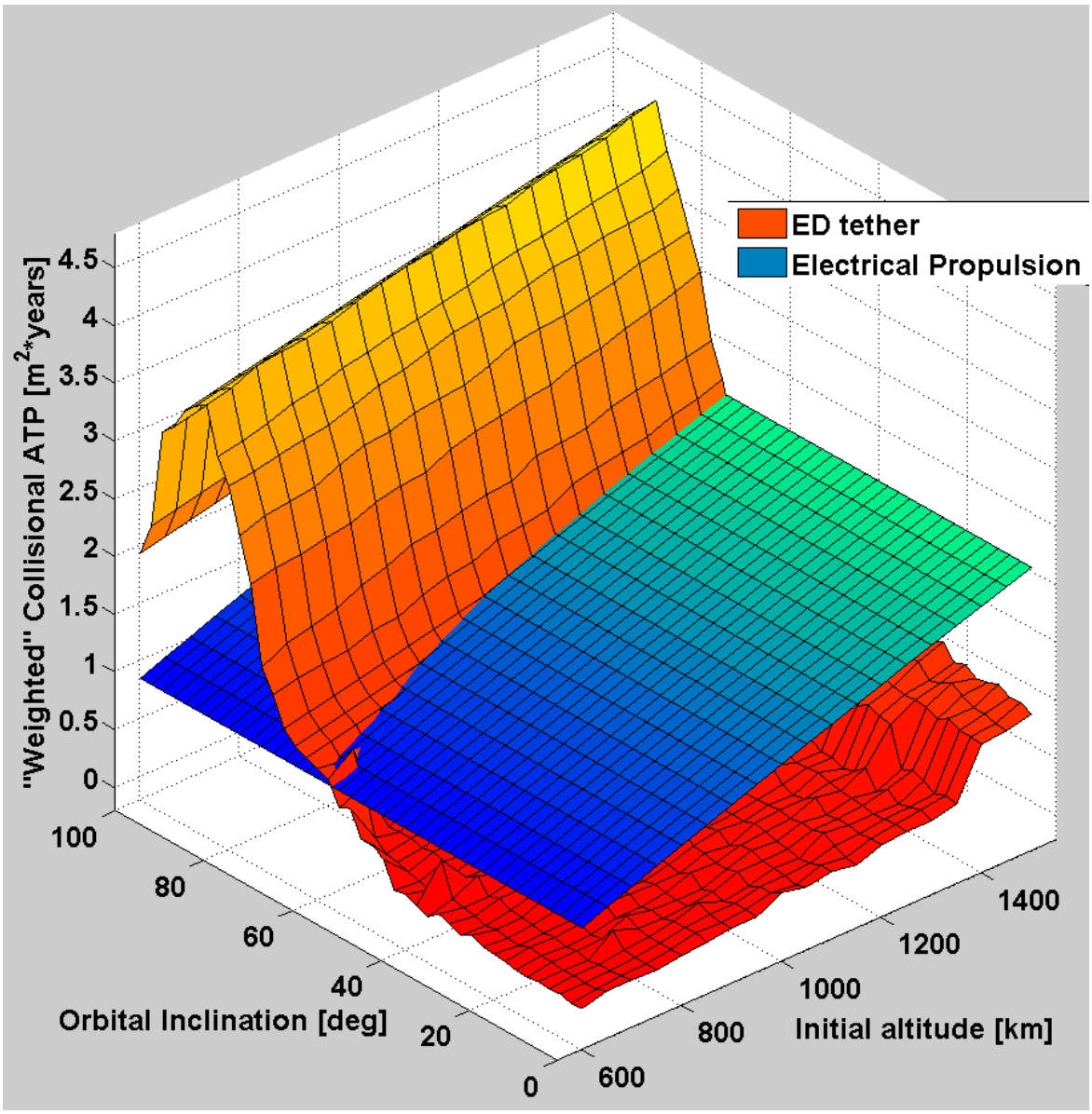

Figure 3.18: *3D Plot showing ATP with respect to both initial altitudes and inclinations*

3.9.3 Comparison based on Additional Mass

Before presenting the results, it is important to highlight that the additional mass of the EDT system was accurately calculated with data found in literature for the mass of each hardware component of the system; additionally, the Xenon mass (used by the cathode) was accounted, with mass flow rate depending on the cathode choice, as already described in Sec.[3.7.1].

A table reporting the various components of the EDT system, and respective mass values, is posted below:

Component	Mass [kg]
Conductive Tether	20.33
Ejection Mechanism (part of endmass)	3.5
Electron Emitter (Cathode)	1.2
Electronics to control tether	3.7
Spool Assembly (part of endmass)	5.8
Shroud	2.1
Tether Anchor	0.15
Battery for deployment (part of endmass)	3
Inert Tether	2.16
Endmass	20.00
Ballast mass	7.70
Xenon consumption [mg/s]	0.0589
Xenon consumption [kg/s]	5.89E-08
Xenon propellant for hollow cathode [kg/year]	1.86
De-Orbit time [years]	1.30
Total Mass of Xenon [kg]	2.41
Xenon tank mass fraction (fraction to multiply by total propellant mass)	0.034
Mass of Xenon tank	0.0820584
Total Mass (with Xenon hollow cathode)	**52.13**
Total Mass (with FEAC cathode)	**49.64**

Figure 3.19: *Table reporting all components of the EDT system, and respective mass. Values of rows from 2 to 7 are taken from Ref.[17]. Mass of conductive and inert segments of tether are calculated from geometry and density of their respective materials. The conductive tether is made of* Al 1100-H19 *(density of* $2710\,\mathrm{kg/m^3}$*)and measures* $5\,\mathrm{km} \times 3\,\mathrm{cm} \times 50\,\mu\mathrm{m}$*. The inert tether is made of* Kevlar *(density of* $1440\,\mathrm{kg/m^3}$*) and measures* $1\,\mathrm{km} \times 3\,\mathrm{cm} \times 50\,\mu\mathrm{m}$*. Values regarding Xenon consumption are provided by a cathode manufacturer at* Colorado State University*. The Xenon mass is computed for the worst case of longest deorbit time: about* 1.3 *years, from initial altitude of* $1500\,\mathrm{km}$ *and* $i = 85°$*. Due to high initial altitude the cathode limited to* $1\,\mathrm{A}$ *is used, with Xenon consumption of* $0.0589\,\mathrm{mg/s}$*. Xenon tank mass fraction: value from Ref.[29]. Ejection mechanism, spool assembly and battery for deployment are part of the endmass. It is also reported the mass of the system, in case the FEAC cathode is used, without need of Xenon (whose mass is then subtracted to the total).*

At worst, i.e. for a deorbit from an initial altitude of $1500\,\mathrm{km}$ and $i = 85°$, the total added mass with the EDT system is about $52\,\mathrm{kg}$.

As mentioned in Sec.[2.2] pg. 31, it was proposed in literature to only partially deorbit satellites, located above a certain altitude, when using *chemical propulsion*. After running some simulations, it is seen that this strategy of partial deorbit, from the mass standpoint, is not convenient, or at best only slightly convenient. This is due to the fact that a *partial* deorbit, differently from a *direct* deorbit, would require a perigee burn, in addition to the apogee burn (that is the only burn required in case of *direct* deorbit). The need of a perigee burn, in addition to the apogee burn, increases significantly the required propellant mass. From computations with the personal code, it turns out that for a satellite of 1000 kg mass (excluding additional mass for deorbit), from an altitude of 1000 km, the amount of hydrazine propellant required for direct deorbit is approximately equal to the amount required for a partial deorbit to a final altitude of 500 km. Moreover, the second option would be worse also because with a partial deorbit the spacecraft would remain much longer in orbit, increasing ATP and risk of collision.
When starting from lower orbits, partial deorbit might be sligthly convenient, but the low gain in terms of mass is paid with a much higher ATP. Consequently, it is possible to conclude that it is generally always better to perform a *direct* reentry with chemical propulsion instead of a *partial* orbit lowering.

Also the solution of partial lowering without perigee burn is not effective, since there would be mass savings but the deorbit time and ATP would increase exponentially since the satellite would continue to orbit in the Hohmann transfer orbit.

For both *chemical* and *electrical* propulsion deorbit options, the propellant mass is calculated using the *Tsiolkovsky equation*, after setting the specific impulse I_{sp} and computing the required difference of velocity ($I_{sp} = 220\,\mathrm{s}$ for the monopropellant hydrazine system, and $I_{sp} = 1500\,\mathrm{s}$ for the *SPT-70 Hall Thruster*).

In the mass calculation for EP, also mass of additional solar panels and additional attitude control hardware is included, as already described in Sec.[3.5].

All the subsequent plots reveal these facts:

- the EDT system is always the best option, from the mass standpoint, for all combinations of initial altitudes and inclinations. In other words, for all inclinations and initial altitudes, the EDT system is the option that allows the minimum additional mass to be carried onboard, in order to implement deorbit.
- the *chemical* propulsion system is in every case the worst option from the mass standpoint, in the entire plotted range of initial altitudes, between 600 km and 1500 km.
- the additional mass is constant with respect to variable inclination, for EP and CP systems, as expected. For the EDT system, the variation in the required mass of Xenon for the cathode is very low, even for high inclinations where deorbit times are longer. Instead, the additional mass of propellant, for the CP and EP

systems, varies significantly with initial altitude: especially for CP, there is a very steep increase.

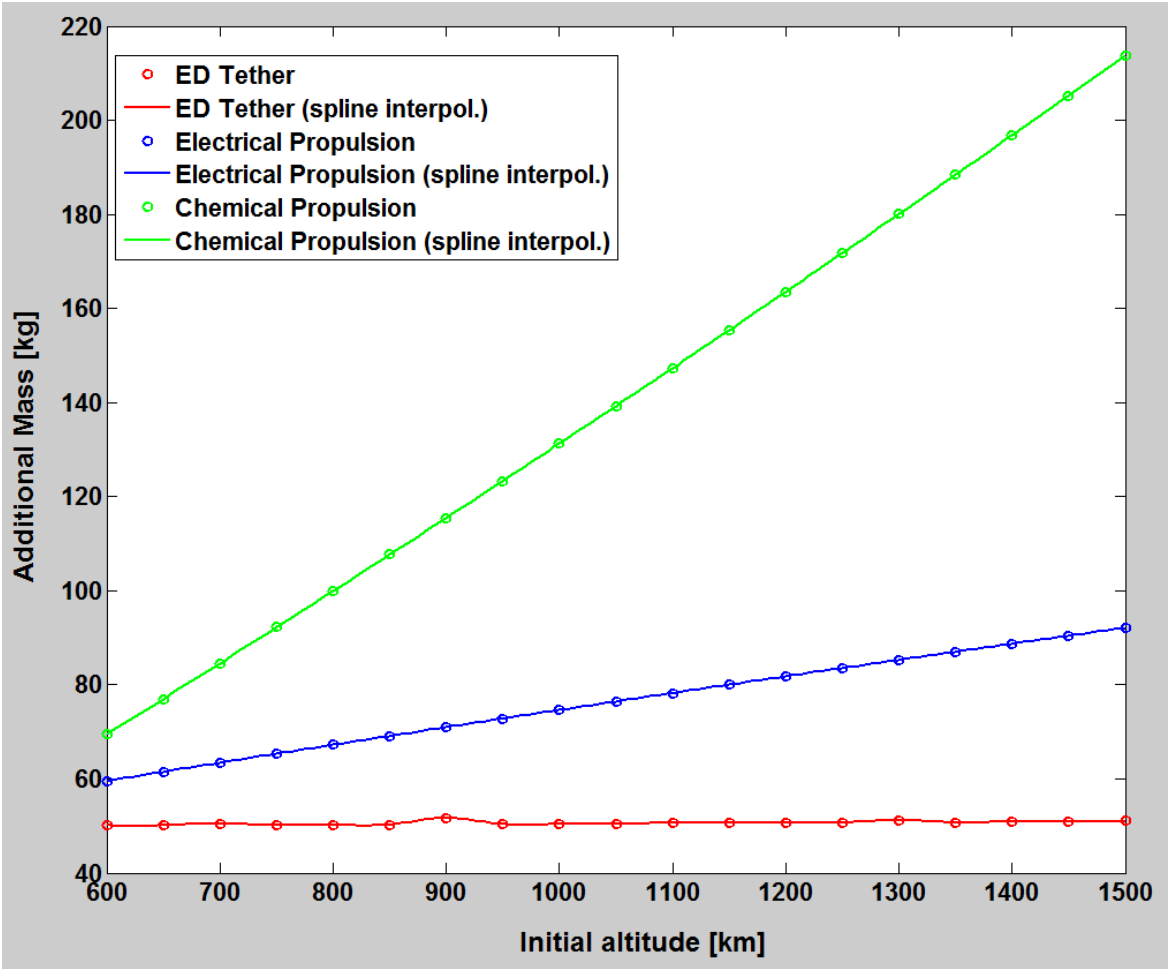

Figure 3.20: *Additional Mass for deorbit VS Initial Altitude, for a constant inclination of* 65°. *Profile for EDT system with conductive tether of* $5\,\mathrm{km} \times 3\,\mathrm{cm} \times 50\,\mu\mathrm{m}$ *followed by an inert tether of* $1\,\mathrm{km} \times 3\,\mathrm{cm} \times 50\,\mu\mathrm{m}$. *An* average solar flux *is used (average electron density over a solar cycle) for the EDT system computations. Profile for* electrical propulsion *using the* SPT-70 Hall Thruster. *Profile for* chemical propulsion *using Hydrazine monopropellant. The final deorbit altitude is set to* 120 km.

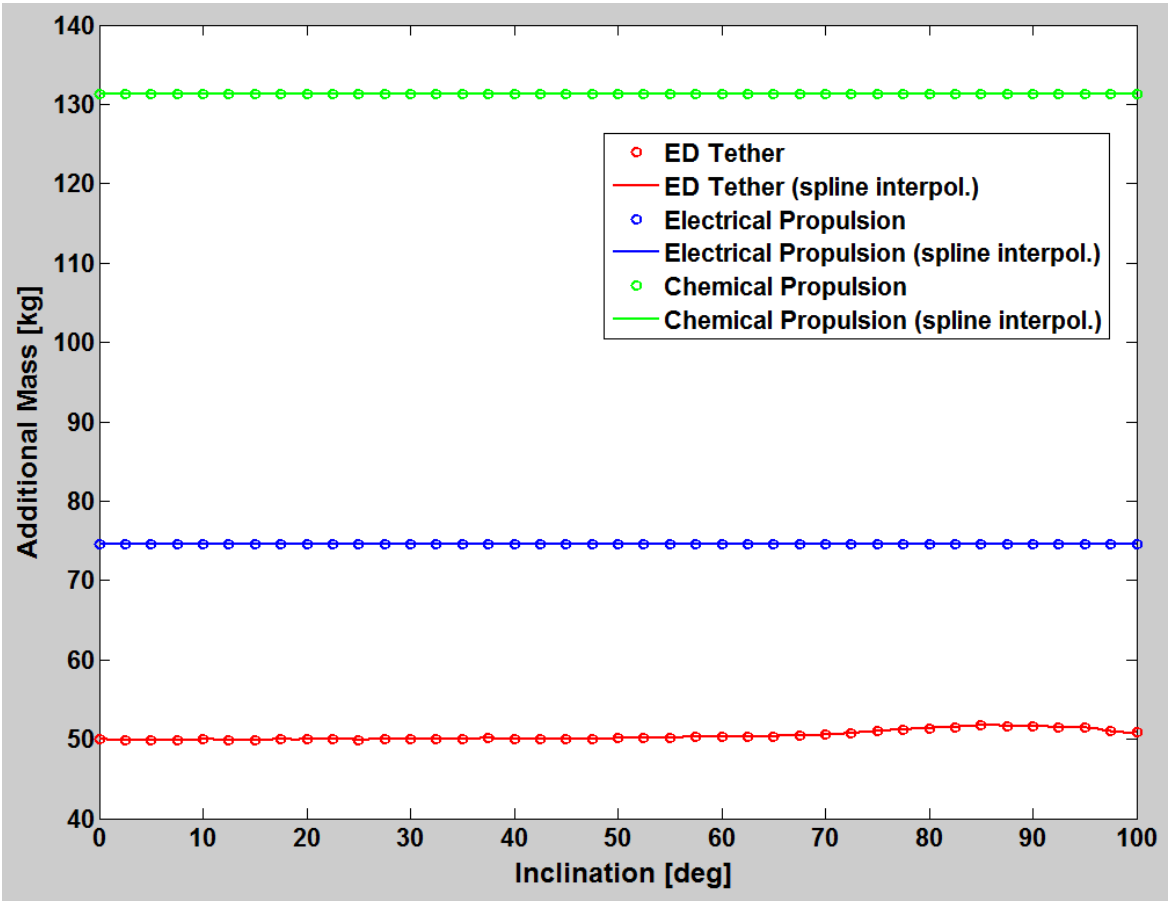

Figure 3.21: *Additional Mass for deorbit VS Orbital Inclination, for a constant constant initial altitude of* 1000 km. *Profile for EDT system with conductive tether of* 5 km × 3 cm × 50 μm *followed by an inert tether of* 1 km × 3 cm × 50 μm. *An* average solar flux *is used (average electron density over a solar cycle) for the EDT system computations. Profile for* electrical propulsion *using the* SPT-70 Hall Thruster. *Profile for* chemical propulsion *using Hydrazine monopropellant. The final deorbit altitude is set to* 120 km.

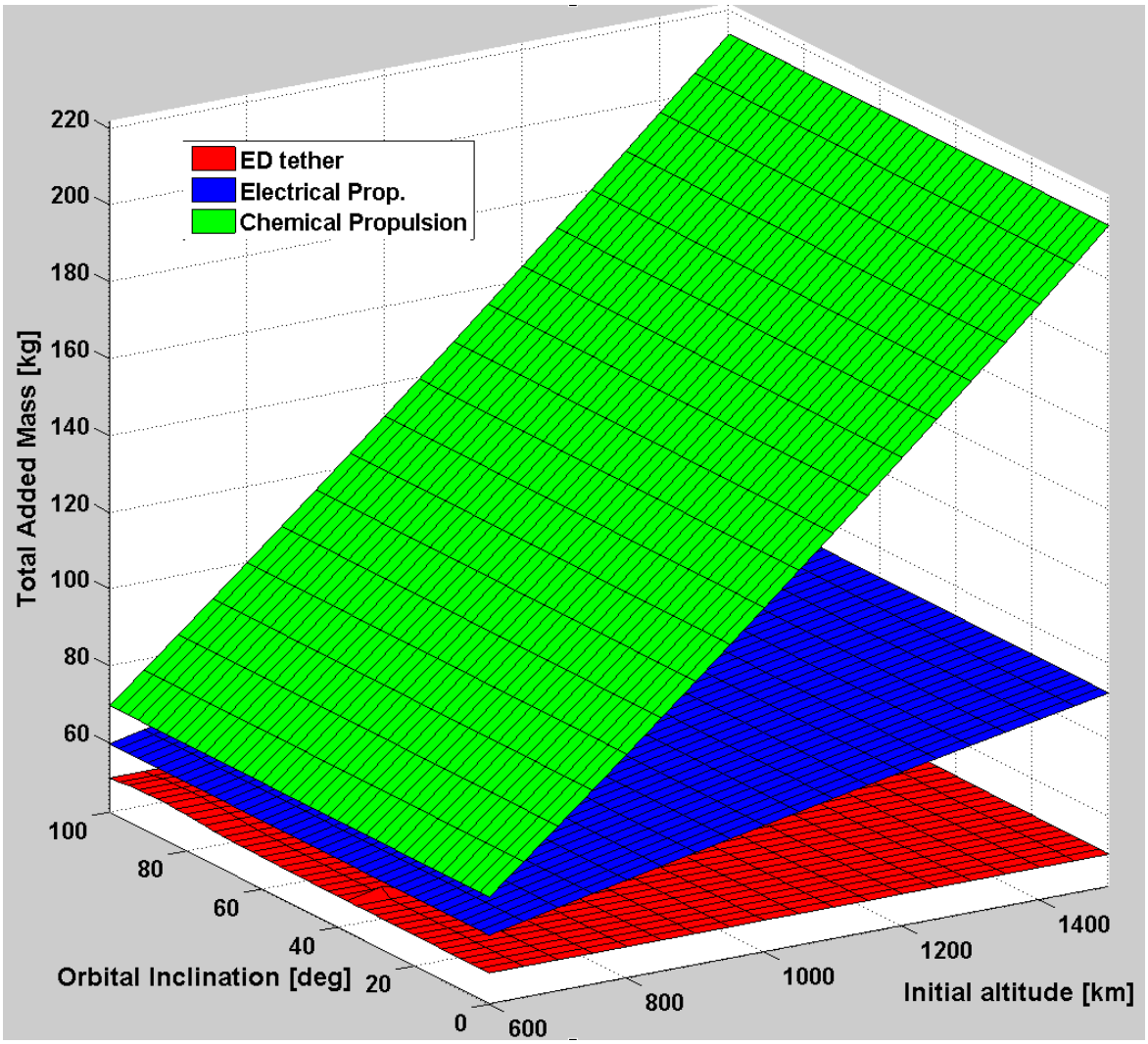

Figure 3.22: *3D Plot showing the* additional mass *required for deorbit, with respect to both initial altitudes and inclinations*

3.9.4 Results in numerical form for selected cases

The most populated LEO inclinations and perigee altitudes are selected, from catalog data described in Section 1.1. The selected inclinations are: 65°, 75°, 82.5° and 97.5°. The selected initial altitude are: 800 km, 900 km and 1400 km. 12 cases are derived from the combination of these 4 inclinations with these 3 altitudes. In the image below, results from the computational analysis of these cases are posted. Anyhow, the codes written for this work are extremely flexible and can accept in input any initial orbital altitude and inclination, so any case not reported here can be easily computed.

Initial Altitude [km]	Inclination [°]	Deorbit Time EDT system[years]	Deorbit Time Electrical P. [years]	ATP EDT system [m^2 * years]	ATP Electrical P. [m^2 * years]
800	65	**0.34**	0.44	1.20	**1.18**
900	65	**0.37**	0.50	**1.30**	1.34
1400	65	**0.51**	0.79	**1.78**	2.10
800	75	0.67	**0.44**	2.34	**1.18**
900	75	0.70	**0.50**	2.48	**1.34**
1400	75	0.86	**0.79**	3.04	**2.10**
800	82.5	0.95	**0.44**	3.35	**1.18**
900	82.5	0.99	**0.50**	3.47	**1.34**
1400	82.5	1.12	**0.79**	3.94	**2.10**
800	97.5	0.68	**0.44**	2.41	**1.18**
900	97.5	0.71	**0.50**	2.51	**1.34**
1400	97.5	0.85	**0.79**	2.99	**2.10**

Figure 3.23: *Table reporting numerical results of deorbit times and ATP, for selected cases.*

Initial Altitude [km]	Inclination [°]	Add. Mass EDT system [kg]	Add. Mass Electrical Propulsion [kg]	Add. Mass Chemical Propulsion [kg]
800	65	**50.27**	67.23	99.94
900	65	**50.32**	70.97	115.50
1400	65	**50.58**	88.72	196.81
800	75	**50.87**	67.23	99.94
900	75	**50.94**	70.97	115.50
1400	75	**51.24**	88.72	196.81
800	82.5	**51.41**	67.23	99.94
900	82.5	**51.47**	70.97	115.50
1400	82.5	**51.72**	88.72	196.81
800	97.5	**50.91**	67.23	99.94
900	97.5	**50.96**	70.97	115.50
1400	97.5	**51.21**	88.72	196.81

Figure 3.24: *Table reporting numerical results of additional mass, for selected cases.*

In the results table, it is highlighted in boldface every best deorbit time (between EDT and EP), ATP (between EDT and EP) and additional mass (between EDT, EP and CP).

Once again, the following facts are confirmed also by numerical values:

- on the deorbit time standpoint, for the case of inclination $i = 65°$, the EDT system is the best option for all the altitudes in the table. For the other inclinations, as expected since they are higher than 70° the EP becomes the best option. However, it has to be pointed out that the difference in deorbit time, between the two options, is not very high. At worst, there is a difference of about half year.
- the previous fact is also reflected in the ATP, where EP is the best option for all inclinations except for $i = 65°$. The tether, being 6 km long and 3 cm wide, adds a significant contribution to the total WCCSA area, increasing the gap between ATP of the EDT system and of the EP system. For the lower altitudes, the ATP of electrical propulsion is generally about half of the ATP of the EDT system (on all inclinations in the table, except for $i = 65°$). For higher altitudes ($h_0 = 1400$ km), the difference in ATP between the two deorbit options is lower.
- on the additional mass standpoint, the EDT system is always the best option. EP is the second best option, whereas CP is, in any case, the worst solution requiring the largest additional mass. Whereas the mass of the EDT is always around 50–52 kg, for the EP it can reach a maximum value of about 90 kg, and for CP it can reach about 215 kg for the 1000 kg satellite, at initial altitude of 1500 km. Moreover, it is important to remember that for even more massive satellites, the gap between EDT and the other two options might increase even more (the propellant mass augments significantly with increasing mass to deorbit), i.e. the EDT becomes even more convenient for deorbit of higher mass satellites.

Chapter 4

Conclusion

From the results presented in Chapter [3], it is clear that the quest for the optimal solution for deorbit has not a unique response, since it depends on the specific initial altitude and inclination. Moreover, it also generally depends on what driver (among *deorbit time*, *ATP* and *additional mass*) is assigned the top priority, since there is no solution that performs always, in any case of initial altitude and inclination, better than all the others, on every driver.

It is considered as reference Fig.[1.6] pg. 21. This figure shows all catalog objects (of any size), but the same profile, proportionally rescaled, can be reasonably applied to satellites and spent stages only (that are the potential targets for future implementation of an onboard deorbit system).
Detailed conclusions will be then provided differentiating between four different ranges inside the LEO region:

- **Range 1: initial altitudes lower than 500 km**. Only 10%, at most, of LEO satellites and spent stages are orbiting with perigee at these low altitudes.
- **Range 2: initial altitudes between 500 km and 700 km**. About 25% of LEO satellites and spent stages are orbiting with perigee constrained in this range.
- **Range 3: initial altitudes between 700 km and 1500 km**. This is, by a large extent, the most populated range, with about 62% of all LEO satellites and spent stages.
- **Range 4: initial altitudes above 1500 km**. Above 1500 km there are very few LEO satellites and spent stages (about 3% of the total).

4.1 Range 1

For satellites (or spent stages) orbiting with perigee lower than 500 km, *Natural Decay* is a considerable option, particularly for the reason that it is cost-free. Especially for bodies with large drag area over mass ratio, the time of reentry via aerodynamic drag

is normally always lower than 5 years in this altitude range. Hence, a much lower deorbit time with respect to the maximum of 25 years imposed by the guidelines.

In case the fastest deorbit is preferred for some reason, a *Chemical Propulsion* deorbit system is the most convenient option, ensuring the lowest deorbit time and ATP with respect to all other solutions. Moreover, when starting deorbit from such low altitudes, the mass of propellant required for the single burn, to inject the satellite into the direct reentry orbit, is comparable or even lower than the mass of the EDT system.

Drag augmentation devices are a potential option, but from the mass standpoint, ATP and deorbit time, they perform worse than both CP and EDT systems.

Electrical Propulsion is a viable option too, but it is surely much more expensive to implement than the CP solution (a CP system is generally always present onboard for mission life in LEO, instead the EP system would be added only for the purpose of deorbit). Moreover, deorbit times and ATP are surely much higher than with CP.

In conclusion, for satellites and spent stages orbiting at altitudes lower than 500 km, the optimal solutions are either *Natural Decay*, if higher deorbit time and ATP can be accepted. Otherwise, in case it is desired a fast deorbit, the most convenient option, on all standpoints, is surely *Chemical Propulsion*.

4.2 Range 2

Natural Decay should generally not be considered, since deorbit times can range typically between 5 years to considerably more than 25 years (violating the guidelines), depending on ratio between drag area and mass, in addition to initial altitude.

From deorbit time and ATP standpoints, *Chemical Propulsion* is surely the most convenient option. The additional mass is always larger than with the EDT system in the entire range, almost twice for a 1000 kg satellite starting deorbit at an altitude of 700 km.

Drag augmentation devices are a potential option, generally allowing times of deorbit lower than 2-3 years, but however not convenient with respect to *chemical propulsion* due to higher additional mass, higher deorbit time, and extremely higher ATP, due to the much larger drag area. This brings, as consequence, a higher indeed risk of collision during deorbit.

Electrical Propulsion is a considerable option, requiring lower total mass than CP, but with higher deorbit times and higher ATP with respect to both *Chemical Propulsion*

and *EDT system*.

EDT system is consistently more convenient, on the additional mass standpoint, with respect to CP, but of course it implies higher deorbit times and higher ATPs, with respect to CP.

In conclusion, for satellites and spent stages orbiting at altitudes between 500 km and 700 km, the optimal solutions are either *Chemical Propulsion*, if shortest deorbit time and lowest ATP are top priorities. Otherwise, the *EDT system* is expected to be the most economically convenient option since it leads to an additional mass that is considerably lower, in some cases about half, than the additional mass required with *Chemical Propulsion*.

4.3 Range 3

Natural Decay and *Drag Augmentation devices* are surely discarded as non-acceptable solutions, due to the excessive deorbit times that, in most of this altitude range, largely surpass the 25 years maximum constraint. Refer to diagrams in Fig.[3.4] at pg. 74 and Fig.[3.7] at pg. 79 for reference.

Chemical Propulsion is, as usual, the most convenient option from deorbit time and ATP standpoints, being a *direct* deorbit method. The major problem is that, for initial altitudes above 700 km, it becomes critical from the additional mass standpoint, especially for massive satellites, with respect to the EDT and EP systems.

Electrical Propulsion is an optimal solution. On deorbit time and ATP standpoints, it outperforms the EDT system only at high inclinations, approximately higher than 70°. A problem of the EP, with respect to the EDT system, is the additional mass, that is higher, almost twice in the worst cases. See Fig.[3.22] at pg. 107 as reference.

EDT is, on the mass standpoint, the best solution in all cases with respect to all other systems. See Fig.[3.22] at pg. 107 as reference. Deorbit times and ATPs are better than with EP in a very broad range of altitudes and inclinations, excluding the region of high inclinations between about 70° and 100°. See Fig.[3.15] at pg. 99 and Fig.[3.18] at pg. 102 as references.

In conclusion, for satellites and spent stages orbiting at altitudes between 700 km and 1500 km, i.e. the most densely populated LEO region, the optimal solutions are: *EDT* is the system that always performs way better than any other option, on the mass standpoint (requiring the lowest additional mass for implementation); *Chemical Propulsion* can be considered for lower orbits in this range, or when the fastest deorbit is strictly necessary for some reasons; *Electrical Propulsion* is the strongest competitor of EDT, with shorter deorbit times and lower ATPs at high inclinations, but always higher mass required (even if much lower than with CP).

4.4 Range 4

Above 1500 km, many of the conclusions that were stated for the previous range are valid. The only variation could be that *chemical propulsion*, at such high altitudes, would never be acceptable due to the extraordinarily high mass of propellant that would be required. In this range EDT and EP systems are the viable solutions, with EDT performing much better on the mass standpoint; regarding deorbit time and ATP, only at very high inclinations the EP would perform better than EDT. However, **in order to avoid the much larger mass required by the EP system, the EDT is, overall, the best solution in this last range. Anyhow, this is the range of lowest concern, since only very few satellites are orbiting at such high LEO altitudes.**

4.5 Final Comment

It is important to highlight, from all the conclusions reported above, based on analysis results presented in Chapter [3], that the *Electro-Dynamic Tether* system is the solution that, for more than 85% of all LEO satellites and spent stages, is most convenient on the mass standpoint. In other words, the additional mass required onboard to implement this deorbit solution on future satellites (assuming for them the same distribution in LEO region as the current debris population in LEO) is the lowest among all proposed deorbit options, for all inclinations and initial altitudes above 500 km. Moreover, exception made for *chemical propulsion*, that, however, for altitudes above 500 km would require a higher or much higher mass, also deorbit times and ATPs granted by the EDT system are lower than with other competing solutions, particularly the EP system, in a broad range of initial altitudes and inclinations.

Consequently, the *Electro-Dynamic Tether* system is surely worth of further research, development and testing, as the most promising solution for a new era of space activity in LEO, with deorbit implemented as a routine procedure. An essential measure that would finally invert the trend of increasing debris population in space: one of the most urgent problems to be solved, in order to progressively achieve a safer space environment for future missions.

Appendix A

Rudiments about Plasma

Plasma is conventionally considered the fourth state of matter. It is defined as an ionized gas made of positive ions and electrons, in such number that the gas is globally neutral. Whether a gas is categorized as *plasma* or not, it strictly depends on the degree of ionization. The presence of only few ions or molecules in a gas does not make it a plasma. Instead, when the degree of ionization becomes sufficient to make electro-dynamic or magneto-hydrodynamic effects dominate the behavior of the material then it can be considered as a *plasma*. A widely accepted criterion for a gas to be considered a *plasma* is the existence of *Debye shielding* and the presence of a large number of electrons/ions inside a region called *sheath*.

From several studies, it emerges that most of the matter in the universe is theoretically in plasma state. as reported in Ref. [13].
Plasma is characterized by three fundamental parameters, as pointed out in Ref. [5]:

1. the particle volumetric density n (measured in particles per cubic meter)
2. the temperature T of each species (usually measured as energy in eV)
3. the steady state magnetic field B (measured in tesla, T)

Relevant bibliographical references about plasma are Ref.[5] and [13].

Appendix B

Probability of tether being cut

It is written a *Matlab*® code (named "LcutTAPE.m") to implement the verification of compliance with the NASA guideline in Ref.[1] pg.3-4. This guideline has the aim of preventing release in space of additional debris coming from the tether. For deorbit application, no tether will be intentionally released in orbit; instead, the tether will remain attached to the satellite until burn out at low altitudes. Therefore, this guideline only applies, in the case of this project, in regard to the potential release of debris due to the tether being cut off during deorbit.

The guideline considers the flux of either orbital debris or meteoroids potentially hitting the tether. It has to be determined the minimum diameter of impactor that causes the tether to be cut. The NASA guideline, on pg. 3-4, recommends, unless specific data is available, to use 1/5 of the tether's diameter or a chosen equivalent dimension of the cross-section. From experimental tests, it turns out that it is possible to use, for a tape tether like the one chosen in this work, a ratio of 1/3 of the tether's characteristic size, instead of 1/5, as minimum diameter that the impacting object must have in order to cut the tether. The impact can occur at any angle with respect to the tether's exposed area. The personal *Matlab*® code computes an "equivalent edge" of the cross-section, i.e. it averages the width "seen" from every impact angle. If the impact occurs perpendicular to the frontal area of the tether (impact angle $\theta = 0°$), the edge is equal to the width w. If the impact occurs perpendicular to the side area of the tether (impact angle $\theta = 90°$), the edge is the thickness. For every case in between, i.e. for impact angle $0° < \theta < 90°$, the edge is calculated as $w \cdot cos(\theta)$. The "equivalent (or average) edge" length, divided by 3, gives the minimum cutting impactor diameter. Knowing this quantity it is possible to derive the *cumulative cross-sectional area flux* of both meteoroids and debris, per year, from the following diagrams taken from the NASA guideline.

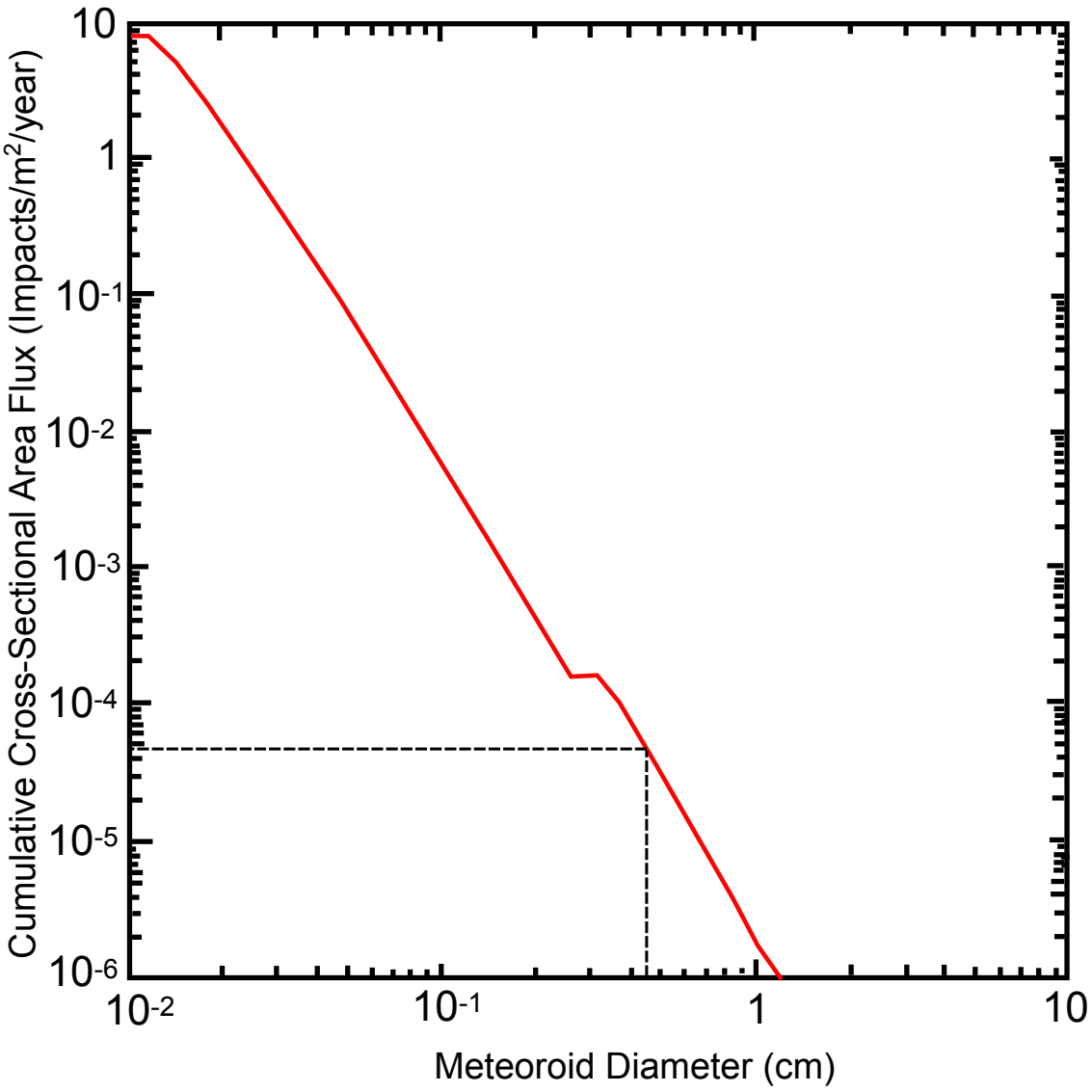

Figure B.1: *Cumulative cross-sectional area flux of meteoroids, per year, as function of meteoroid diameter. For a tape tether* 2 cm *wide, the minimum impactor diameter that determines cut of the tether (calculated as* equivalent edge *divided by 3) is* 0.0046 m = 0.46 cm. *This value corresponds to a flux of* meteoroids *of approximately* $5e-5$ *(impacts/m^2/year). Data from Ref. [1] pg. 5-9.*

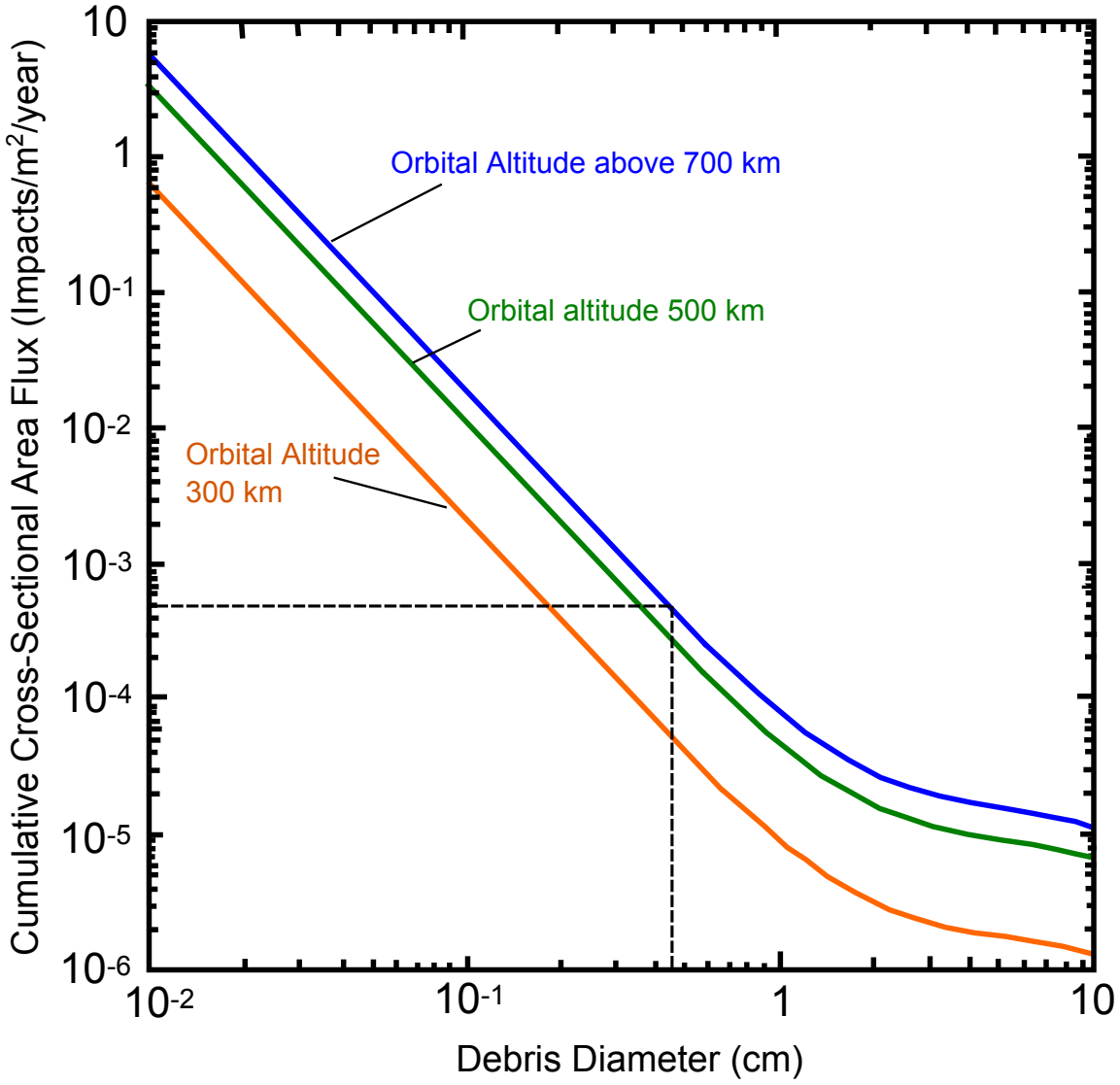

Figure B.2: *Cumulative cross-sectional area flux of debris, per year, as function of debris diameter, for different orbit altitudes. For a tape tether* 2 cm *wide, the minimum impactor diameter that determines cut of the tether (calculated as* equivalent edge *divided by 3) is* 0.0046 m = 0.46 cm. *This value corresponds to a flux of* debris *of approximately* $5e-4$ *(impacts/m*^{2}*/year). Data from Ref. [1] pg. 5-9.*

Two facts are demonstrated by computations:

1. the inefficiency of a tether with a circular cross-sectional area with respect to a tape-like tether of same length and cross-sectional area value, but with different cross-sectional area geometry. One dimension, the width, is orders of magnitude larger than the other dimension, the thickness.
   The lower is the characteristic dimension of the meteoroid that can determine a fatal cut of the tether, the higher is the flux meteoroids of that size. For a circular cross-section tether, the impacting object always "sees" the diameter as characteristic dimension, regardless of the direction of impact. Instead, for

a tape tether, the "characteristic dimension" seen by the impacting meteoroid depends on the angle of impact θ.

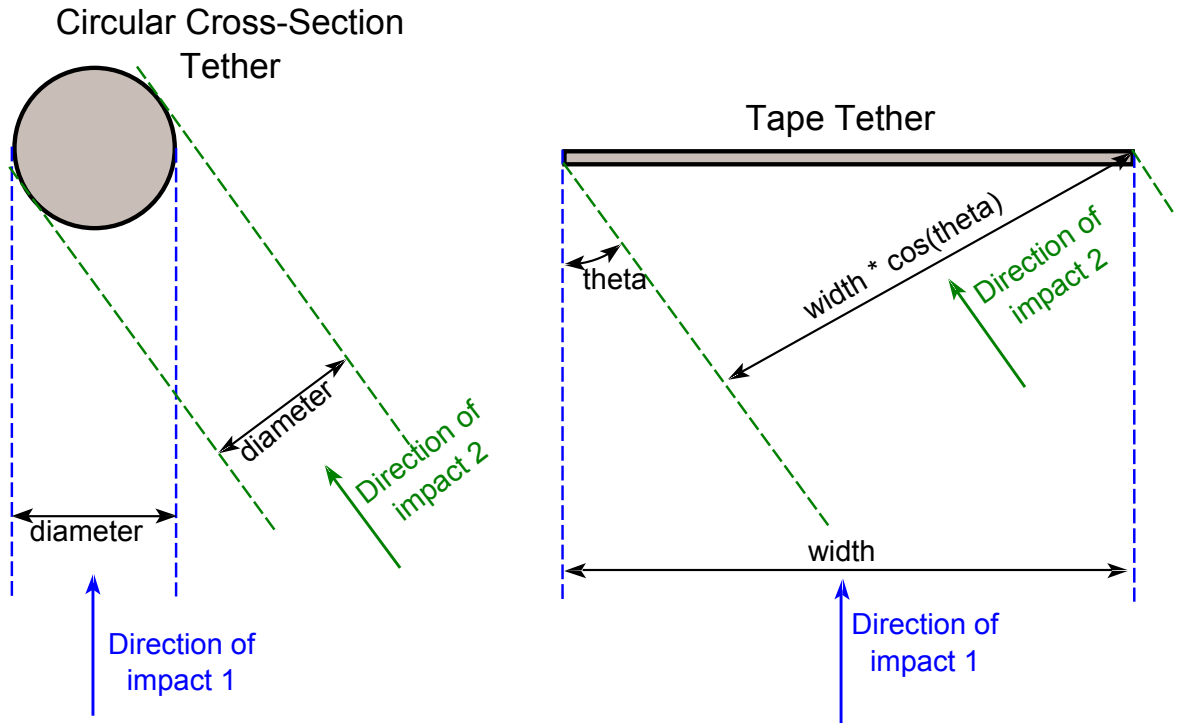

Figure B.3: *Sketch showing the fact that for a circular cross-section tether the characteristic dimension "seen" by the impactor is always equal to the diameter, regardless of the impact direction; instead for a tape tether, the edge "seen" by the impactor changes with the impact angle θ, and therefore it is needed the calculation of an "equivalent edge", averaged on all impacting angles from* $0°$ *to* $90°$.

It turns out that the "equivalent edge" for a $2\,\text{cm}\times 50\,\mu\text{m}$ cross-section, is 0.46 cm. Instead, a circular cross-section of the same area, would have a radius of 0.056 cm, and a minimum cutting impactor diameter of 0.037 cm, leading to a much higher cumulative flux per year of both meteoroids and debris. This in turn leads to a much higher risk of being cut for the circular cross-section tether with respect to the tape tether.

2. the full compliance of the tape tether considered in this work with the NASA safety guideline. The typical times of reentry, using tethers that are between 3 to 6 km long, according to analyses results discussed in Sec.[3.9], are always lower than 2 years, even for the highest inclinations and altitudes in LEO. In most cases they are lower than 1 year. Considering the worst case, of 6 km tether and deorbit lasting for 2 years, the computed length L_{cut} is 0.05 km for the meteoroids flux, and about 0.48 km for the debris flux. The length $L_{max} = \frac{1}{T}$, already described in Sec.[2.5] pg. 40, is 0.5. Therefore, since $L_{cut} < L_{max}$ for both debris and meteoroids, the EDT system successfully complies with the debris release NASA guideline in Ref.[1].

Appendix C

Coordinate Systems

For attitude work, the most commonly used reference systems are centered on the orbiting spacecrafts (see Ref.[36] at pg. 26). In the case of this work, focused on the orbital scale not on the local attitude scale, the reference systems that are used are all Earth-centered, i.e. *geocentric* systems. Follows a list of the reference systems used for computations in the personally written *Matlab*® codes:

1. **Cartesian Geocentric Equatorial Inertial (CGEI)** system.
   This is the principal reference frame. It is centered on the Earth, but stationary, not rotating with it. It can be considered inertial for Earth's orbits (in fact this is not a truly inertial frame since the center of the Earth is accelerating with respect to a third body, e.g. the Sun, but it can be considered inertial for a satellite orbiting the Earth). The x_I axis lies on the Earth's equatorial plane and points towards the *vernal equinox*; the z_I axis is aligned on the Earth's rotation axis and points northward. The y_I axis completes the right-hand orthonormal triad.

2. **Cartesian Geocentric Equatorial Rotating (CGER)** system: centered on the Earth and rotating with it. The x_I axis lies on the Earth's equatorial plane and points towards the Greenwich meridian; the z_I axis is aligned on the Earth's rotation axis and points northward. The y_I axis completes the right-hand orthonormal triad.

3. **Spherical Geocentric Equatorial Rotating (SGER)** system. Coordinates (r,θ,ϕ) where r is the direction pointing from the Earth's center to the spacecraft location in space; θ is the co-latitude direction at the generic location, i.e. measured from the North pole and pointing southward (positive direction); ϕ is the longitude direction at the generic location, from the Greenwich meridian and pointing eastward (positive direction). This is the reference system in which the coordinates of the magnetic field vector are first computed from database, as described in Appendix [E].

4. **Cartesian Geocentric Orbital Rotating (CGOR)** system: reference system with x and y axes lying on the orbital plane, and z axis perpendicular to this plane and oriented with the right-hand rule, once defined the x and y axes. The system is rotating with the satellite orbiting along a generic circular orbit: the

x axis is pointing in the outward radial direction; the y axis is parallel to the local instantaneous tangent to the orbit; the z closes the right-hand triad and is perpendicular to the orbital plane. This system is very convenient for defining any cinematic parameter associated to the orbit: for instance, the position vector in any instant of time is $\vec{r} = [r, 0, 0]$ and the orbital velocity vector is simply $\vec{v} = [0, v, 0]$.

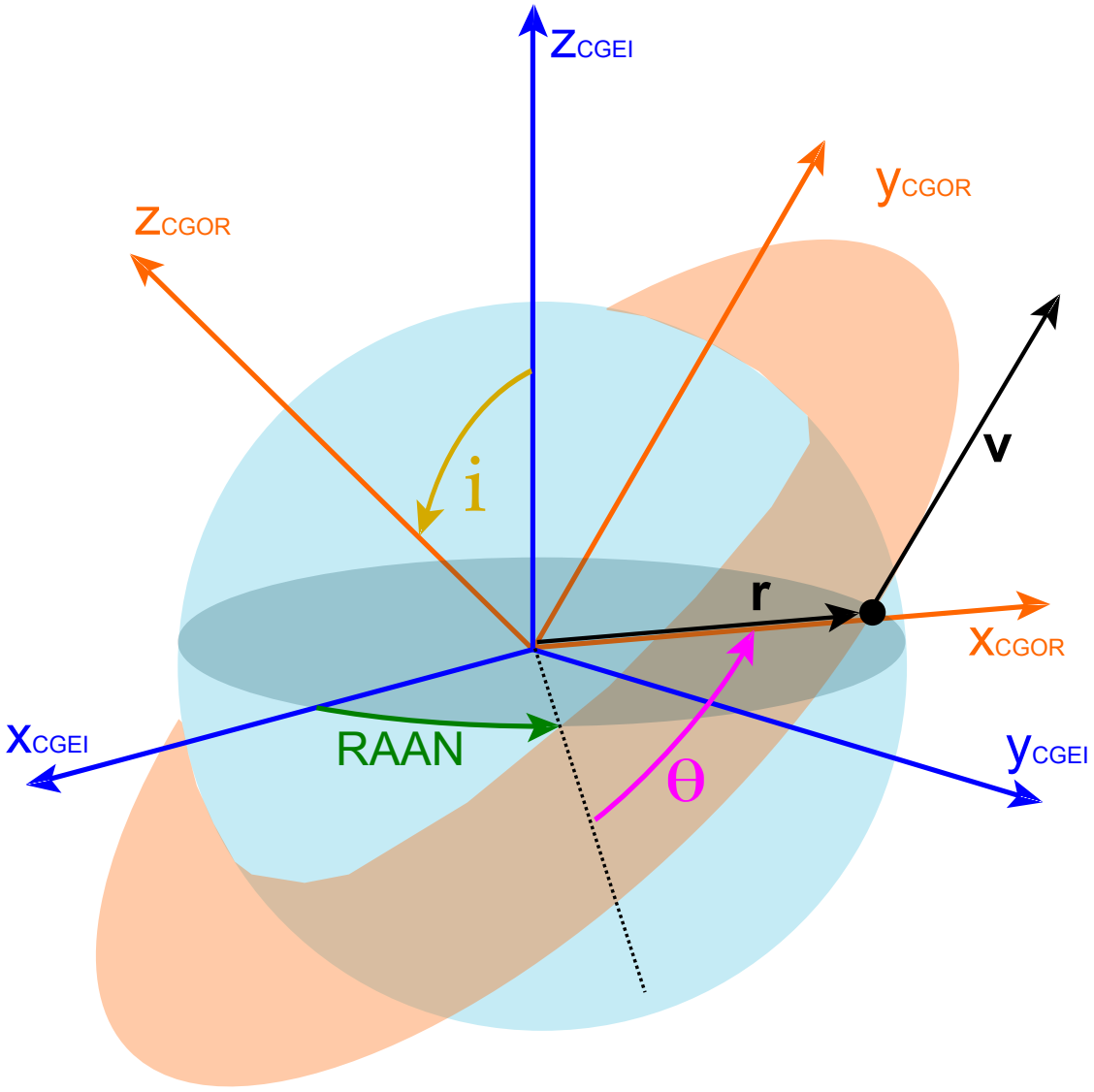

Figure C.1: CGOR *and* CGEI *reference systems. Position vector and velocity vector of the satellite are displayed, and all the angles necessary for the transformation of coordinates between the two reference systems*

Appendix D

Architecture of the *Matlab*® code for EDT analysis

For the computation of 2D and 3D plots with comparison between many different cases of initial altitude and inclination, the set of codes inside the folder 'DIAGRAMS' is used. This set of *Matlab*® codes works according to the architecture described in the image posted below. The core file is called 'DIAGRAMS.m'; this file calls all the other ancillary codes. In addition to all the plots this code also reports all the results for each case in an output *Excel*® file, where each row shows results for one case, i.e. for a specific combination of initial altitude and inclination.

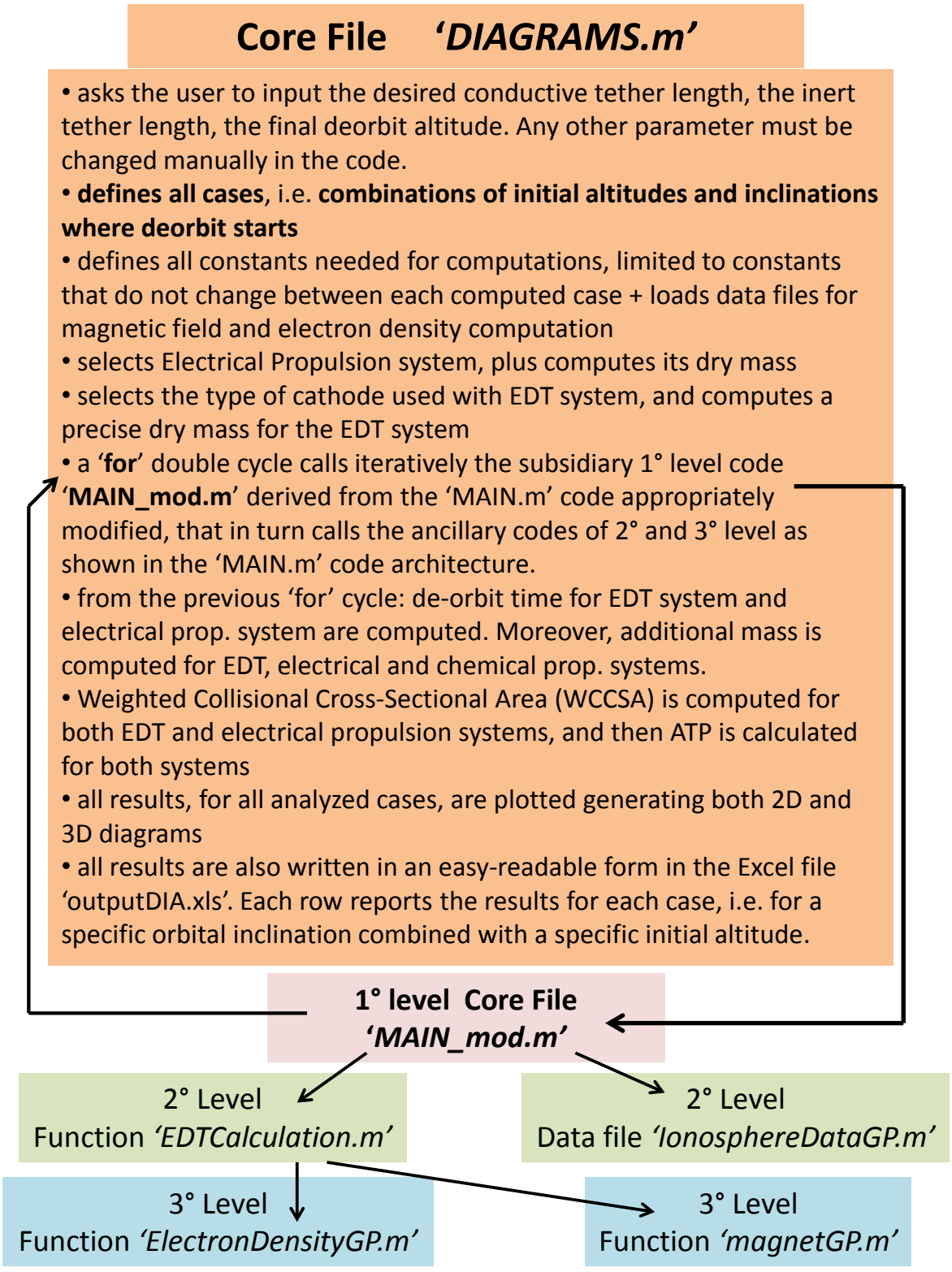

Figure D.1

Instead, for the computations of single cases in detail, the set of files inside the 'SINGLE_CASE' folder is used. This set of *Matlab*® codes works according to the architecture described in the image posted in the following page. The core file is called 'MAIN.m'; this file calls all the other ancillary codes.

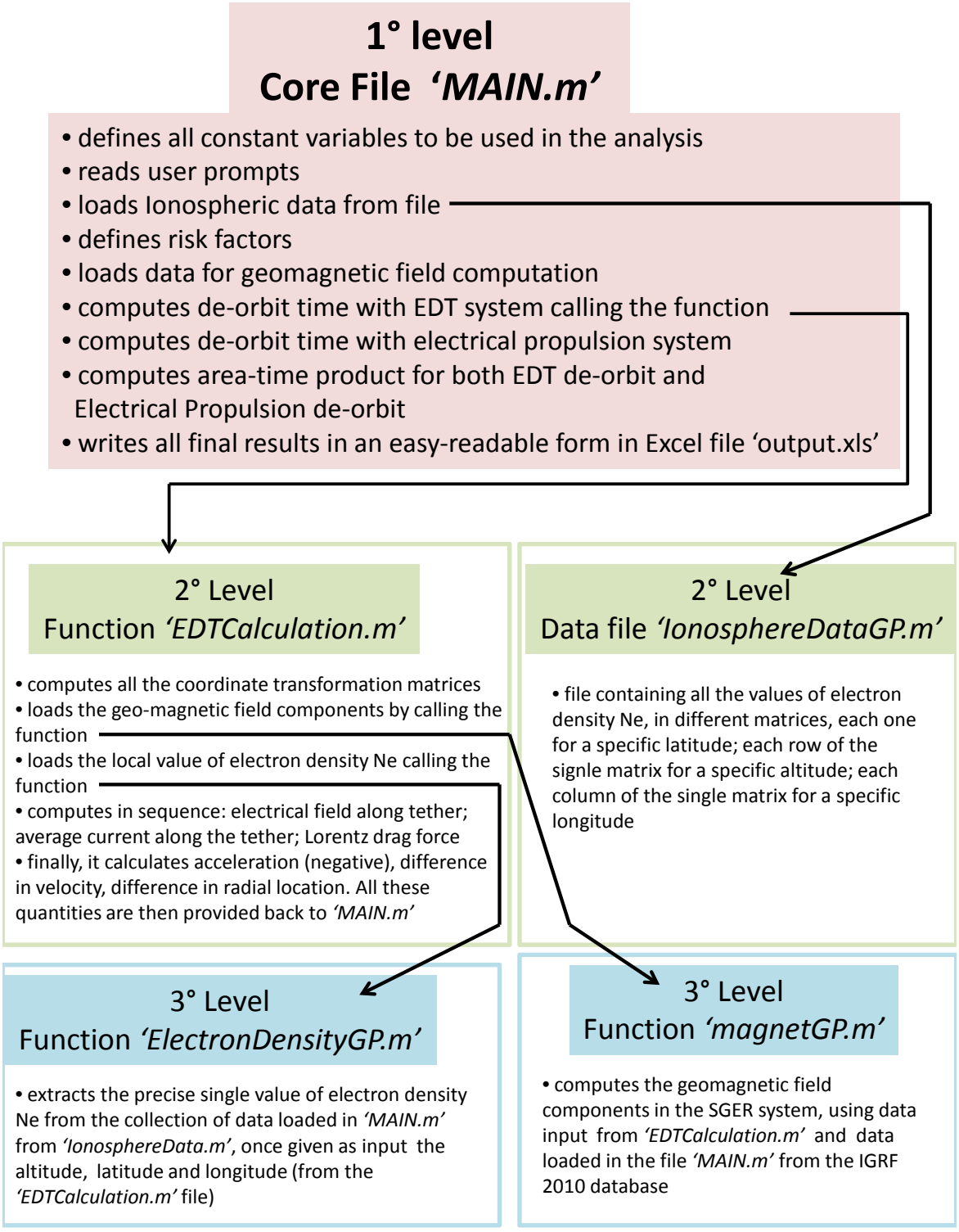
1° level
Core File 'MAIN.m'
• defines all constant variables to be used in the analysis
• reads user prompts
• loads Ionospheric data from file
• defines risk factors
• loads data for geomagnetic field computation
• computes de-orbit time with EDT system calling the function
• computes de-orbit time with electrical propulsion system
• computes area-time product for both EDT de-orbit and Electrical Propulsion de-orbit
• writes all final results in an easy-readable form in Excel file 'output.xls'
2° Level
Function 'EDTCalculation.m'
• computes all the coordinate transformation matrices
• loads the geo-magnetic field components by calling the function
• loads the local value of electron density Ne calling the function
• computes in sequence: electrical field along tether; average current along the tether; Lorentz drag force
• finally, it calculates acceleration (negative), difference in velocity, difference in radial location. All these quantities are then provided back to 'MAIN.m'
2° Level
Data file 'IonosphereDataGP.m'
• file containing all the values of electron density Ne, in different matrices, each one for a specific latitude; each row of the signle matrix for a specific altitude; each column of the single matrix for a specific longitude
3° Level
Function 'ElectronDensityGP.m'
• extracts the precise single value of electron density Ne from the collection of data loaded in 'MAIN.m' from 'IonosphereData.m', once given as input the altitude, latitude and longitude (from the 'EDTCalculation.m' file)
3° Level
Function 'magnetGP.m'
• computes the geomagnetic field components in the SGER system, using data input from 'EDTCalculation.m' and data loaded in the file 'MAIN.m' from the IGRF 2010 database

Figure D.2

Appendix E

Computation of Earth's Magnetic Field

The geomagnetic field components are derived from data in the *IGRF* reference model. The *Matlab*® function *'magnetGP.m'* is written in order to compute the geomagnetic field vector components B_r,B_θ, B_ϕ in the SGER spherical coordinate system (r, θ, ϕ) (see Appendix [C] for more details about this coordinate system). B_r is the component along the local radial direction (positive if pointing outwards from the Earth's center); B_θ is the component in the co-latitude direction (positive if pointing southward); B_ϕ is the component in the longitude direction (positive if pointing eastward from the reference Greenwich meridian).

The function *'magnetGP.m'* requires some inputs defined in the *'MAIN.m'* file, and is called by the other function *'EDTcalculation.m'* as described in the analysis scheme in Appendix [D]. These are the inputs required by the *'magnetGP.m'* function:

- the instantaneous radial distance r of the spacecraft from the Earth's center
- the co-latitude θ, i.e. the angle from the Earth's spin axis to the vector $\vec{r}$. This means that the unit vector $\hat{u}_\theta$ is positive in southward direction
- the longitude angle ϕ measured eastward from the Greenwich reference meridian. The positive unit vector $\hat{u}_\phi$ lies then parallel to the Earth's equatorial plane and points eastward.
- the time (in decimal days) starting from January 1^{st}, 2010.

E.1 Dipole Model

The simplest model for the geomagnetic field is the *dipole* model, with dipole axis tilted of an angle $\theta_m \approxeq 11.5°$ with respect to the Earth's spin axis; the dipole model corresponds to considering only the contributions of spherical harmonics of degree 1, and orders 0 and 1, (see Ref.[30]) in the analytic calculation of magnetic field. It is important to remember, in order to assign the correct direction to magnetic

field vectors, that the polarity of the magnetic dipole is opposite to the geographical polarity, i.e. the geomagnetic South Pole is close to the geographical North Pole, and the geomagnetic North Pole is close to the geographical South Pole. Magnetic field lines are oriented such that they "exit" from the North Magnetic Pole (close to the South Geographical pole) and go towards the South Magnetic Pole (close to the North Geographical pole). Hence, the direction of local magnetic field vector $\vec{B}$ points precisely in the direction shown in the picture below, it is tangent to the local field line, and lying on the plane of this line.

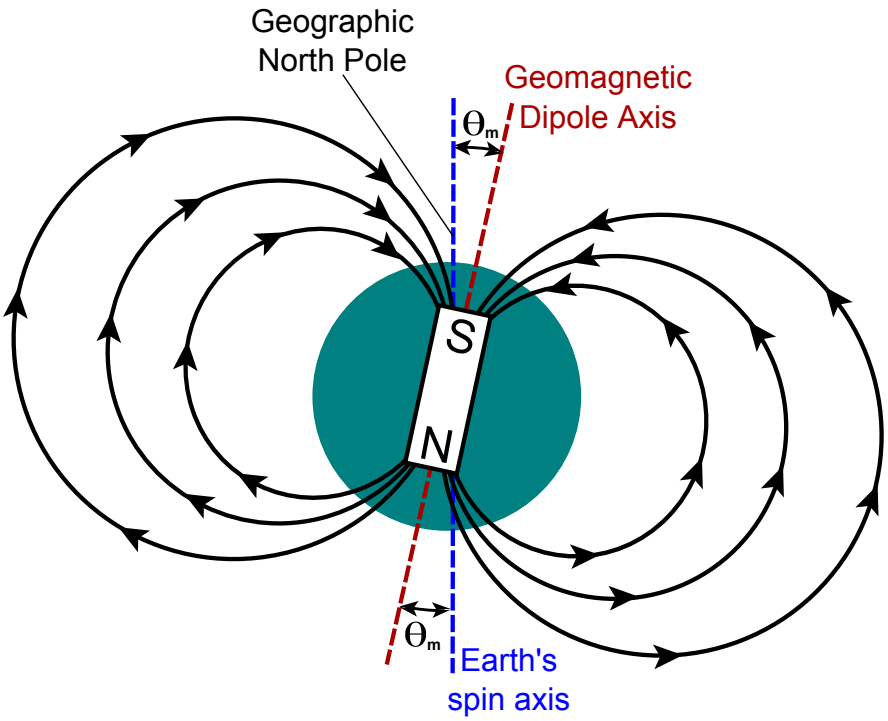

Figure E.1: *Geomagnetic dipole model*

E.2 Higher Harmonics model

Earth's magnetic field vector is computed as the gradient of a potential function that, in turn, is derived from a series of spherical harmonics. An infinite number of these harmonics would be required to achieve the exact value of the magnetic field components, at every location in space. Refer to [30] and [37] for detailed information. In the present project the notation system from Ref. [37] will be used.

The magnetic field vector **B** is computed as:

$$\mathbf{B} = -\nabla V \tag{E.1}$$

i.e. $\mathbf{B}$ is the negative of the spatial gradient of a scalar potential function V, that can be in turn derived as:

$$V = \sum_{n=1}^{\infty} \sum_{m=0}^{n} V^{n,m} \tag{E.2}$$

where

$$V^{n,m} = a \left(\frac{a}{r}\right)^{n+1} \left[g^{n,m} cos(m\phi) + h^{n,m} sin(m\phi)\right] P^{n,m} \tag{E.3}$$

- $a = 6371.2\,\text{km}$ is the mean radius of the Earth
- r is the magnitude of $\mathbf{r}$, i.e. the position vector from the center of the Earth to the generic point Q in space, where the magnetic field vector has to be computed.
- ϕ is the geographic longitude of point Q measured eastward from the Greenwich meridian.
- n is the degree of the specific spherical harmonic under consideration
- m is the order of the specific spherical harmonic under consideration
- $g^{n,m}$ and $h^{n,m}$ are Gauss-normalized coefficients of degree n and order m
- $P^{n,m}$ are Gauss-normalized functions, derived from Legendre polynomials. They are functions of θ, namely the co-latitude (or co-elevation) of generic point Q in space (i.e. $90° - latitude$).

It is defined as *spherical harmonic* of *degree* n and *order* m, the single contribution to $\mathbf{B}$, i.e.:

$$\mathbf{B^{n,m}} = -\nabla V^{n,m} \tag{E.4}$$

Therefore:

$$\mathbf{B} = \sum_{n=1}^{\infty} \sum_{m=0}^{n} \mathbf{B^{n,m}} \tag{E.5}$$

Gauss-normalized coefficients can be derived from *Schmidt Quasi-Normalized* (or *Semi-Normalized*) coefficients extracted from the *International Geomagnetic Reference Field (IGRF)* database. It is used the most up-to-date version, i.e. the 11th Generation IGRF, with the most recent values of coefficients computed for January 1st, 2010. This data was released by the International Association of Geomagnetism and Aeronomy (IAGA) in December 2009. The values of all coefficients reported in the IGRF model are determined experimentally. The IGRF is the result of a collaboration between magnetic field modellers and the institutes involved in collecting magnetic field data from satellites and from observatories around the world. There are some model limitations, to be aware of; for additional details see Web Ref.[16].

It is downloaded an *Excel*® spreadsheet from Web Ref. 4 with the *11th generation IGRF* data. It is named *igrf11coeffs.xls*. This spreadsheet includes all the *Schmidt Quasi-Normalized* (or *Semi-Normalized*) coefficients up to the 13th degree and order ($n_{max} = 13$ and $m_{max} = 13$) in units of nT (nano-tesla). Every column reports the values computed every five years. It is used the column of IGRF-2010. When the subsequent IGRF-2015 will be computed, the IGRF-2010 will become DGRF (Definitive Geomagnetic Reference Field). This file also contains the secular variations, used for the computation of "corrected" values of these coefficients, at any time between January 1st, 2010 and January 1st, 2015. In fact, *secular variations* represent correction factors, in units of *nano-Tesla/year*, that multiplied by the time in years elapsed from January 1st 2010, return an estimate of the variation of *Schmidt Quasi-Normalized* coefficients in that time period.

For all analyses in this work, it is chosen to start deorbiting on January 1st, 2010: this means to set the decimal number of days to zero, at the start of every deorbit simulation. Then, at every consecutive time step, it is calculated the variation of *Schmidt Quasi-Normalized* coefficients, using *secular variations*; thereafter, it is updated the value of magnetic field accounting for these variations. It is possible to start simulations even at a later date, but in order for the secular variation values to be valid, the entire deorbit phase should be constrained between 2010 and 2015. Consequently, it is not recommended to start the simulation on 2014 since, if deorbit time is higher than one year, secular variations after January 1st, 2015 are not available.

The *'MAIN.m'* or the *'DIAGRAMS.m' Matlab*® codes import the *Schmidt Quasi-Normalized* coefficients, from the *igrf11coeffs.xls* file, in units of nT. These values are then converted to units of *tesla* (T) and used for the following computations.

Schmidt quasi-normalized coefficients are converted to *Gauss-normalized* coefficients. The *Schmidt quasi-normalized* coefficients are denoted with a tilde sign on the top and by placing only m as superscript, and n as subscript ($\widetilde{g_n^m}$ and $\widetilde{h_n^m}$), in order to distinguish them from the *Gauss-normalized* coefficients ($g^{n,m}$ and $h^{n,m}$). The conversion from *Schmidt quasi-normalized* to *Gauss-normalized* coefficients is performed using the following equations:

$$g^{n,m} = S_{n,m}\widetilde{g_n^m} \tag{E.6}$$

$$h^{n,m} = S_{n,m}\widetilde{h_n^m} \tag{E.7}$$

where factors $S_{n,m}$ are independent of local spherical coordinates r, θ, ϕ of the generic point Q where the magnetic field is computed. The same is true also for the *Schimdt quasi-normalized* coefficients and, consequently, for the *Gauss-normalized* coefficients. Therefore, the code has to perform these operations, described up to now, only once in an entire simulation, not for every single location covered by the object during deorbit. This is an advantage granted by the usage of these coefficients, that allow a

more efficient computational method.

$S_{n,m}$ factors are derived using the following recursive equations:

$$S_{0,0} = 1 \tag{E.8}$$

$$S_{n,0} = S_{n-1,0}\left[\frac{2n-1}{n}\right] \qquad n \geq 1 \tag{E.9}$$

$$S_{n,m} = S_{n,m-1}\sqrt{\frac{(n-m+1)(\delta_m^1+1)}{n+m}} \qquad m \geq 1 \tag{E.10}$$

where δ_m^1 is the *Kronecker delta* defined as $\delta_i^j = 1$ if $i = j$ and $\delta_i^j = 0$ otherwise. In this equation $j = 1$; therefore, only when $m = 1$ the delta is $\delta_1^1 = 1$. In all other cases $\delta_{m\neq 1}^1 = 0$.

The Gauss functions $P^{n,m}$ can be recursively obtained too, with a similar procedure:

$$P^{0,0} = 1 \tag{E.11}$$

$$P^{n,n} = sin(\theta)P^{n-1,n-1} \tag{E.12}$$

$$P^{n,m} = cos(\theta)P^{n-1,m} - K^{n,m}P^{n-2,m} \tag{E.13}$$

where

$$K^{n,m} = 0 \qquad n = 1 \tag{E.14}$$

$$K^{n,m} = \frac{(n-1)^2 - m^2}{(2n-1)(2n-3)} \qquad n > 1 \tag{E.15}$$

It is set the maximum *degree* of contributing spherical harmonics, to be considered in the analysis, as n_{max}. In the IGRF datasheet the maximum degree is $n = 13$, but n_{max} can be even lower than 13. In all analyses in this thesis, it is used $n_{max} = 13$, i.e. the maximum degree of spherical harmonics available. For each degree value n, there is a set of values of order m ranging from 0 to n, for g coefficients; from 1 to n for h coefficients. The maximum value of order m equals the maximum value of n considered in the calculation, i.e. $m_{max} = n_{max}$. Hence, in all analyses for this thesis it is used $m_{max} = 13$, i.e. the highest number of available harmonics order. Consequently, it is important to point out that the values of magnetic field used in all analyses, they are the most precise values possible, since all 13×13 available harmonics are considered. This is done since it is detected that computational time did not increase significantly by using all the available harmonics, with respect to using a lower number of harmonics. References regarding the geomagnetic field computation are Ref. [14] and Ref. [37] at Appendix H.

By applying the gradient in spherical coordinates, the magnetic field components can be eventually calculated with the following equations:

$$B_r = -\frac{\partial V}{\partial r} = \sum_{n=1}^{n_{max}} \left(\frac{a}{r}\right)^{n+2} (n+1) \sum_{m=0}^{n} \left[g^{n,m} cos(m\phi) + h^{n,m} sin(m\phi)\right] P^{n,m} \tag{E.16}$$

$$B_\theta = -\frac{1}{r}\frac{\partial V}{\partial \theta} = -\sum_{n=1}^{n_{max}} \left(\frac{a}{r}\right)^{n+2} \sum_{m=0}^{n} \left[g^{n,m} cos(m\phi) + h^{n,m} sin(m\phi)\right] \frac{\partial P^{n,m}}{\partial \theta} \tag{E.17}$$

$$B_\phi = -\frac{1}{r sin\theta}\frac{\partial V}{\partial \phi} = -\frac{1}{sin\theta} \sum_{n=1}^{n_{max}} \left(\frac{a}{r}\right)^{n+2} \sum_{m=0}^{n} m \left[-g^{n,m} sin(m\phi) + h^{n,m} cos(m\phi)\right] P^{n,m} \tag{E.18}$$

Computation is performed using a recursive method in order to improve code efficiency, and the expressions are such that singularity is avoided when the magnetic field is evaluated at points that lie on the polar axis.

The results for geomagnetic field computed by this code are successfully validated by comparing them with the values output from NASA applet at Web Ref. 5. Validation procedures are described in detail at Sec.[3.8.1].

The components B_r, B_θ and B_ϕ are computed, using the equations described above, in the SGER system (see Appendix [C] for definition), i.e. a non-inertial geocentric system.

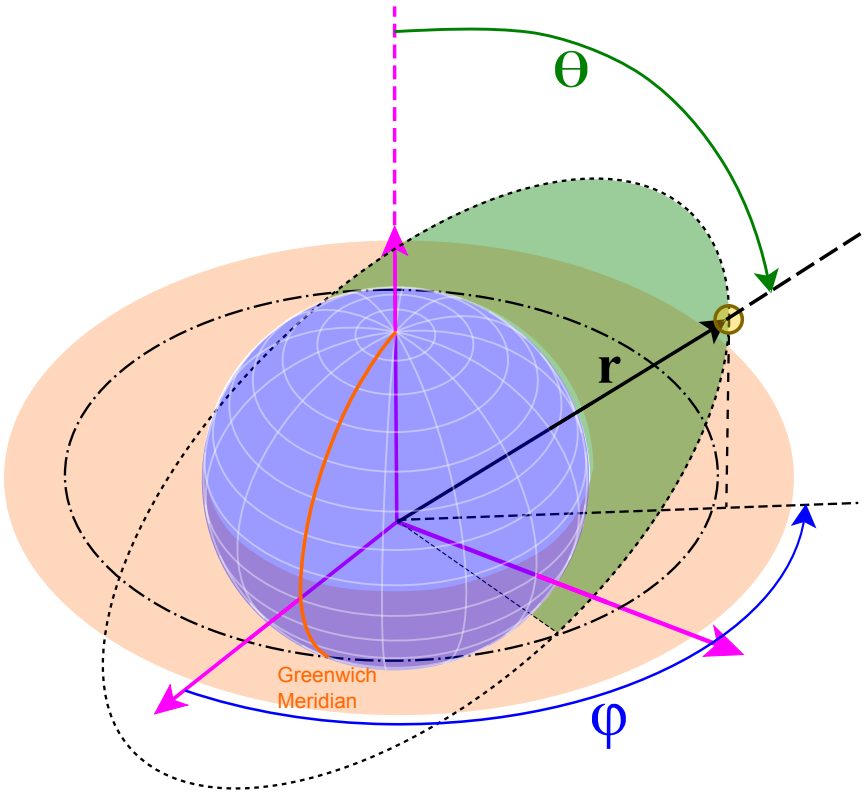

Figure E.2: *Reference Frame (SGER) in which magnetic field components are originally computed using data from the IGRF-2010 model.*

Therefore, the magnetic field components must be converted from the non-inertial SGER system, to the CGEI inertial system (see Appendix [C] for definition). This conversion is performed in the *Matlab*® function *'EDTCalculation.m'* using two transformation matrices. One transformation matrix, reported below, is necessary to convert the geomagnetic field components from SGER to CGER system.

$$\begin{bmatrix} B_x \\ B_y \\ B_z \end{bmatrix}_{CGER} = \begin{bmatrix} sin\theta cos\phi & cos\theta cos\phi & -sin\phi \\ sin\theta sin\phi & cos\theta sin\phi & cos\phi \\ cos\theta & -sin\theta & 0 \end{bmatrix} \begin{bmatrix} B_r \\ B_\theta \\ B_\phi \end{bmatrix}_{SGER} \tag{E.19}$$

namely

$$\vec{B}_{CGER} = [R]^{SGER}_{CGER}\, \vec{B}_{SGER} \tag{E.20}$$

where $[R]^{SGER}_{CGER}$ is the transformation matrix from SGER coordinates to CGER coordinates.

The second matrix converts the components from CGER system to CGEI system.

The CGER system has the same z axis as the CGEI system but it rotates about this axis with angular velocity Ω_E, i.e. Earth's angular velocity about its spin axis. The transformation matrix from CGER system coordinates to CGEI coordinates is:

$$[R]_{CGEI}^{CGER} = \begin{bmatrix} cos(\Omega_E t) & -sin(\Omega_E t) & 0 \\ sin(\Omega_E t) & cos(\Omega_E t) & 0 \\ 0 & 0 & 1 \end{bmatrix} \tag{E.21}$$

Consequently, the magnetic field vector in CGEI system can be finally computed as:

$$\vec{B}_{CGEI} = \begin{bmatrix} B_{x_I} \\ B_{y_I} \\ B_{z_I} \end{bmatrix} = [R]_{CGEI}^{CGER}\ \vec{B}_{CGER} \tag{E.22}$$

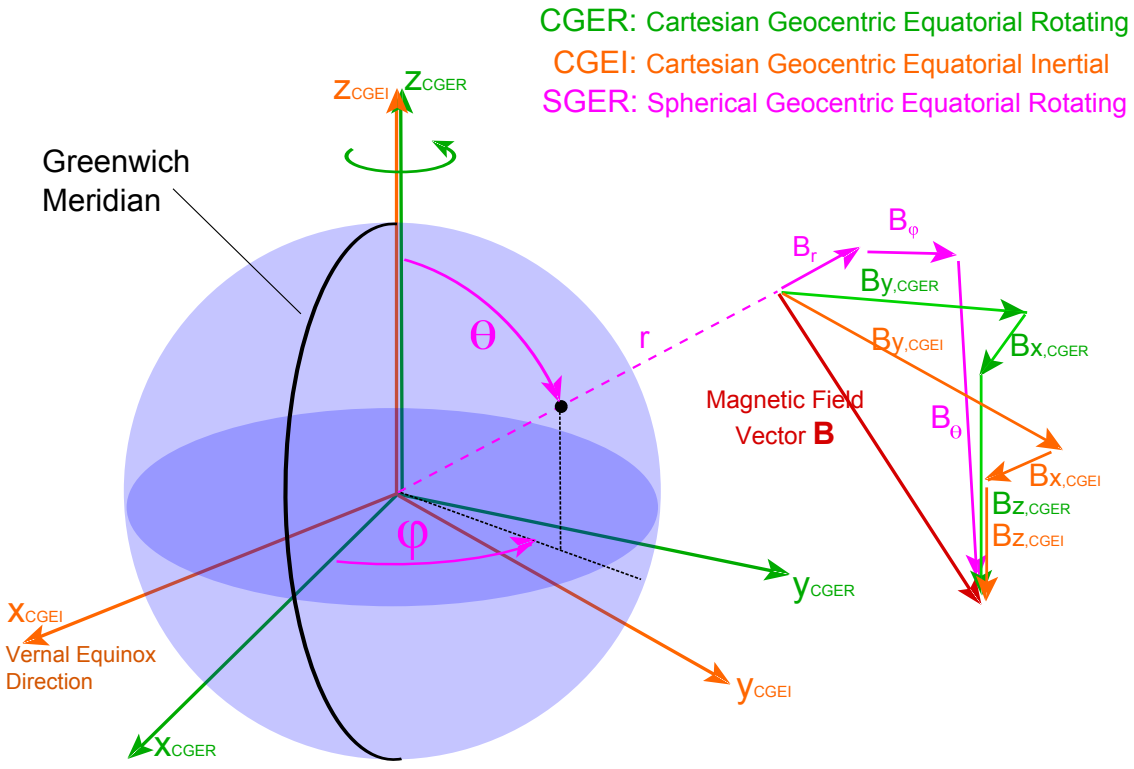

Figure E.3: *Geomagnetic Field vector $\vec{B}$, showing components in all different reference systems*

Appendix F

Ionosphere Modeling

For the computation of the current generated along the ED tether, it is necessary to know the value of *electron density* N_e at every location in space of the satellite during deorbit. Values of N_e are extracted from ionospheric data in the *International Reference Ionosphere (IRI) 2007* database. This database is written in *Fortran*. *Intel Parallel Studio Fortran* compiler is used to launch a *Fortran* code called 'Map.f90'(provided by D. Zanutto, see Additional References [G]), in Linux operating system, in order to create a *Matlab*® file called *'IonosphereData.m'*, by calling another *Fortran* file named 'IRI.for' that accesses the database. The 'IRI.for' code was adapted by H. Urrutxua and C. Bombardelli. The only input requested by the 'Map.f90' code, when compiled, is the precise Julian Day (JD) at which to compute the *electron density* data. In fact, *electron density* is variable over time, even on the same specific location. The major influencing factor is the *solar flux*. Higher solar flux leads to higher *electron densities*.

A re-computation of *electron density* data at each time step of the deorbit is not possible, with the set of *Fortran* routines available. This is also not necessary since, with the approximations already considered, (such as no inclination change, only circular initial orbits, tether as a rigid dumbbell, etc.) it is surely reasonable to use only one single set of data for *electron density*, for the entire deorbit.
Therefore, it is chosen, for *electron density* computation, a Julian Day such that the solar flux on that day is as close as possible to an average value over one complete solar cycle. Since deorbit times with EDT system range from few months to about 1.3 years as maximum, the *electron density* is sort of "averaged" during such time (even if this time is considerably lower than the 11 years of one typical solar cycle). The error related to considering a mean solar flux over one solar cycle, and to using constant values for *electron density* over time, is lower the higher is deorbit time. This is because for longer deorbits the mean solar flux over deorbit time is closer to the mean solar flux over an entire solar cycle that lasts for about 11 years.

It is then found from scientific literature an average value of $F10.7$ index, i.e. the measure of the solar radio flux per unit frequency at a wavelength of 10.7 cm, near the peak of the observed solar radio emission. $F10.7$ is generally measured in SFU, i.e. *Solar Flux Units* ($1\ \text{SFU} = 10^{-22}\,\frac{\text{W}}{\text{m}^2\text{Hz}}$). The $F10.7$ is then a direct indicator of the

intensity of solar activity.

Using this average $F10.7$, it is found a Julian Day when the $F10.7$ was as close as possible to this mean value. Finally, by inputting this JD when compiling the 'Map.f90' *Fortran* routine, the ionosphere data associated to that JD is computed. This collection of data can be consequently treated as a "mean ionosphere" over an 11 years solar cycle. After compiling, and inserting the JD, the code writes the *'IonosphereData.m'* *Matlab*® file. This file reports several matrices containing all values of electron density N_e for different altitudes, longitudes, and latitudes. The file 'IonosphereData.m' was then slightly edited and renamed to 'IonosphereDataGP.m'. This file is loaded by the core files 'MAIN.m' or 'DIAGRAMS.m', in order to import all the N_e values (as shown in the code architecture diagram in Section [D]).

Appendix G

Additional References

Web References

1. http://en.wikipedia.org/wiki/Electrodynamic_tether#Orbit_motion_limited_.28OML.29_theory
2. http://en.cnki.com.cn/Article_en/CJFDTOTAL-JSGC200903018.htm
3. http://www.tethers.com/bibliography.html
4. http://www.ngdc.noaa.gov/IAGA/vmod/igrf.html
5. http://ccmc.gsfc.nasa.gov/modelweb/models/igrf_vitmo.php
6. http://iri.gsfc.nasa.gov/
7. http://omniweb.gsfc.nasa.gov/vitmo/iri2012_vitmo.html
8. http://www.webmo.net/support/ifort11.html
9. http://irimodel.org/#ftpweb
10. http://www.ndt-ed.org/GeneralResources/MaterialProperties/ET/Conductivity_Al.pdf
11. http://plasma.physics.swarthmore.edu/ssx/lab.html
12. http://en.wikipedia.org/wiki/Electric_current
13. http://www.moog.com/products/propulsion-controls/spacecraft/sub-systems/
14. http://space.skyrocket.de/index.html
15. https://directory.eoportal.org/web/eoportal/satellite-missions/s/space-tethers
16. http://www.ngdc.noaa.gov/IAGA/vmod/igrfhw.html
17. http://aoss-research.engin.umich.edu/sets/FEAC/
18. http://www.ips.gov.au/Satellite/6/2

19. http://www.universetoday.com/106284/goce-spacecraft-will-likely-make-uncontrolled-re-entry-this-weekend/

20. http://roma2.rm.ingv.it/en/research_areas/4/ionosphere

Other

- *Stela* ® software, version 2.5.1, has been used for simulations of reentry via *natural decay* and via *drag augmentation devices*. With courteous permission of CNES (Centre National d'études Spatiales), http://logiciels.cnes.fr/STELA/en/logiciel.htm
- Slides from lecture about *Micrometeorites and Space Debris*, *Astrodynamics* class, Prof. Lorenzini E.C., Università di Padova.
- A set of *Matlab*® codes, strictly regarding only deorbit via ED tether, was provided by D. Zanutto and, for a very limited part, used as reference. Nonetheless, all the *Matlab*® codes used in this work are absolutely original and completely created from zero by the author of this thesis. Only original *Matlab*® codes written by Pastore Guido are used to compute results presented in this thesis work. The only exception is the ancillary *Fortran* file used to extract ionospheric data from the IRI database and convert it to a *Matlab*® data file. This *Fortran*® code was used as provided by D. Zanutto, without modifications.
- Tutorial "Deorbiting Performance" by D. Zanutto.

Bibliography

[1] Nasa safety standard: Guidelines and assesment procedures for limiting orbital debris. Technical report, August 1995. NSS 1740.14. Office of Safety and Mission Assurance, Washington D.C.

[2] A.P. Alpatov, V.V. Beletsky, V.I. Dranovskii, V.S. Khoroshilov, A.V. Pirozhenko, Troger H., and A.E. Zakrzhevskii. *Dynamics of Tethered Space Systems*. CRC Press, 1st edition, 2010.

[3] Vladimir S. Aslanov and Alexander S. Ledkov. *Dynamics of Tethered Satellite Systems*. Woodhead Publishing, 1st edition, 2012.

[4] Roger R. Bate, Donald D. Mueller, and Jerry E. White. *Fundamentals of Astrodynamics*. Dover Publications Inc., 1st edition, 1971.

[5] Paul M. Bellan. *Fundamentals of Plasma Physics*. Cambridge University Press, 1st edition, 2006. ISBN-10 0-521-82116-9.

[6] D.M. Blash and J.D. Williams. Determination of hollow cathode plasma contactor system requirements using an electrodynamic tether system simulation tool.

[7] Claudio Bombardelli, Jesus Pelaez, and Manuel Sanjurio. *Asymptotic Solution for the Current Profile of Passive Bare Electrodynamic Tethers. Journal of Propulsion and Power*, 2010. Vol. 26, No. 6, pp. 1291-1304, DOI: 10.2514/1.46808.

[8] Claudio Bombardelli, Denis Zanutto, and Enrico Lorenzini. *Deorbiting Performance of Bare Electrodynamic Tethers in Inclined Orbits. Journal of Guidance, Control and Dynamics*, September-October 2013. Vol.36, No.5.

[9] Eric Choinière. *Theory and Experimental Evaluation of a Consistent Steady State Kinetic Model for 2-D Conductive Structures in Ionospheric Plasmas with Application to Bare Electrodynamic Tethers in Space*. PhD thesis, University of Michigan, 2004.

[10] M.L. Cosmo and E.C. Lorenzini. *Tethers In Space Handbook*. Smithsonian Astrophysical Observatory, 3rd edition, 1997.

[11] National Research Council. *Orbital Debris: A Technical Assessment*. National Academies Press, 1st edition, 1995. ISBN 1558671587.

[12] Howard D. Curtis. *Orbital Mechanics for Engineering Students*. Elsevier Butterworth Heinemann, 1st edition, 2005.

[13] A C Das. *Space Plasma Physics, An Introduction*. Narosa Publishing House, 1st edition, 2004. ISBN 81-7319-575-7.

[14] Jeremy Davis. *Mathematical Modeling of Earth's Magnetic Field*. Technical report, Virginia Tech, Blacksburg, VA 24061. May 2004.

[15] Luigi T. De Luca. *Problemi Energetici in Propulsione Aerospaziale*. Politecnico di Milano, 1998.

[16] Robert L. Forward and Robert P. Hoyt. *Application of the Terminator Tether^{TM} Electrodynamic Drag Technology to the Deorbit of Constellation Spacecraft*. Technical report, Tethers Unlimited, Inc. Published by AIAA (American Institute of Aeronautics and Astronautics).

[17] Robert L. Forward and Robert P. Hoyt. *The Terminator Tether^{TM}: Autonomous Deorbit of LEO Spacecraft for Space Debris Mitigation*. Technical report, Tethers Unlimited, Inc. AIAA-00-0329.

[18] Keith R.P. Fuhrhop. *Theory and Experimental Evaluation of Electrodynamic Tether Systems and Related Technologies*. PhD thesis, University of Michigan, 2007.

[19] Dan M. Goebel and Ira Katz. *Fundamentals of Electric Propulsion: Ion and Hall Thrusters*. Wiley, 1st edition, 2008.

[20] Robert P. Hoyt. *Tether Systems for Satellite Deployment and Disposal*. Technical report, Tethers Unlimited, Inc. IAF-00-S.6.04.

[21] L. Iess. *Space tethers: an overview*. Technical report, Dipartimento Ing. Aerospaziale, Università *La Sapienza*, Roma.

[22] A. M. Jablonski. *Deorbiting of microsatellites in Low Earth Orbit (LEO): An Introduction*. Technical report, June 2008. Defence R&D Canada - Ottawa.

[23] Heiner Klinkrad. *Space Debris Models and Risk Analysis*. Praxis Publishing Ltd., 1st edition, 2006.

[24] E. Levin. Orbital debris: Time to remove, August 2011. Google TechTalk.

[25] P. Mazzoldi, M. Nigro, and C. Voci. *Elementi di Fisica - Elettromagnetismo*. Edises, 2nd edition, 2005.

[26] Kim Minkyu. *ECE Radiation Analysis of the Hall Thruster*. PhD thesis, University of Texas, 2007.

[27] H. M. Mott-Smith and I. Langmuir. *The Theory of Collectors in Gaseous Discharges. Physical Review*, October 1926. Vol. 28, pp. 727-763.

[28] Kerry T. Nock, Kim M. Aaron, and Darren McKnight. *Removing Orbital Debris with Less Risk. Journal of Spacecraft and Rockets*, March-April 2013. Vol. 50, No. 2, pp. 365-379, DOI: 10.2514/1.A32286.

[29] D. Oh, S. Benson, K. Witzberger, and M. Cupples. Deep space mission applications for next: Nasa's evolutionary xenon thruster. American Institute of Aeronautics and Astronautics.

[30] M. Carlos Roythmayr. *Contributions of Spherical Harmonics to Magnetic and Gravitational Fields.* Technical report, Langley Research Center, Hampton, Virginia. NASA/TM-2004-213007, March 2004.

[31] R. M. Sanjurjo. *Self balanced bare electrodynamic tethers. Space debris mitigation and other applications.* PhD thesis, Escuela Tecnica Superior De Ingenieros Aeronauticos, 2009.

[32] J. R. Sanmartin, E. C. Lorenzini, and M. Martinez-Sanchez. *Electrodynamic Tether Applications and Constraints.* Technical report, Universidad Politécnica de Madrid, University of Padova, Massachussets Institute of Technology. Journal of Spacecraft and Rockets, Vol.47, No.3, May-June 2010.

[33] Nickolay N. Smirnov. *Space Debris Hazard Evaluation and Mitigation.* Taylor and Francis, 1st edition, 2002.

[34] P. Stuckey, C. Clauss, M. Day, V. Murashko, N. Maslennikov, K. Kozubsky, R. Gnizdor, B. Arhipov, G. Popov, V. Kim, V. Kozlov, and D. Grdlichko. *SPT-140 High Performance Hall System (HPHS) Development.* Technical report, Air Force Research Laboratory (AFMC), AFRL/PRS, Edwards, AFB, CA. July 1998.

[35] Eric J. Van der Heide and Michiel Kruijff. *Tethers and debris mitigation. Acta Astronautica Vol.48, No.5-12, pp.503-516*, March-June 2001. Published by *Elsevier Science Ltd.*

[36] James R. Wertz. *Spacecraft Attitude Determination and Control.* D. Reidel Publishing Company, 1st edition, 1978.

[37] James R. Wertz. *Space Debris Models and Risk Analysis.* Praxis Publishing Ltd., 1st edition, 2006.

[38] James R. Wertz and Wiley J. Larson. *Space Mission Analysis and Design.* Space Technology Library, 3rd edition, 1999.

[39] D. Zanutto, E. C. Lorenzini, R. Mantellato, G. Colombatti, and A. Sanchez-Torres. *Orbital debris mitigation through deorbiting with passive electrodynamic drag.* Technical report, University of Padova, Universidad Politécnica de Madrid, 2012. 63rd International Astronautical Congress, Naples, Italy.

[40] Denis Zanutto. Deorbiting performance.

[41] Denis Zanutto. *Analysis of propellantless tethered system for the de-orbiting of satellites at end of life.* PhD thesis, Universita' degli Studi di Padova, 2013.

[42] Z. H. Zhu and Rui Zhong. *Deorbiting Dynamics of Electrodynamic Tether. International Journal of Aerospace and Lightweight Structures, Vol.1, No.1, pp.47-66*, 2011. DOI: 10.3850/S2010428611000043.